THE UNIVERSITY OF ALABAMA

COLLEGE OF ENGINEERING
BUREAU OF ENGINEERING RESEARCH

FINAL REPORT

on

Contract NAS8-25562

THRESHOLD DETECTION IN AN ON-OFF BINARY COMMUNICATIONS CHANNEL WITH ATMOSPHERIC SCINTILLATION

by

William E. Webb
Principal Investigator

Prepared for

National Aeronautics and Space Administration
George C. Marshall Space Flight Center
Marshall Space Flight Center, Alabama 35812

January 1975

BER Report No. 186-70

UA ··· UNIVERSITY, ALABAMA 35486

FINAL REPORT

on

Contract NAS8-25562

THRESHOLD DETECTION IN AN ON-OFF BINARY COMMUNICATIONS CHANNEL WITH ATMOSPHERIC SCINTILLATION

by

William E. Webb
Principal Investigator

Prepared for

National Aeronautics and Space Administration
George C. Marshall Space Flight Center
Marshall Space Flight Center, Alabama 35812

January 1975

BER Report No. 186-70

In the course of this contract a number of individual tasks have been performed in direct support of NASA-MSFC's airborne optical communications experiment (project AVLOC) and a proposed satellite optical communications test. All work performed on this contract has been previously reported either in interim technical reports or by informal reports delivered to the MSFC-COR. In this final report we summarize the more significant accomplishments of this project as follows:

Appendix 1. Threshold Detection in an On-Off Binary Optical Communications System with Atmospheric Scintillation

Appendix 2. Near Field Antenna Patterns of Obstructed Cassegrainian Telescopes

Appendix 3. Study of Atmospheric Effects on Laser Communications Systems

Appendix 4. Requirements Study for the AVLOC Experiment

Appendix 5. Data Analysis for AVLOC Project

In addition to the preceding tasks, the project director has (1) prepared a study on the state of the art in atmospheric communications, (2) prepared a measurements program document for the AVLOC project, (3) served as co-principal investigator on both the AVLOC and ATS-G communications experiments, and performed various other tasks at the request of the project contracting officer's technical representative.

APPENDIX 1

THRESHOLD DETECTION IN AN ON-OFF BINARY COMMUNICATIONS CHANNEL WITH ATMOSPHERIC SCINTILLATION

ABSTRACT

The optimum detection threshold in an on-off binary optical communications system operating in the presence of atmospheric turbulence has been investigated assuming a poisson detection process and log normal scintillation. The dependence of the probability of bit error on log amplitude variance and received signal strength has been analyzed and semi-emperical relationships to predict the optimum detection threshold derived. On the basis of this analysis a piecewise linear model for an adaptive threshold detection system is presented. The bit error probabilities for non-optimum threshold detection systems have also been investigated.

INTRODUCTION

It is well known that atmospheric scintillation not only increases the bit error probability in a pulse code modulated optical communications channel but also influences the decision level for optimum threshold detection. The later effect is of considerable practical importance to the design of efficient pulse code modulated optical communications systems regardless of whether fixed or adaptive threshold detection is used. Fried and Schmelzer[1] have considered the bit error rates in an optical communications channel by assuming gaussian detection statistics, an approximation which is valid only for large numbers of signal photons. Titterton and Speck[2] have treated the problem using Poisson statistics so that their results are valid for small numbers of signal photons also. Although both previous investigators have recognized that the optimum detection threshold changes in the presence of scintillation, neither has studied the effect in depth.

In this paper we investigate the optimum detection threshold in an on-off binary optical communications channel as a function of the number of received photoelectrons and the strength of scintillation. Poisson detection statistics and log normal scintillation are assumed and, on the basis of this model, expressions to predict the optimum detection threshold are derived. In addition, we have investigated the bit error probabilities for sub-optimum choices of detection

threshold. This is of importance to the design and analysis of optical communications systems since exact optimization of the threshold level is never possible, especially in the presence of atmospheric effects. Application of these results to the design of fixed and adaptive threshold optical receivers is discussed.

ERROR PROBABILITY IN THE OPTICAL CHANNEL.

We shall consider an on-off binary optical communications channel in which the laser transmitter may send either a '1', which corresponds to a pulse being transmitted, or a '0' which corresponds to no pulse transmitted. Let S be the number of signal photoelectrons per pulse received at the detector when a '1' is transmitted and εS be the number of received signal photoelectrons when a '0' is transmitted. Here ε is the reciprocal of the modulator extinction ratio. We will assume that in addition to the signal photoelectrons the detector receives N noise photoelectrons per pulse, mostly due to background. In a threshold detection system the receiver interprets the received signal as either a '1' or a '0' depending on whether the total number of received photoelectrons is greater or less than some threshold level T.

In the presence of scintillation the probability of a detection error is

$$P_E = P(0)P_{FA} + P(1)(1-P_D) \qquad (1)$$

Where P(0) and P(1) are the apriori probabilities of sending '0' and a '1' respectively, P_{FA} is the false alarm probability, ie. the probability of a '1' being received given that a '0' was sent, and P_D is the detection probability, ie. the probability of a '1' being received given that a '1' was sent. P_D and P_{FA} are given by

$$P_{FA} = \int_0^\infty \sum_{j=t}^{\infty} \exp\left[-(N+\varepsilon S)\right] \frac{(N+\varepsilon S)^j}{j!} f(S)dS \qquad (2)$$

$$P_D = \int_0^\infty \sum_{j=t}^{\infty} \exp\left[-(N+S)\right] \frac{(N+S)^j}{j!} f(S)dS \quad . \qquad (3)$$

Assuming log normal scintillation and a symmetrical pulse code we obtain

$$P_E = \frac{1}{8C_\ell} + \left(\frac{e^{C_\ell 2T(T-1)}}{4\sqrt{2\pi C_\ell}}\right)\left(-(S_0)^T \int_{-\infty}^{\infty} e^{-8C_\ell Z_1^2} \gamma^*(T, S_0 e^{(Z_1+4C_\ell(T-1/2))})dZ_1\right.$$

$$\left. + ((S_0-N)\varepsilon+N)^T \int_{-\infty}^{\infty} e^{-8C_\ell Z_0^2} \gamma^*(T, ((S_0-N)\varepsilon+N)e^{(Z_0+4C_\ell(T-1/2))})dZ_0\right) \qquad (4)$$

where γ^* is the incomplete gamma function

$$\gamma^*(T,n) = \frac{1}{n^T} \sum_{X=T}^{\infty} \frac{e^{-n} n^X}{X!} \qquad (5)$$

S_0 is the average number of signal photoelectrons per pulse and C_ℓ is the variance of ln(S).

The bit error probability has been evaluated by numerical integration of equation 4 on a UNIVAC 1108 computer. The threshold T was initially taken to be the no scintillation optimum threshold given by 3

$$T_0 = \frac{S(1-\varepsilon) + \ln(P(0)/P(1))}{\ln((S+N)/(N+\varepsilon S))} \quad . \tag{6}$$

An iterative procedure was then used to minimize the error probability as a function of T, while holding S_0, N, ε and C_ℓ constant. In this way we were able to simultaneously determine the optimum threshold in the presence of scintillation and study the effect of sub-optimum threshold on the error rates. Calculations were repeated for values of the parameters S_0, ε, N and C_ℓ over the ranges likely to be encountered in practice.

Figure 1 shows the probability of a bit error at optimum threshold as a function of the number of received signal photoelectrons and the log amplitude variance of scintillation with one background photoelectron and an extinction ratio of 15 db. The computed values of bit error probability agree with those previously published by Titterton and Speck[2].

One feature of figure 1 which deserves note is the difference in the slope of the curves for large and small values of the log amplitude variance. When C_ℓ is less than about 0.02 the error probability decreases rapidly with increasing number of signal photo-

electrons, whereas for large values of C_ℓ the error probability tends to become relatively independent of the number of signal photoelectrons provided that S_0 is not too small. Thus there appears to be two regions, one in which the error probability is determined primarily by scintillation and the other in which it is mainly determined by signal strength. This dicotomy, which we might call the signal limited and scintillation limited cases, will be seen more clearly when we consider the optimum detection threshold in the presence of scintillation.

An alternate method of displaying these results is in terms of the transmitted power required to achieve a given bit error rate in the presence of scintillation as compared to the power required when there is no scintillation. In figure 2 the required power margin is shown as a function of bit error rate and log amplitude variance. These results are essentially independent of the choice of N and ϵ as long as both are relatively small. Fried and Schmeltzer[1] have developed a similar set of curves based on the assumption of gaussian detection statistics. Comparison of our results with those of Fried and Schmeltzer shows that the two models agree reasonably well in predicting the required power margin for values of C_ℓ less than about 0.02, but that the gaussian model may underestimate the necessary power margin by as much as 8 db for C_ℓ equal to 0.03 and 30 db for C_ℓ equal to .05 at error rates of 10^{-6}. For a log amplitude variance of 0.1 the difference in the power margins predicted by the gaussian

and Poisson models may exceed 80 db. Thus the gaussian model is reasonably accurate in the case of weak scintillation but gives an extremely over-optimistic estimate of a communications system performance in the presence of strong scintillation.

Since the Poisson distribution approaches a gaussian distribution as the mean increases, it might be expected that our results should reduce to those of Fried and Schmeltzer in the case of a large average number of received signal photoelectrons. However, for the system under consideration a large value of S_0 is not sufficient to insure that the Poisson counting statistics can be adequately approximated by a gaussian distribution. The means of the Poisson distributions in question are not S_0 but $(N + S)$ and $(N + \varepsilon S)$, where the variable S is averaged over all values from zero to infinity. Thus if N is small, the mean of the Poisson distribution will be small over part of the range of S, even though S_0 is large. Clearly, when C_ℓ is large the contribution to the error probability from that part of the range of S in which the gaussian approximation is invalid will be greater. Physically this means that during a deep fade there are only a few photoelectrons per pulse; therefore gaussian statistics can not be used. A second, and perhaps more significant, problem with Fried and Schmeltzer's model is the assumption of additive noise independent of the signal strength. This assumption is equivalent to approximating the Poisson distribution by a gaussian distribution with constant variance. Since the variance of a Poisson distribution is

equal to the mean, this assumption is valid only if

$$N + S \simeq N + \varepsilon S \simeq \text{constant} \tag{7}$$

for all values of S with non negligible probability of occurance. In particular, unless N is very large compared to S_0, the noise associated with a zero being received is different from the noise associated with a one. Therefore Fried and Schmeltzer's analysis can only be valid if the number of noise photoelectrons per pulse is much greater than the number of signal photoelectrons. In this case the two analyses should yield the same results.

As a check on our results we have calculated the error probabilities assuming fourty noise photoelectrons per pulse, log amplitude variances of 0.0 and 0.05 and error probabilities from 10^{-1} to 3×10^{-3}. For these cases the computed power margin required to compensate for scintillation agreed with that reported by Fried and Schmeltzer to within one db. The residual error is due to the fact that even for fourth noise photoelectrons the condition of equation 7 is only approximately satisfied.

On the basis of our analysis we conclude that Fried and Schmeltzer's results contain a fundamental inconsistancy; namely, the number of signal photoelectrons required to obtain error probabilities less than about 10^{-3} is so large that equation 7 can not be satisfied unless the log amplitude variance is very small. Thus the assumption of background limited operation is invalid except for the case of weak scintillation or very high bit error rates.

OPTIMUM THRESHOLD

The optimum threshold in the presence of scintillation is shown in figure 3 as a function of the average number of received signal photoelectrons per pulse. As is to be expected the optimum threshold decreases with increasing scintillation. For S_0 greater than about 10 the curves are very nearly straight lines whose slopes are dependent on the strength of the scintillation. This linearity can be understood in the no scintillation case by noting that when εS is large compared to N equation 6 reduces to

$$T = \frac{1-\varepsilon}{\ln(1/\varepsilon)} S. \tag{8}$$

With scintillation we may replace equation 8 by a linear relation of the form

$$T = \alpha(C_\ell)S_0 + \beta \tag{9}$$

where the parameters α and β can be determined by linear least mean square fits to the data of figure 3. To a reasonable approximation we may take β to be 2.5, independent of C_ℓ. The slope α, on the other hand, is strongly dependent on C_ℓ as shown in figure 4. The dependence of the slope on C_ℓ can be represented by the relation

$$\alpha(C_\ell) \simeq .145(e^{7.5X10^3 C_\ell^2} + 1) \tag{10}$$

Perhaps the most striking feature of figure 4 is the distinct knee that occurs for values of C_ℓ near 0.02, and corresponds to the transition from signal strength limited to scintillation limited conditions. For C_ℓ much larger than 0.02 the slope of the threshold curve varies only slowly with increasing C_ℓ whereas for weak scintillation the slope is a very strong function of C_ℓ. In fact we can approximate α fairly well in these two regions by straight lines as shown by the dashed curves in figures 4. Hence

$$T_0 = a_i C_\ell S_0 + b_i S_0 + C \qquad (11)$$

where the coefficients a_i and b_i take on either one of two values depending upon whether C_ℓ is greater or less than the break point. A piecewise linear approximation of this sort is appealing from an engineering point of view since it provides a convenient model for implementing an adaptive threshold detection system. One could envision, for example, a detection system in which the mean and variance of the received signal power were continuously monitored and the threshold set in accordance with equation 11. Such a system would require only linear operations and a single discrete discontinuity to control the threshold level.

As Titterton and Speck have pointed out (footnote 4 of reference 2) this analysis is applicable to systems in which the threshold is varied on the basis of a long term estimate (ie. on the order of seconds) of scintillation and is limited to systems with bit rates

of 10^7 or less. Tycz, Fitzmaurice and Premo [5] have considered a perfectly adaptive threshold system for both the log normal and beta channels.

SUB-OPTIMUM THRESHOLDS

In practice the detection threshold of an optical communications system operating through the atmosphere will never be perfectly optimized. If the threshold is fixed then changing atmospheric conditions will deoptimize the system and even if an adaptive threshold is used the system will be incapable of precisely tracking changes in signal strength and turbulence. In order to properly predict a communication system's performance it is necessary to know the expected bit error probabilities for non-optimum detection thresholds. Investigation of the performance of non-optimum threshold detection is also necessary to the design of adaptive threshold systems.

Figure 5 shows the bit error probability as a function of detection threshold with log amplitude variance as a parameter. The data plotted is for the case of 40 signal photoelectrons and no background photoelectrons per pulse and an extinction ratio of 15 db. Other choices of parameters yielded curves which were essentially similar.

Inspection of figure 5 shows that with a fixed detection threshold a decrease in scintillation will always result in an improvement in system performance even though decreasing the scintillation deoptimizes the system. That is to say that the bit error probability

decreases more rapidly with decreasing log amplitude variance than it is increased by the corresponding deoptimization of the threshold level. Thus if one selects the detection threshold that is optimum for the strongest expected scintillation and predicts the error rate on this basis, one is assured that the system performance will not be worse under conditions of weaker scintillation. This strategy might be appropriate if one wishes to insure that a given error rate will be obtained under all expected conditions.

ACKNOWLEDGMENT

This research was supported by the National Aeronautics and Space Administration under Contract NAS8-25562 with the Astrionics Laboratory, George C. Marshall Space Flight Center, Huntsville, Alabama.

REFERENCES

1. D. L. Fried and R. A. Schmeltzer, Appl. Opt. 6, p 1729-1737, 1967.

2. P. J. Titterton and J. P. Speck, Appl. Opt. 12, p 425-426, 1973.

3. This corresponds to Titterton and Speck's (op. cit.) equation 5. However these authors' expression contains a typographical error in that two pairs of parenthesis in the denominator were omitted.

4. M. Tycz, M. W. Fitzmaurice and D. A. Premo, IEEE Trans. on Communications, p 1069-1071, 1973.

Figure 1. Probability of bit error for an on-off binary PCM optical communications system as a function of the number of signal photoelectrons for log amplitude variances between 0,0 and 0.1. One background photoelectron per pulse and a modulation extinction ratio of 15 db. was assumed.

Figure 2. The Loss Factor, defined as the additional transmitted power required to compensate for atmospheric scintillation, is given as a function of the number of received photoelectrons per pulse and the log-amplitude variance of scintillation. Other parameters are the same as the preceeding figure.

Figure 3. The optimum detection threshold as a function of number of signal photoelectrons per pulse and log amplitude variance of scintillation. Other parameters are the same as in the preceeding figures.

Figure 4. The slope of the linear portion of the detection threshold curves (figure 3) as a function of the log amplitude variance of scintillation. The dashed lines indicate a piecewise linear approximation discussed in the text.

Figure 5. Dependence of the bit error probability on detection threshold for non-optimum detection. Error probability is plotted as a function of the normalized threshold, T/S_0, for $S_0 = 40$.

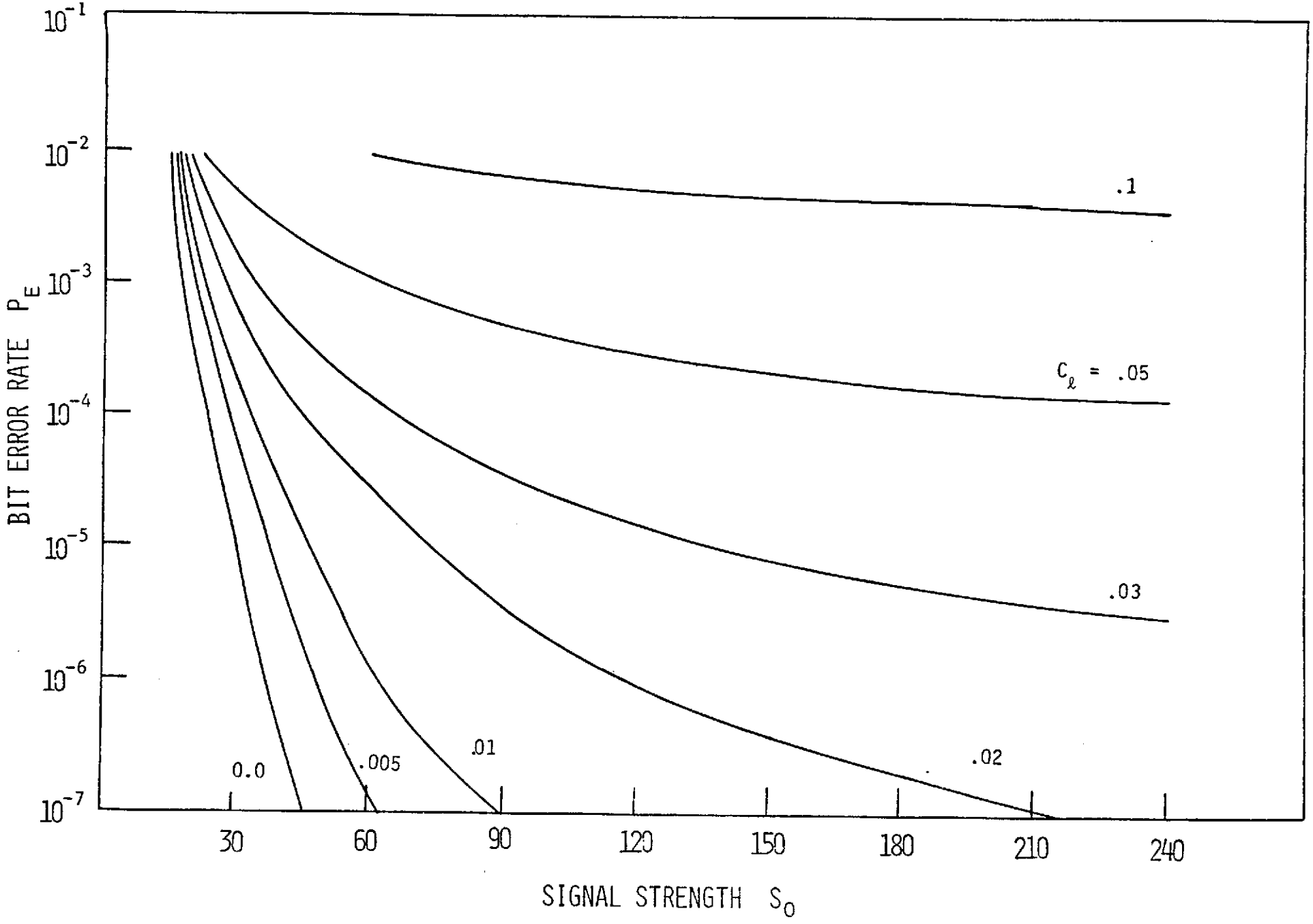
10^{-1}
10^{-2}
10^{-3}
10^{-4}
10^{-5}
10^{-6}
10^{-7}
BIT ERROR RATE P_E
.1
C_ℓ = .05
.03
.02
.01
.005
0.0
30
60
90
120
150
180
210
240
SIGNAL STRENGTH S_0

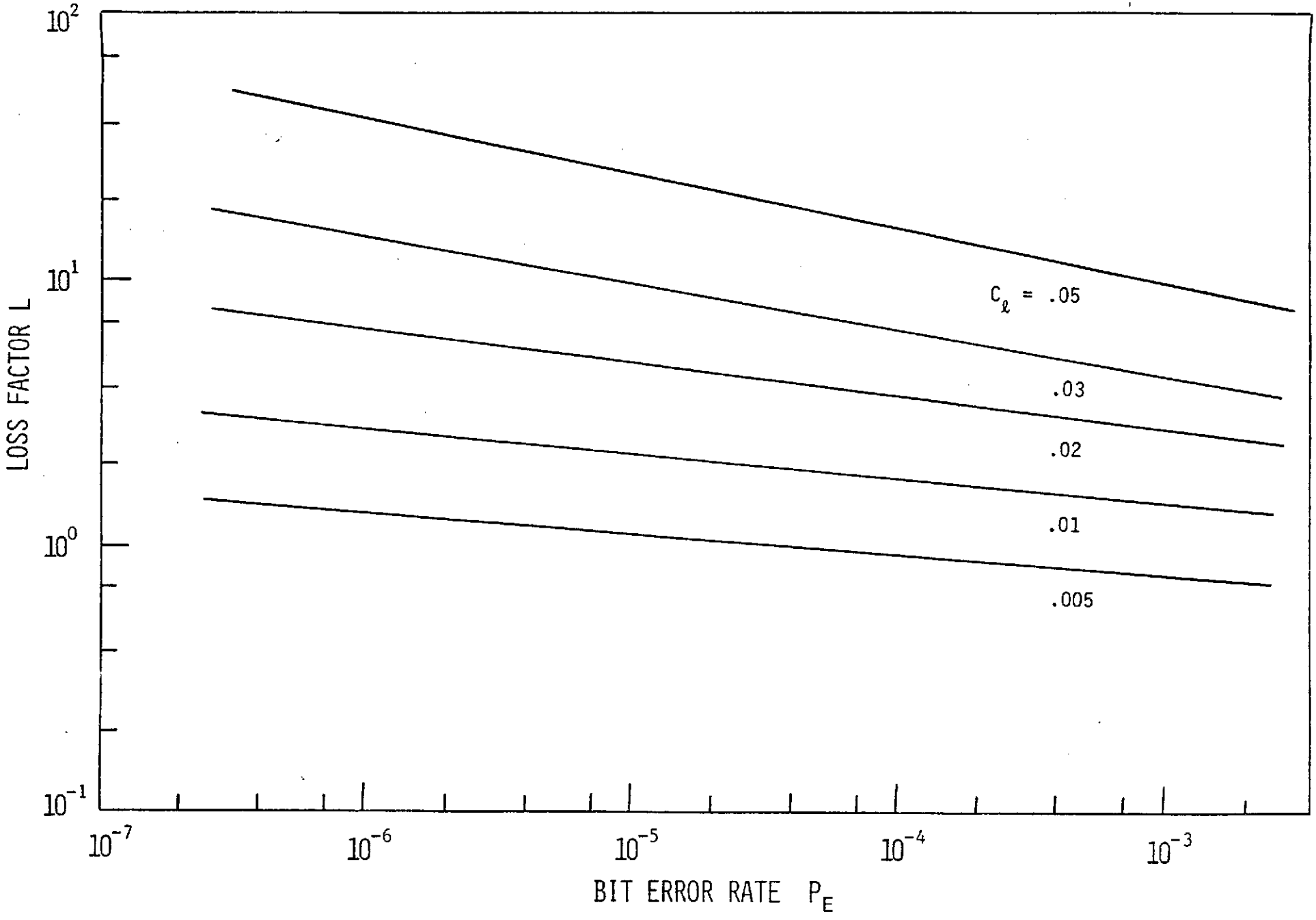
10^2
10^1
10^0
10^{-1}
LOSS FACTOR L
C_ℓ = .05
.03
.02
.01
.005
10^{-7}
10^{-6}
10^{-5}
10^{-4}
10^{-3}
BIT ERROR RATE P_E

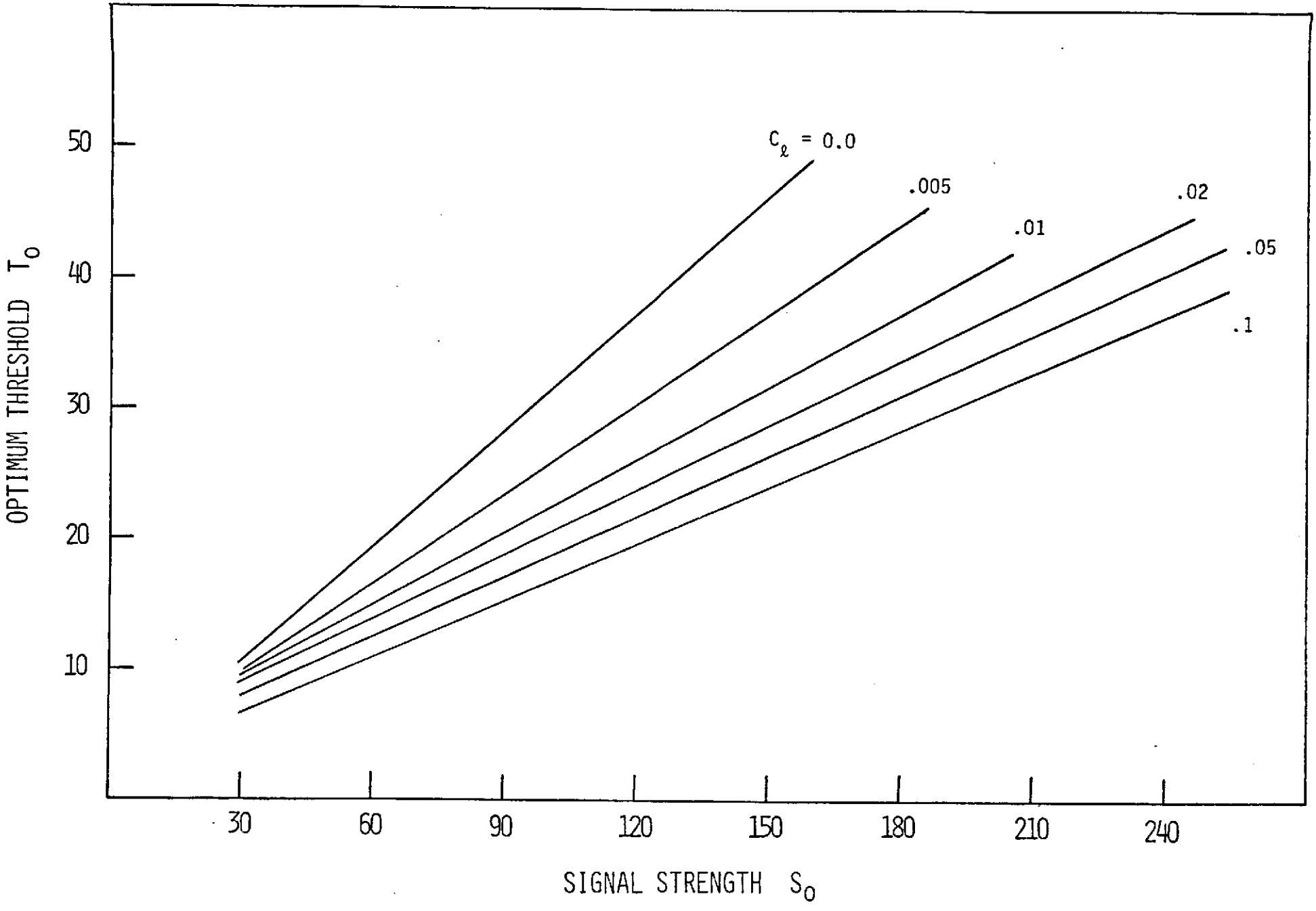
OPTIMUM THRESHOLD T_o
50
40
30
20
10
C_ℓ = 0.0
.005
.01
.02
.05
.1
30
60
90
120
150
180
210
240
SIGNAL STRENGTH S_o

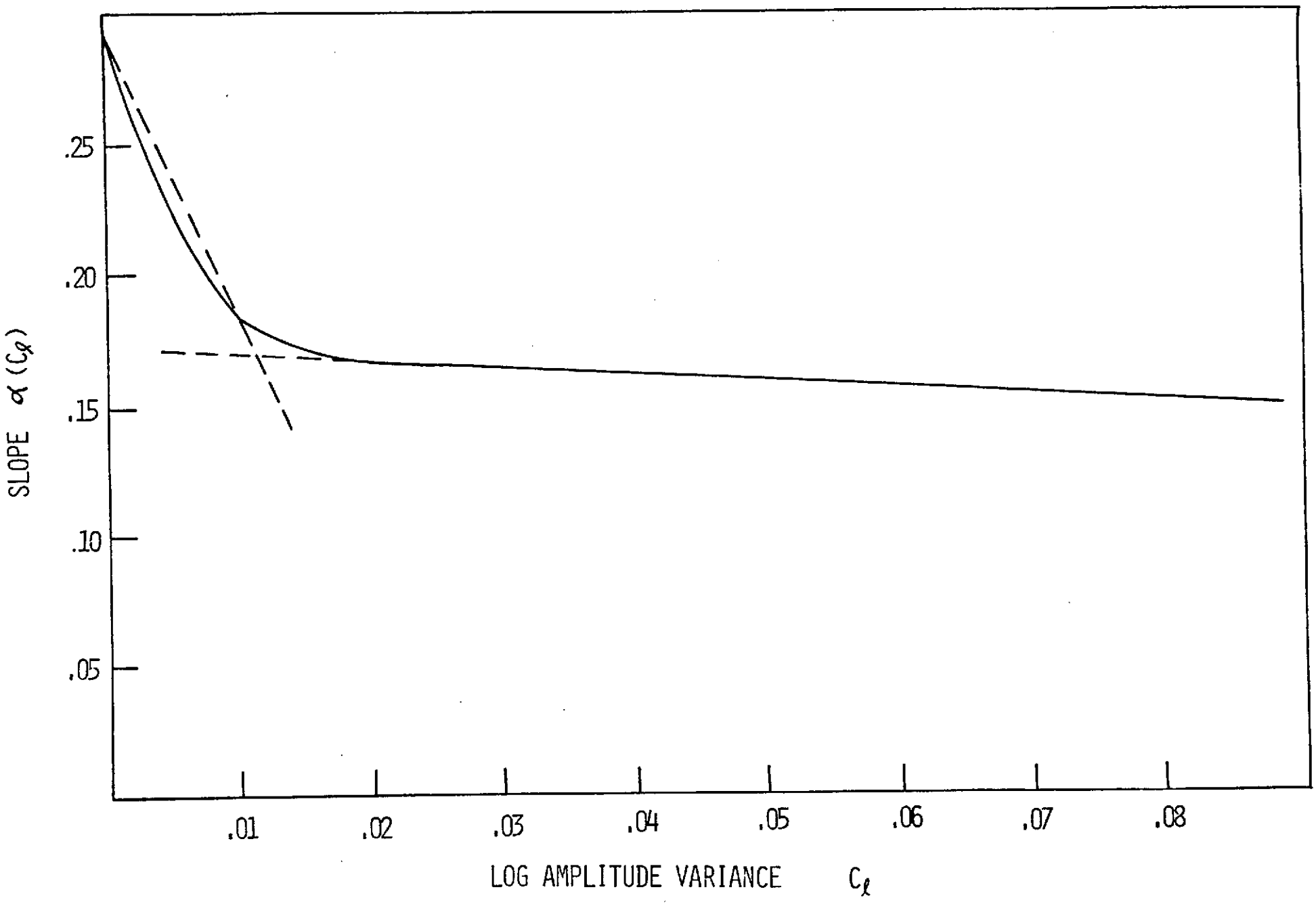
.25
.20
.15
.10
.05
SLOPE $\alpha(C_\ell)$
.01
.02
.03
.04
.05
.06
.07
.08
LOG AMPLITUDE VARIANCE C_ℓ

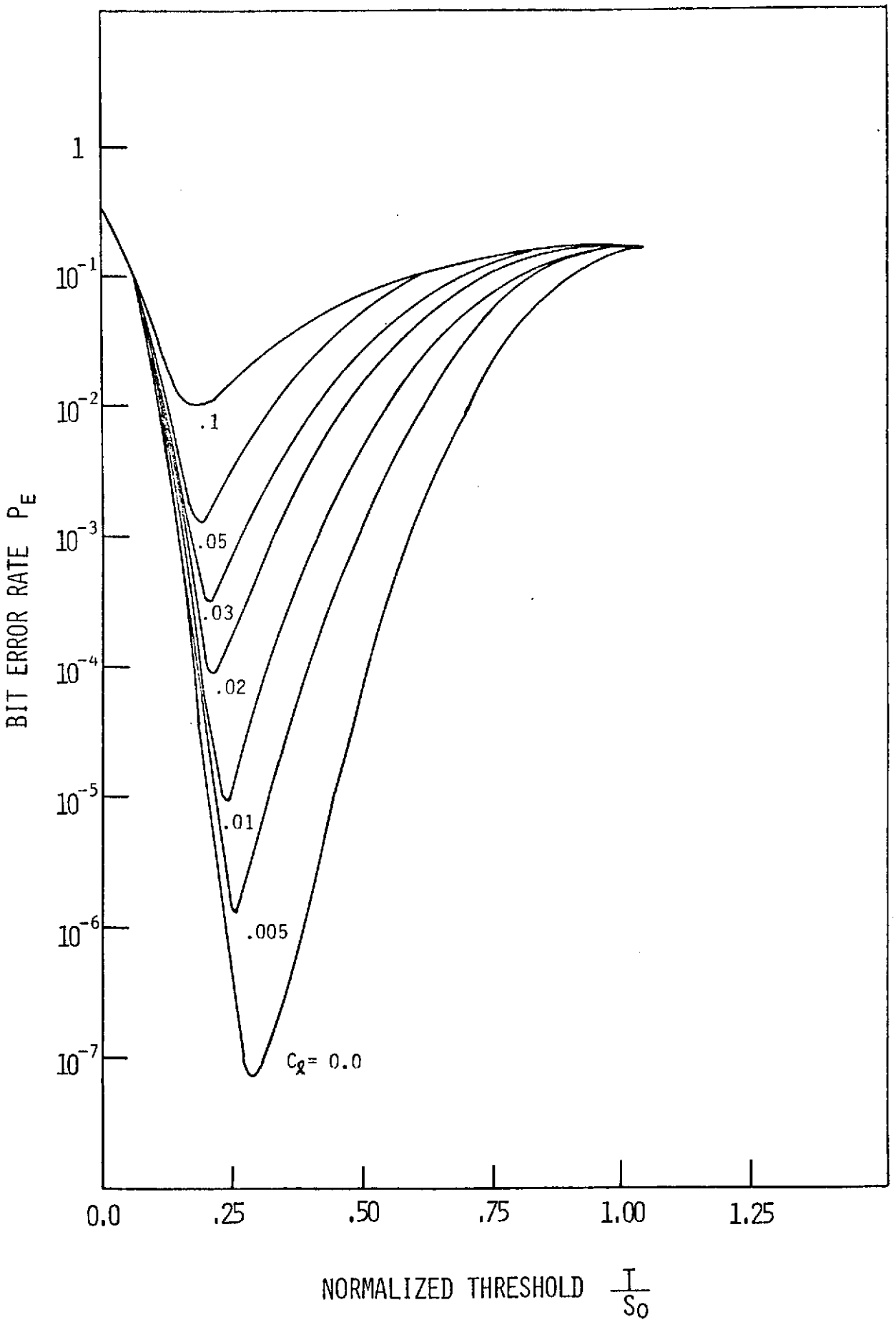
1
10^{-1}
10^{-2}
10^{-3}
10^{-4}
10^{-5}
10^{-6}
10^{-7}
BIT ERROR RATE P_E
.1
.05
.03
.02
.01
.005
C_ℓ = 0.0
0.0
.25
.50
.75
1.00
1.25
NORMALIZED THRESHOLD $\frac{I}{S_0}$

APPENDIX 2

NEAR FIELD ANTENNA PATTERNS OF OBSTRUCTED CASSEGRAINIAN TELESCOPES

ABSTRACT

The near field antenna pattern of an obstructed optical transmitter, such as a cassegrainian telescope, has been computed using the Fresnel approximation to the scalar diffraction integral. A number of cases have been considered. These include uniformly illuminated, obstructed circular apertures, and apertures coherently illuminated with a divergent gaussian beam wave such as may be obtained from the TEM_{oo} mode of a laser. Other beam profiles that may also been considered.

The techniques used for the numerical evaluation of the Fresnel integral are discussed and results for the optical systems to be used on the Marshall Space Flight Center's High Altitude Aircraft Optical Communications Experiment are presented.

TABLE OF CONTENTS

LIST OF FIGURES

INTRODUCTION

The Marshall Space Flight Center's High Altitude Aircraft Test for Visible Laser Optical Communications (AVLOC) will use cassegrainian telescopes as transmitting optics on both the air-to-ground and ground-to-air links.[1] For very long ranges, such as earth to satellite, cassegrainian optics will cause no difficulty provided that collimated or focused beams are used. Under these conditions the shadow of the secondary mirror will be filled with diffracted light and the intensity maximum of the telescope's antenna pattern will lie on the optical axis of the telescope. That is to say that the far field diffraction pattern does not contain the shadow of the central obstruction. Many optical tracking and communication systems, including those employed on the AVLOC experiment, operate over much shorter path lengths so that both receivers are in the near field of their respective transmitters and hence see a doughnut shaped radiation pattern with a dark shadow on the optical axis. Even very long path lengths will not eliminate the central shadow if the transmitted beam has a divergence greater than the beam spreading due to diffraction by the aperture. In the case of divergent beams, one is in effect always in the near field.

Since most optical communications systems require a divergent transmitted beam to keep the pointing errors less than the beam spread, it would appear that some technique must be used to eliminate the central shadow, or else cassegrainian optics (or any other obstructed

optical system) cannot be used. One might, for example, offset the transmitted beam with respect to the axis of the tracking system by an angle sufficient to remove the receiver from the dark central portion of the beam. This is undesirable, however, since the inclusion of such a point-ahead angle will complicate the pointing and tracking problems and is also wasteful of the transmitted energy. A more attractive solution would be to reduce the diameter of transmitted beam and displace it laterally from the optical axis of the telescope so that it uses a small transmitter aperture located in the unobstructed portion of the telescope. Other techniques, such as dithering the beam at a high rate to effectively smear it over a large area, or including diffusers in the optical system at appropriate points, might also be considered.

In the case of the AVLOC test, there are two effects which could conceivably make the inclusion of a pointing offset or other technique unnecessary. The ranges to be employed in the experiment are such that the receiver is not located very deep in the Fresnel region. This is especially true of the downlink where the receiver will lie in the transition region between the near and far fields. At these distances there may be enough spreading of the beam by diffraction to provide usable levels of illumination near the axis. In addition atmospheric effects will tend to smear the beam and help to eliminate the central shadow.

The primary purpose of this report is the compute the antenna patterns for the transmitting optics to be used in the AVLOC communications system and to estimate the amount of illumination in the central

shadow of the cassegrainian obscuration. The theoretical relations and computer programs developed are quite general however, and can be directly applied to any obstructed optical system. Although other investigators have studied the far field patterns of obstructed optical systems [2], to our knowledge the near field region has never been analyzed.

We have computed the near field diffraction patterns for a cassegrainian telescope system transmitting a coherent gaussian beam. Numerical calculations have been made for a number of ranges and beam divergence angles typical of the conditions which will be encountered during the AVLOC test. Calculations have also been made for shorter ranges representative of the Marshall Space Flight Center Optical Range between Madkin and Bradford Mountains. These calculations were performed for the purpose of comparison with beam profile measurements made by MSFC personnel on the ground transmitter system. In addition we have investigated the near field pattern of an obstructed telescope in which the beam profile has been redistributed by means of an optical axicon. The effect of atmospheric turbulence in helping to fill the central shadow is also considered.

THEORETICAL BACKGROUND

We may consider the diffraction pattern of the cassegrainian telescope as that of a circular aperture containing a central opaque disk and illuminated with a divergent gaussian beam.* Let $U(x_o, y_o)$ be the complex representation of the field at an observation point (x_o, y_o, z) and $U(x_1, y_1)$ be the field at a point $(x_1\ y_1\ o)$ within the aperture, z being the distance between the receiver and transmitter. We also define

a = radius of the central obstruction

b = radius of the telescope objective

λ = wavelength

k = the propagation number

P = laser power

R = radius of curvature of laser beam

ω = beam width

θ = beam divergence (half angle)

In the near field, the field distribution of a coherently illuminated aperture is given by the Fresnel approximation [3]

---

*The uplink beam is in fact not gaussian due to the inclusion of an energy redistribution device in the optical system. The effects of the beam redistribution will be considered separately.

$$U_o(x_o,y_o) = \iint_{A'} U_1(x_1,y_1)\,\frac{e^{jkz}}{j\lambda z}\exp\left\{\frac{jk}{2z}\left[(x_1-x_o)^2 + (y_1-y_o)^2\right]\right\}\,dx_1dy_1 \tag{1}$$

where A' is the unobstructed portion of the aperture. We will assume that the laser is operated in the TEM_{oo} mode so that $U_1(x_1,y_1)$ is given by the gaussian beam approximation

$$U_1(x_1,y_1) = \sqrt{\frac{2P}{\pi\omega^2}}\exp\left[\frac{jkr_1^2}{2R} - \frac{r_1^2}{\omega^2}\right] \tag{2}$$

where $r_1^2 = x_1^2 + y_1^2$. The factor $(2P/\pi\omega^2)^{1/2}$ is included so that $|U|^2$ will be the illuminance in watts per square meter. Substituting equation 2 into equation 1 and converting to polar coordinates we obtain

$$U_o(r_o,\theta_o) = \frac{1}{\lambda z}\sqrt{\frac{2P}{\pi\omega^2}}\int_0^{2\pi}\int_a^b \exp\left[jk\,\frac{r_1^2}{2R}\right]\exp\left[-\frac{r_1^2}{\omega^2}\right]$$

$$\exp\left[\frac{jk}{2z}\left[r_1^2 + r_o^2 - 2r_1r_o\cos(\theta_1-\theta_o)\right]\right] r_1dr_1d\theta_1 \tag{3}$$

A phase factor $-je^{-jkz}$ has been dropped from equation 3 since it will not effect the intensity $I = |U_o|^2$. It should also be noted that contrary to common usage ω is the distance at which the field, rather than the intensity, falls to 1/e of its maximum value and that the signs in the exponents have been chosen to make R positive for divergent beams instead of for focused beams. We now apply a well known integral representation for the Bessel Function.

$$J_o(\xi) = \frac{1}{2\pi} \int_0^{2\pi} \exp\{-j\ \xi\ \cos(\theta-\phi)\}\, d\theta \qquad (4)$$

to obtain

$$U_o(r_o) = \frac{2\pi}{\lambda z} \sqrt{\frac{2P}{\pi\omega^2}} \int_a^b \exp\{\frac{-r_1^2}{\omega^2}\} \exp\{j\ \frac{k}{2}\ (\frac{1}{R} + \frac{1}{z})\ r_1^2\}\ J_o(\frac{kr_1r_o}{z})\ r_1 dr_1 \qquad (5)$$

Again a phase factor which will not influence the intensity has been omitted.

Equation 5 is the Fresnel Diffraction pattern for an obscured aperture illuminated by a gaussian beam and is valid for all ranges likely to be of interest in optical communications. The persistence of the central shadow for large values of z can be understood by inspection of equation 5. Consider for a moment the case of a collimated beam. The radius of curvature of the beam is infinite and equation 5 reduces to

$$U(r_o) = \frac{2\pi}{\lambda z} \sqrt{\frac{2P}{\pi\omega^2}} \int_a^b \exp\{\frac{-r_1^2}{\omega^2}\} \exp\{j\ \frac{k}{2z}\ r_1^2\}\ J_o\{\frac{kr_1r_o}{z}\}\ r_1 dr_1 \qquad (6)$$

for z small $U_o(r)$ must approach the geometrical optics limit of a gaussian beam with sharp central and peripheral shadows. However, for large z the term $\{\frac{jkr_1^2}{2z}\}$ vanishes and equation 6 further reduces to the well known Fraunhoffer approximation

$$U(r_o) = \frac{2\pi}{\lambda z} \sqrt{\frac{2P}{\pi\omega^2}} \int_a^b \exp\{\frac{-r_1^2}{\omega^2}\}\ J_o\{\frac{kr_1r_o}{z}\}\ r_1 dr_1 \qquad (7)$$

which has an intensity maximum at $r_o = 0$. Thus the condition for the elimination of the central shadow for a collimated beam is that

$$z >> \left|\frac{kr_1^2}{2}\right|_{max.} \tag{8}$$

i.e., the range must be great enough to place the observer well into the far field. Now for the case of an uncollimated beam this condition becomes

$$\frac{1}{R} + \frac{1}{Z} << \left|\frac{2}{kr_1^2}\right|_{min.} \tag{9}$$

If the beam is converging the Fraunhoffer condition is satisfied near the focus (R = -Z). However, if R is small and positive, as it is for a divergent beam, the inequality of equation 9 cannot be satisfied for any value of Z, no matter how large. Hence one is in effect always in the near field and the central shadow will be observed at all ranges. For R small compared to Z equation 9 may be written as

$$R >> \left|\frac{kr_1^2}{2}\right|_{max} \tag{10}$$

or

$$R >> \frac{kb^2}{2}$$

which corresponds to a beam divergence half angle of

$$\theta_m < \frac{2}{kb} \tag{11}$$

Here θ_m is the largest beam divergence for which the central shadow will disappear at long ranges.

The preceding result may be interpreted physically as follows. For a divergent beam the geometric shadow of the central obscuration is a cone with it's apex located at the center of curvature of the wave front and a half angle θ. Light from the unobscured part of the aperture will be spread by diffraction; the angular divergence due to diffraction being of the order of λ/b. If θ is less than λ/b then for large distances the light will eventually fill the central shadow, however, if θ is greater than λ/b the spreading due to diffraction is not great enough to compensate for the beam divergence and the shadow is never illuminated.

ON AXIS ILLUMINANCE

On the z axis equation 5 takes a particularly simple form since here $r_o = 0$ and $J\left(\frac{k\, r_1 r_o}{z}\right) = 1$. Then

$$U_o(0) = \frac{k}{z}\sqrt{\frac{2P}{\pi\omega^2}} \int_a^b e^{-\alpha r_1^2} r_1 dr_1 \tag{12}$$

where

$$\alpha = \frac{-1}{\omega^2} + j\frac{k}{2}\left(\frac{1}{R} + \frac{1}{z}\right) \tag{13}$$

It will be useful to investigate the on axis illuminance since it will provide a check on the accuaracy of the numerical integration needed to evaluate the off axis intensity. Equation 12 may be integrated directly to yield

$$U_o(0) = \frac{k}{z}\sqrt{\frac{2P}{\pi\omega^2}}\, \frac{1}{2\alpha}\left[e^{+\alpha b^2} - e^{-\alpha a^2}\right] \tag{14}$$

The intensity along the axis is then given by

$$I(0) = \left|U_o(0)\right|^2 \tag{15}$$

$$I(0) = \frac{k^2}{4z^2|\alpha|^2}\, \frac{2P}{\pi\omega^2}\, \left(e^{\alpha b^2} - e^{\alpha a^2}\right)\left(e^{\alpha^* b^2} - e^{\alpha^* a^2}\right) \tag{16}$$

which reduces to

$$I(0) = \frac{k^2 P}{2\pi z^2 |\alpha|^2 \omega^2} \left[e^{(\alpha + \alpha^*)b^2} + e^{(\alpha + \alpha^*)a^2} - e^{(\alpha a^2 + \alpha^* b^2)} - e^{(\alpha^* a^2 + \alpha b^2)} \right] \tag{17}$$

$$I(0) = \frac{k^2 P}{2\pi z^2 |\alpha|^2 \omega^2} \left[e^{2Re\alpha a^2} + e^{2Re\alpha b^2} - 2e^{Re\alpha(a^2 + b^2)} \cos(Im\alpha(a^2 - b^2)) \right] \tag{18}$$

$$I(0) = \frac{2P}{\pi\omega^2 \left[(1 + \frac{z}{R})^2 + \frac{4z^2}{k^2 \omega^4} \right]} \left[e^{-2\frac{b^2}{\omega^2}} + e^{-\frac{2a^2}{\omega^2}} - 2e^{-\frac{a^2+b^2}{\omega^2}} \cos\left[\frac{k}{2} \left(\frac{1}{R} + \frac{1}{z} \right)(a^2 - b^2) \right] \right] \tag{19}$$

The first exponential terms in equation 19 arise from the loss of the center portion of the beam from obscuration by the cassegrainian secondary and the loss of the tails of the beam at the objective. The harmonic term is due to the changing number of Fresnel zones contained within the aperture as one moves along the axis. This result is the alternating maxima and minima in the intensity along the axis characteristic of Fresnel diffraction.

For the ranges to be used in the AVLOC experiment $z/R >> 1$ and $(2z/k\omega^2) << 1$. Equation 19 then simplifies to

$$I(0) = \frac{2P}{\pi\omega^2 z^2/R^2}\left[e^{-2(b/\omega)^2} + e^{-2(a/\omega)^2} - 2e^{-(a^2+b^2)/\omega^2} \cos\left\{\frac{k}{2}\left(\frac{1}{R} + \frac{1}{z}\right)(a^2 - b^2)\right\}\right] \tag{20}$$

But since

$$\theta = \omega/R \tag{21}$$

and $\pi(z\theta)^2$ is just the geometrical area of the beam in the receiver plane we may let $I'(0)$ denote the intensity which one would compute neglecting the central obstruction, the gaussian beam shape and all diffraction effects. Then

$$I(0) = I'(0)\ 2\left(e^{-2(a/\omega)^2} + e^{-2(b/\omega)^2} - 2e^{-(a^2+b^2)/\omega^2} \cos\left(\frac{k}{2}\left(\frac{1}{R} + \frac{1}{z}\right)(a^2 - b^2)\right)\right) \tag{22}$$

Clearly I (0) will have maxima and minima when the cosine term is ± 1. Then

$$I_{max/min} = I' \cdot 2\left(e^{-(a/\omega)^2} \pm e^{-(b/\omega)^2}\right)^2 \tag{23}$$

If we choose $\omega = b$ and $a = b/3$ then $I_{max} = 3.18\ I'$ and $I_{min} = 0.55\ I'$, or a factor of about 6 to 1 difference in intensity. If one is going to work on axis it would be worthwhile to choose the aircraft

range so as to take advantage of the maxima. The ability to do this depends, of course, upon the spacing of the maxima being great enough to allow the aircraft to remain near the maxima rather than fluctuating between maxima and minima. We may estimate this spacing by noting that maxima will occur when

$$\frac{k}{2}\left(\frac{1}{z}+\frac{1}{R}\right)\left(b^2-a^2\right)=(2n+1)\,\pi \tag{24}$$

n being an integer. Solving for z we obtain

$$Z_m=\left[\frac{(2n+1)\,\lambda}{(b^2-a^2)}-\frac{1}{R}\right]^{-1} \tag{25}$$

or

$$\Delta Z_m=\frac{1}{\left[\frac{(2n+1)\lambda}{(b^2-a^2)}-\frac{1}{R}\right]}-\frac{1}{\left[\frac{(2n+3)\lambda}{(b^2-a^2)}-\frac{1}{R}\right]} \tag{26}$$

$$\Delta Z_m=Z_m-\frac{1}{\left[1/Z_m+\frac{2\lambda}{b^2-a^2}\right]} \tag{27}$$

$$\Delta Z_m=\frac{2\lambda\,Z_m^{\,2}}{(b^2-a^2)}\Big/\left(1+\frac{2\lambda\,Z_m}{(b^2-a^2)}\right) \tag{28}$$

but $2\lambda\,Z_m/(b^2-a^2) \ll 1$, therefore

$$\Delta Z_m=\frac{2\lambda\,Z_m^{\,2}}{b^2-a^2} \tag{29}$$

We choose a = 10 cm, b = 30 cm, λ = 6328 Å and Z = 20 km. ΔZ then is of the order of 6 km. so that the variation of I(0) with Z is clearly slow enough to allow the aircraft to remain near a maximum. Inspection of equation 25 shows that while the spacing between maxima is independent of R their position is not. Since R can be controlled by adjusting the beam divergence θ it should be possible to locate the receiver near an axis illuminance maxima for both the uplink and downlink beams.

The on axis illuminance which we have computed corresponds to the bright central spot usually observed in the Fresnel diffraction from an opaque disk [6]. The question remains whether or not this spot is broad enough to provide usable powers. In order to answer this question it is necessary to investigate the variation of illuminance with the distance off axis.

ILLUMINANCE OFF AXIS

The illuminance at a point off axis is given from equation 5

$$I(r_o,z) = \frac{2P}{\pi\omega^2}\left(\frac{k}{z}\right)^2 (S^2 + C^2) \tag{30}$$

where

$$S = \int_a^b e^{-(r/\omega)^2} J_o\left(\frac{kr_1 r_o}{z}\right) \cdot \sin(\beta r_1^2)\, r_1 dr_1 \tag{31}$$

and

$$C = \int_a^b e^{-(r/\omega)^2} J_o\left(\frac{kr_1 r_o}{z}\right) \cos(\beta r_1^2)\, r_1 dr_1 \tag{32}$$

$$\beta = \frac{k}{2}\left(\frac{1}{R} + \frac{1}{z}\right) \tag{33}$$

The evaluation of S and C is relatively difficult since the argument of the Bessel function is such that neither the asymptotic nor ascending power expansions coverage rapidly. Furthermore, the trigonometric functions oscillate so rapidly that numerical integrating requires a very large number of points to accurately sample the function. This in turn requires that the integrand be evaluated with high precision to avoid an unacceptable accumulation of round off errors. Several methods of evaluating C and S were considered, including an expansion by repeated integration by parts leading to a series of Bessel functions of increasing order and fixed argument. This series, which resembles

the classical Lommel function expansion, was so weakly convergent that it proved to be even less efficient than direct numerical integration.

The method finally chosen for the evaluation of S and C was a Simpson's Rule integration with two correction terms. The zero order Bessel function was computed using an ascending power series [4]

$$J_o(\xi) = \sum_{r=o}^{\infty} (-1)^r \frac{(\frac{1}{2}\xi)^{2r}}{(r!)^2} \tag{34}$$

for values of ξ less than 10 and Hankel's asymptotic expansion [5]

$$J_o(\xi) = \sqrt{\frac{2}{\pi\xi}} \{P(\xi) \cos \chi + Q(\xi) \sin \chi\} \tag{35}$$
$$\xi \to \infty$$

$$P = 1 - \frac{3^2}{2!(8\xi)^2} + \frac{3^2 \cdot 5^2}{4!(8\xi)^4} - \cdots \tag{36}$$

$$Q = \frac{-1}{8\xi} + \frac{1 \cdot 3^2 \cdot 5^2 \cdot 7^2}{3!(8\xi)^3} - \cdots \tag{37}$$

$$\chi = \xi - \pi/4 \tag{38}$$

for ξ greater than 10. Double precision arithmetic was used throughout.

We have investigated the errors in the numerical integration, both by consideration of the error in the calculation of the integrand, by examining the magnitude of the correction terms in the Simpson's Rule algorithm, and by varying the number of points used in the integration. It is concluded that the maximum error will not exceed 0.1%. Furthermore,

it was found that the value of I(0) calculated from equation 30 agrees very closely with that found from equation 22.

The computer programs used for these calculations are described in Appendix A.

EFFECTS OF ENERGY REDISTRIBUTION

In the previous sections the field distribution in both the ground-based and airborne transmitting apertures was assumed to be a truncated gaussian beam mode. The ground based telescope in fact will not have a gaussian intensity distribution in the exit pupil since it contains a device, called an axicon, which redistributes the beam in such a way that all the energy in the beam is incident upon the unobscured portion of the aperture. For the purpose of estimating the order of magnitude of the illuminance near the axis the truncated gaussian approximation was adequate. It is desirable, however, to be able to compare the theoretical diffraction patterns with beam profiles observed over relatively short horizontal paths. In this way estimates of atmospheric spreading of the beam may be obtained. For this purpose it will be necessary to consider the effect of the energy redistribution of the near field pattern.

Two possible physical realizations of the axicon are shown in figure 1. The axicon shown in Fig. 1a displaces the beam outward in a radial direction producing an energy distribution in the exit pupil usually referred to as a "displaced gaussian" distribution. The axicon illustrated in Fig. 1b not only displaces the energy outward from the optical axis but also inverts the intensity distribution in the sense that light from the center of the entrance pupil is routed to the outside of the exit pupil and visa-versa. This type of

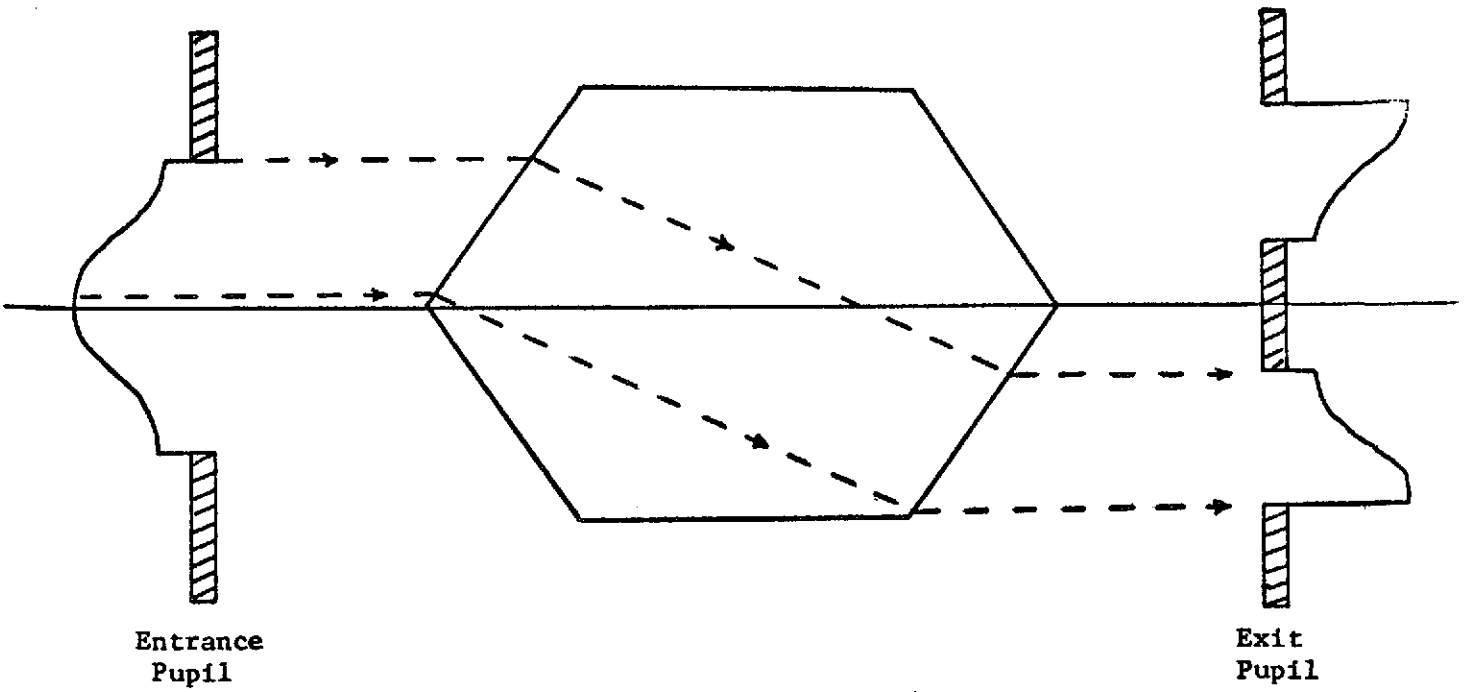

a. plandromic gaussian

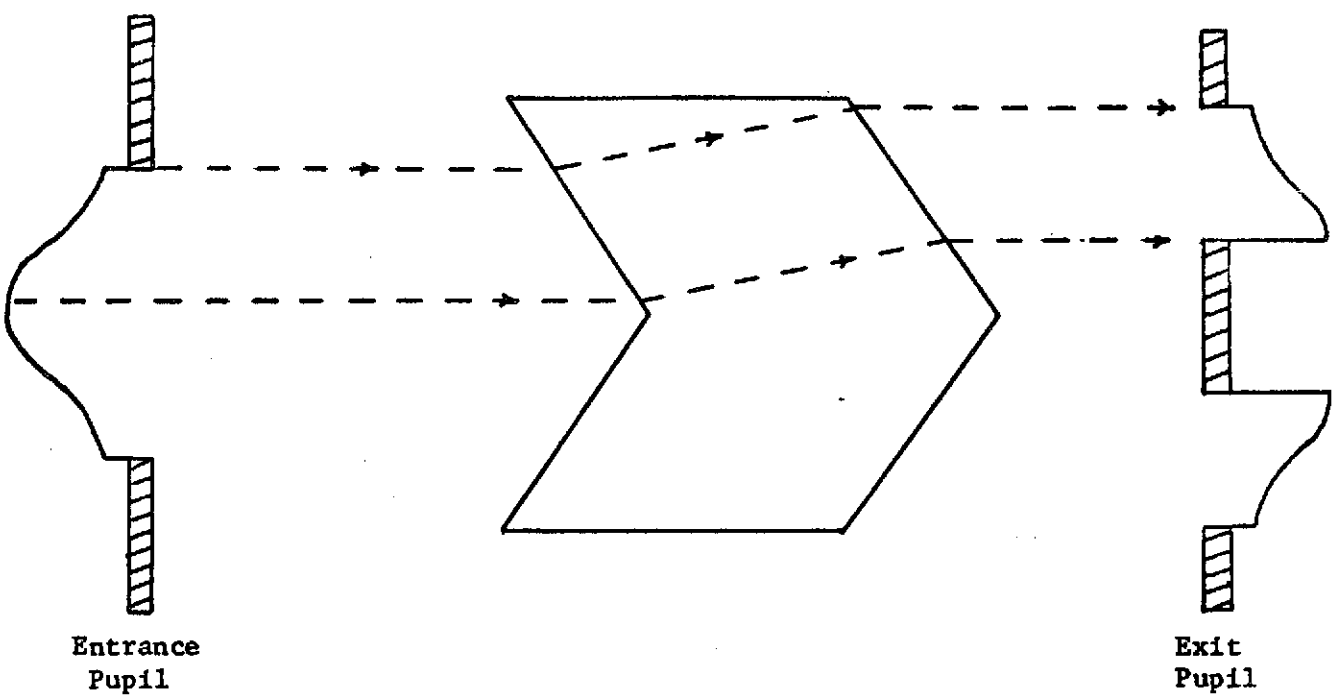

b. displaced gaussian

Figure 1. Two Axicon Devices.

axicon produces an intensity distribution which has been described as "plaindromic gaussian".

We assume that the energy redistribution device in the ground based telescope acts as a plaindromic axicon [7] i.e., it maps the energy contained in an annulus of radius r' in the entrance pupil of the optical system into an annulus of radius r in the exit pupil as shown in Fig. 2a. The radii of the two annuli are related by

$$r = b - \frac{b - a}{T} r' \tag{39}$$

and T is the truncation point of the original beam. This equation is equivalent to Peters and Ledger's equation (9) (reference 7) except that we have allowed an arbitrary truncation point for the original beam while Peters and Ledger have considered only beams which are truncated at a distance equal to the radius of the inner obscuration. Our results are therefore more general in that it will allow for an axicon with a lateral magnification different from unity.

The redistributed beam profile is obtained from the mapping equation (equation 39) and from the conservation of energy.

$$E_p(r) \cdot 2\pi r dr = E_g(r') \cdot 2\pi r' dr' \tag{40}$$

where E_p and E_r are the plaindromic distribution in the exit pupil and gaussian distribution in the entrance pupil respectively. Noting that $E = |U|^2$ we have

$$|U_p(r)| = \left(\frac{r'dr}{rdr}\right)^{1/2} |U_g(r')| \tag{41}$$

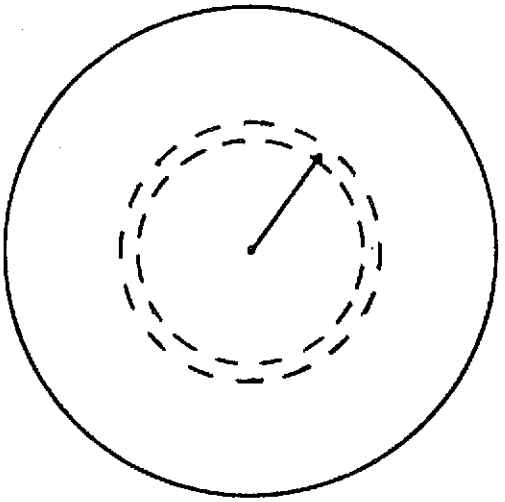

a. entrance pupil

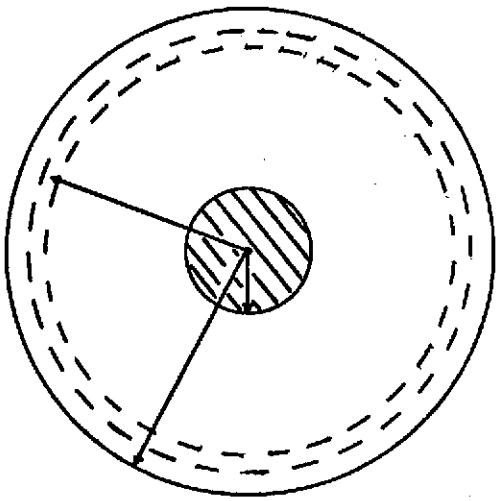

b. exit pupil
plandromic gaussian

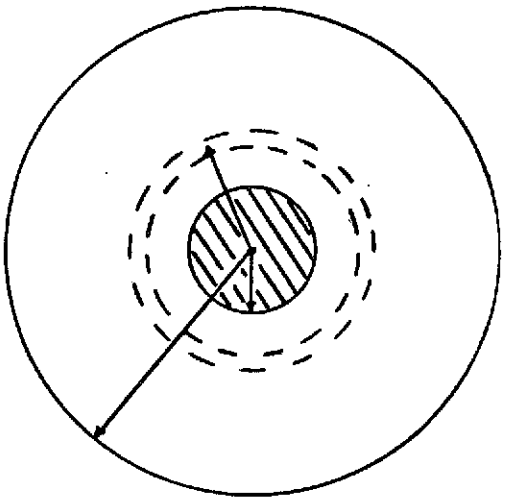

c. exit pupil
displaced gaussian

Figure 2. Energy Mappings for
Plandromic and Displaced
Gaussian Axicons.

$$|U_p(r)| = \left(\frac{T}{b-a}\right)\left(\frac{b-r}{r}\right)^{1/2} \exp\left\{-\left(\frac{T}{\omega(b-a)}\right)^2 (b-r)^2\right\} \qquad (42)$$

Assuming that the beam wave fronts are approximately spherical we may add a phase term and a normalization constant to obtain

$$U_p(r) = \left(\frac{2P}{\pi\omega^2}\right)^{1/2} \frac{T}{b-a}\left(\frac{b-r}{r}\right)^{1/2} \exp\left\{-\left(\frac{T}{\omega(b-a)}\right)^2 (b-r)^2\right\}$$

$$\exp\left\{j\,\frac{k}{2R}\,r^2\right\} \qquad (43)$$

Equation 43 is now substituted into equation 1 and following the same procedure as before we obtain the equivalent forms of equations 30-34, viz.

$$I(r_o,z) = \frac{2P}{\pi\omega^2}\left(\frac{T}{b-a}\right)^2\left(\frac{k}{z}\right)^2 (S_p^2 + C_p^2) \qquad (44)$$

where

$$S_p = \int_a^b \left(\frac{b-r_1}{r_1}\right)^{1/2} e^{-\alpha^2(b-r_1)^2} J_o\left(\frac{kr_1r_o}{z}\right) \sin(\beta r_1^2)\, r_1 dr_1 \qquad (45)$$

and

$$C_p = \int_a^b \left(\frac{b-r_1}{r_1}\right)^{1/2} e^{-\alpha^2(b-r_1)^2} J_o\left(\frac{kr_1r_o}{z}\right) \cos(\beta r_1^2)\, r_1 dr_1 \qquad (46)$$

α and β given by

$$\beta = \frac{k}{2}\left(\frac{1}{R} + \frac{1}{z}\right) \qquad \alpha = \frac{T}{\omega}/(b-a) \qquad (47)$$

Similar expressions can be obtained for a displaced gaussian. In this case equation 37 is replaced by the mapping

$$r = a + \frac{b - a}{T} r' \tag{48}$$

and the remainder of the derivation follows as before. The diffraction pattern from a displaced gaussian is then given by equation (44) with S_p and C_p replaced by S_D and C_D where

$$S_D = \int_a^b \left[\frac{a + r_1}{r_1}\right]^{1/2} e^{-\alpha^2(a + r_1)^2} J_o\left(\frac{kr_1r_o}{z}\right) \sin(\beta r_1^2)\, r_1 dr_1 \tag{49}$$

and

$$C_D = \int_a^b \left[\frac{a + r_1}{r_1}\right]^{1/2} e^{-\alpha^2(a + r_1)^2} J_o\left(\frac{kr_1r_o}{z}\right) \cos(\beta r_1^2)\, r_1 dr_1 \tag{50}$$

Numerical calculations have been made for a number of ranges and divergence using a plaindromic gaussian distribution and a displaced gaussian distribution. The numerical techniques employed were identical to those used for a gaussian distribution except for the choice of the input function. These results are presented in the following sections.

RESULTS

Numerical calculations have been made for the optical communications systems which will be used by the Marshall Space Flight Center's High Altitude Aircraft Optical Communications Experiment (AVLOC). For the ground to air system the transmitter is a 24 inch (61 cm) diameter cassegrainian telescope with an 8 inch (20 cm) diameter central obstruction. The aircraft to ground system employs a 4 inch (10 cm) telescope with a 1 inch (2.54 cm) obstruction. The transmitted powers and wavelengths are 1 watt at 5880 nm. uplink and 5 milliwatts at 632.8 nm. downlink. Ranges from 50,000 feet (15 Km) to 150,000 feet (45 Km) and beam divergence angles from 0 to 150 arc seconds were considered. The parameters for a typical set of calculations are shown in Table I.

Table I

System	Diameter (in) Aperture	Diameter (in) Secondary	Beam Power Watts	Range 1000 ft.	Beam Divergence* Arc Seconds
uplink	24	8	1	80	0
uplink	24	8	1	80	25
uplink	24	8	1	80	50
downlink	4	1	.005	80	25
downlink	4	1	.005	80	50
downlink	4	1	.005	80	75

*half angle

The assumed range (80,000 feet) corresponds to an aircraft approximately 10 miles from the ground station at an altitude of 60,000 feet. For the purpose of these calculations we have assumed a gaussian beam whose beam width equals the outer diameter of the aperture. While this is not the optimum matching to the aperture, it is an adequate approximation, as the final results are not very sensitive to changes in the truncation point except for small changes in the overall amplitude.

The results of these calculations are shown in Figs. 2-8 along with the geometrical optics approximation to the gaussian beam. The geometrical optics approximation was obtained by scaling the beam profile by the relation

$$r_o = \frac{Z + R}{R} r_1 \tag{51}$$

For the uplink beam the diffraction pattern shows the characteristic monotonic decrease of intensity within the geometrical shadows, indicating that one will be deep within the Fresnel region as expected. Examination of the uplink beam patterns indicate that the intensities within the shadow may be expected to be quite low. Furthermore it seems unlikely that smearing by the atmosphere will be sufficient to produce usable illumination in the shadow. In each of these patterns the central maximum (Fresnel-Arago bright Spot) is clearly visible. With the exception of the collimated beam it is far too narrow, however, to be of much use in a practical communications system.

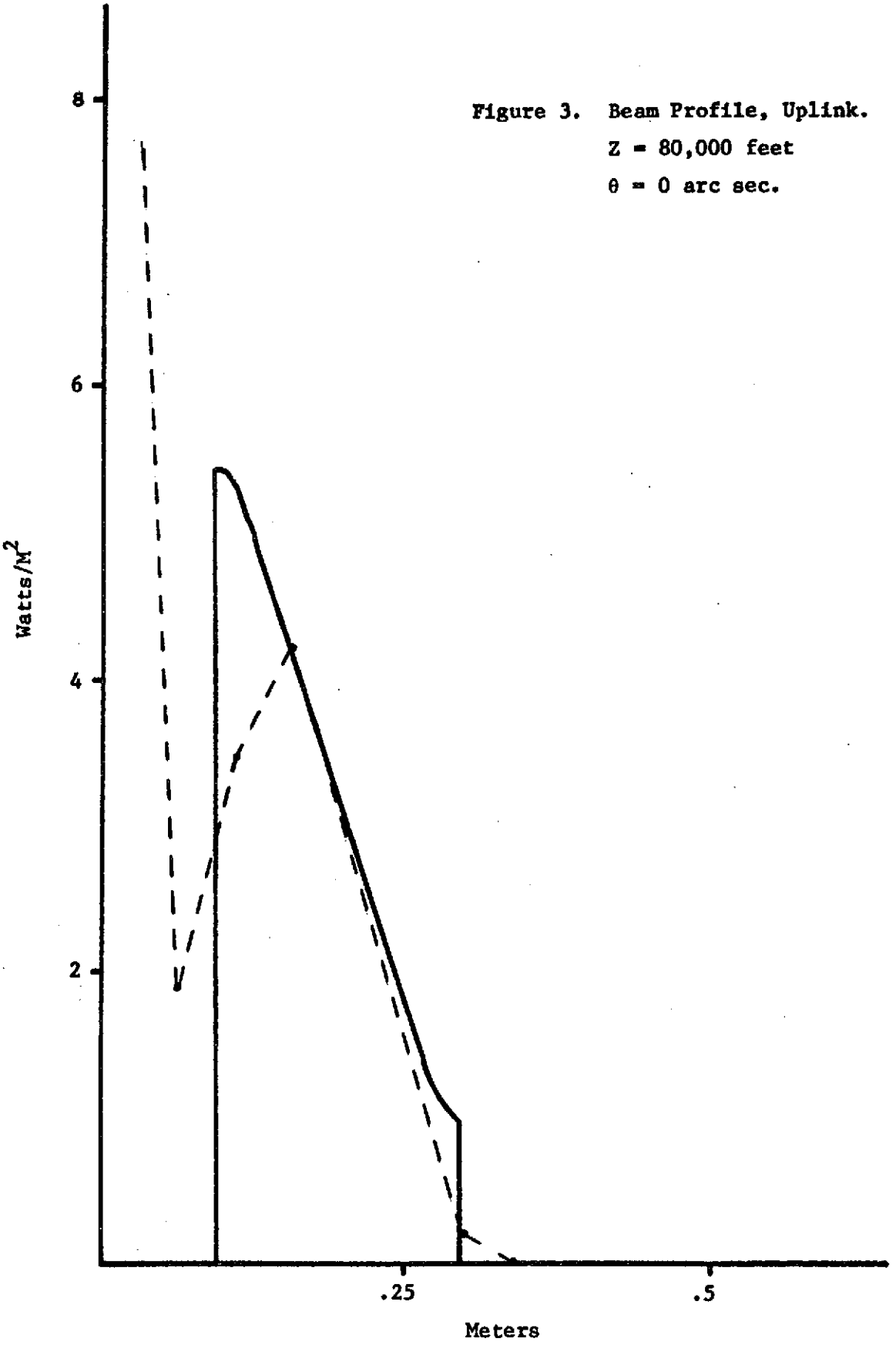

Figure 3. Beam Profile, Uplink.
Z = 80,000 feet
θ = 0 arc sec.

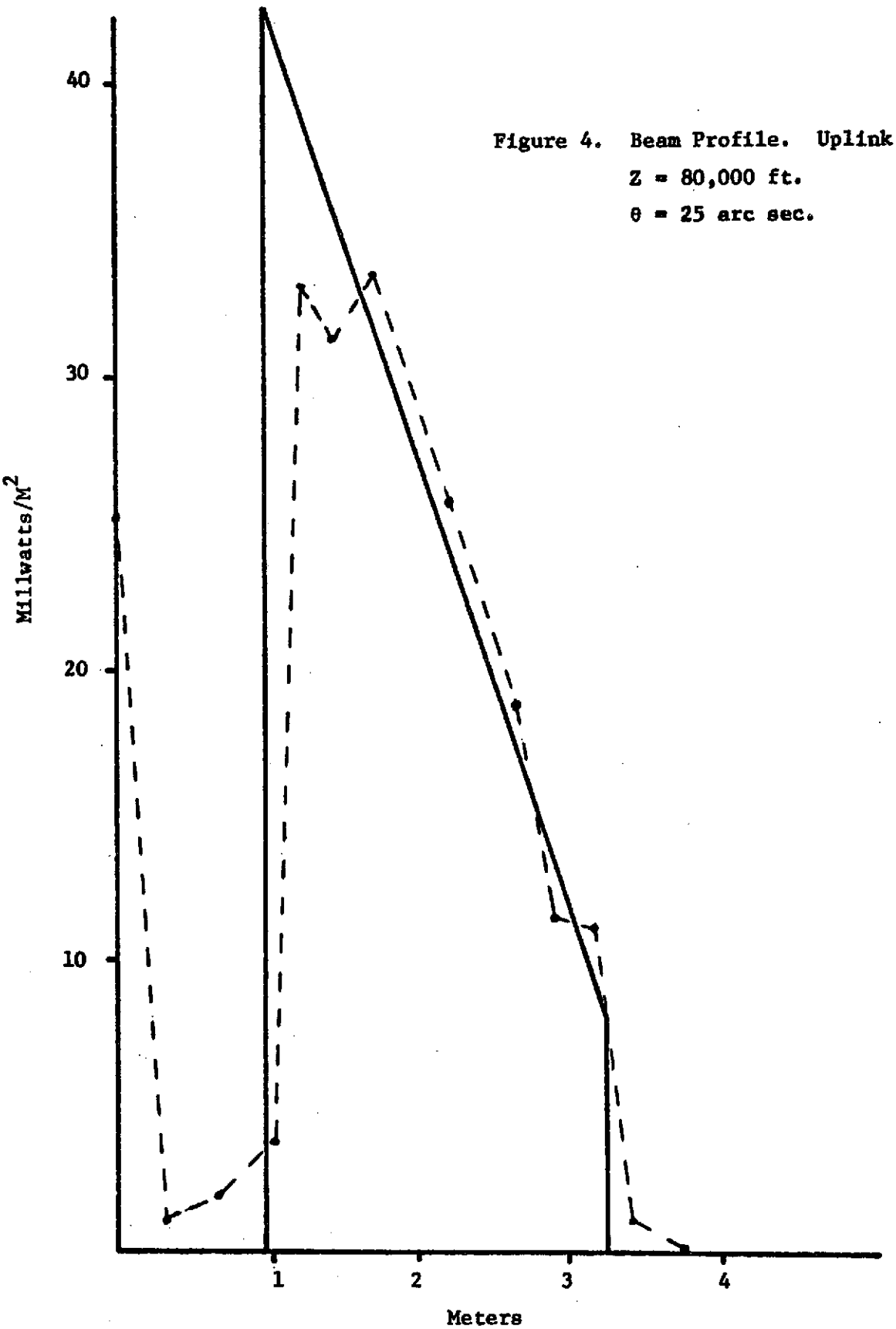

Figure 4. Beam Profile. Uplink
Z = 80,000 ft.
θ = 25 arc sec.

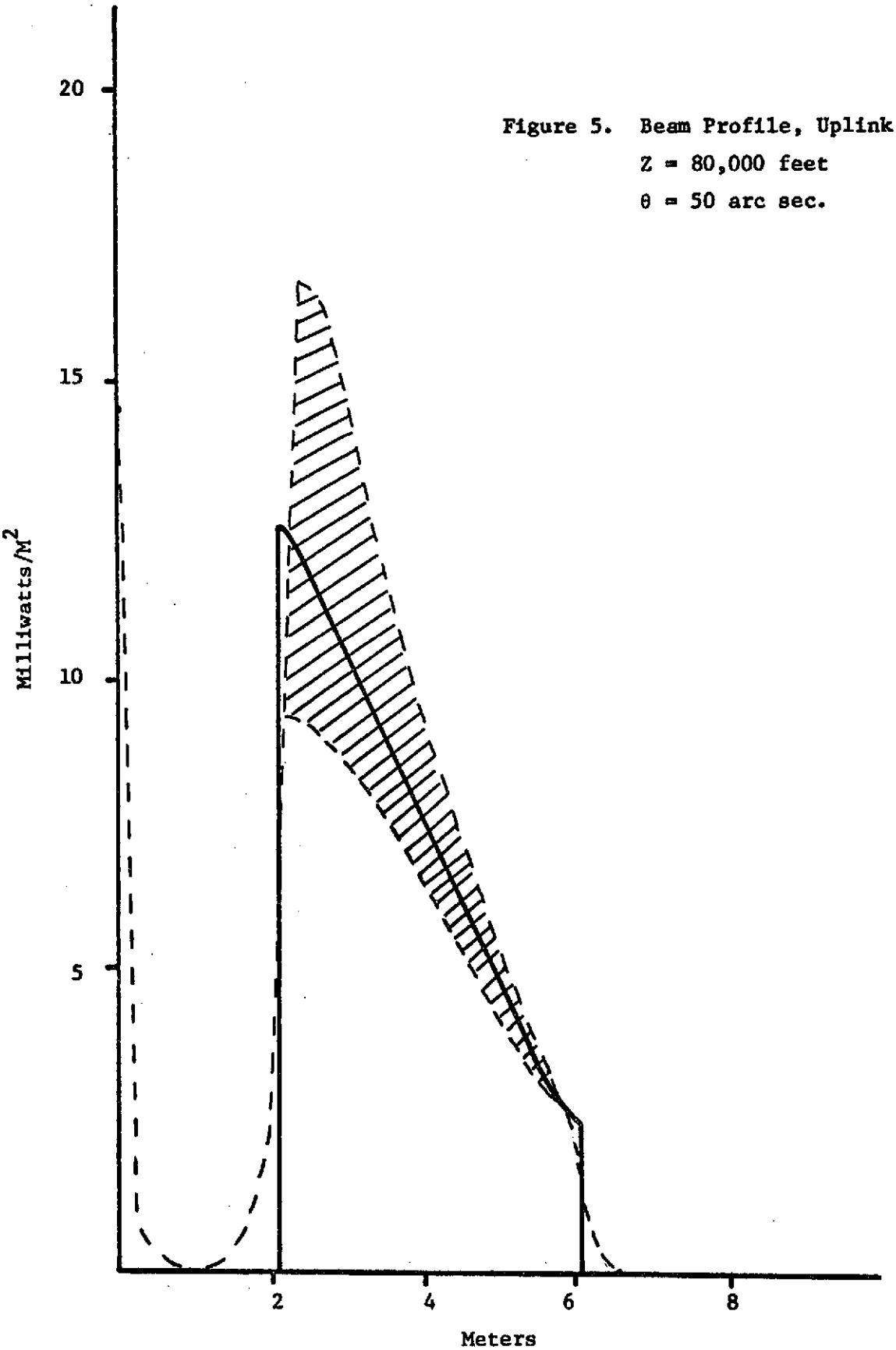

Figure 5. Beam Profile, Uplink.
Z = 80,000 feet
θ = 50 arc sec.

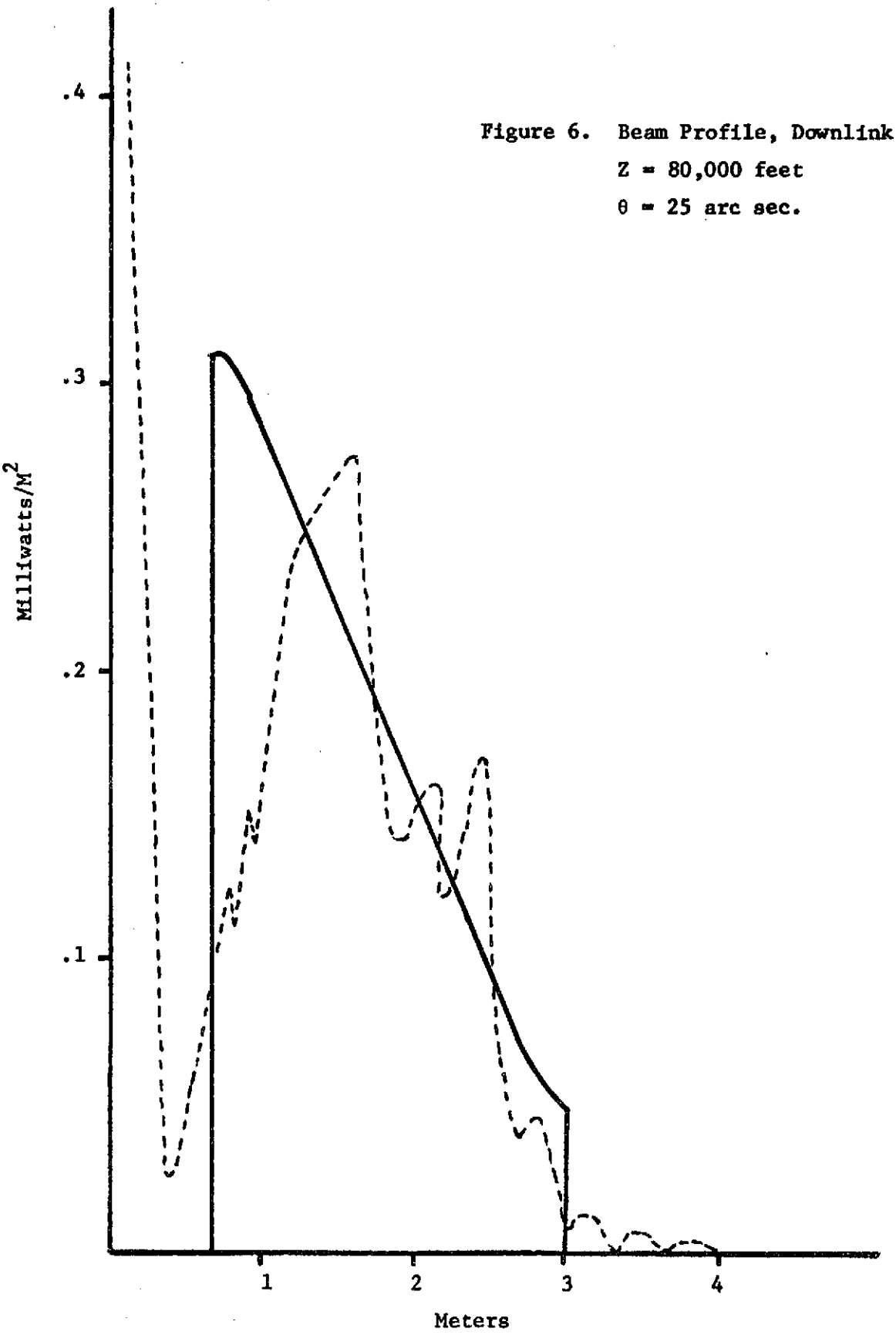

Figure 6. Beam Profile, Downlink.
Z = 80,000 feet
θ = 25 arc sec.

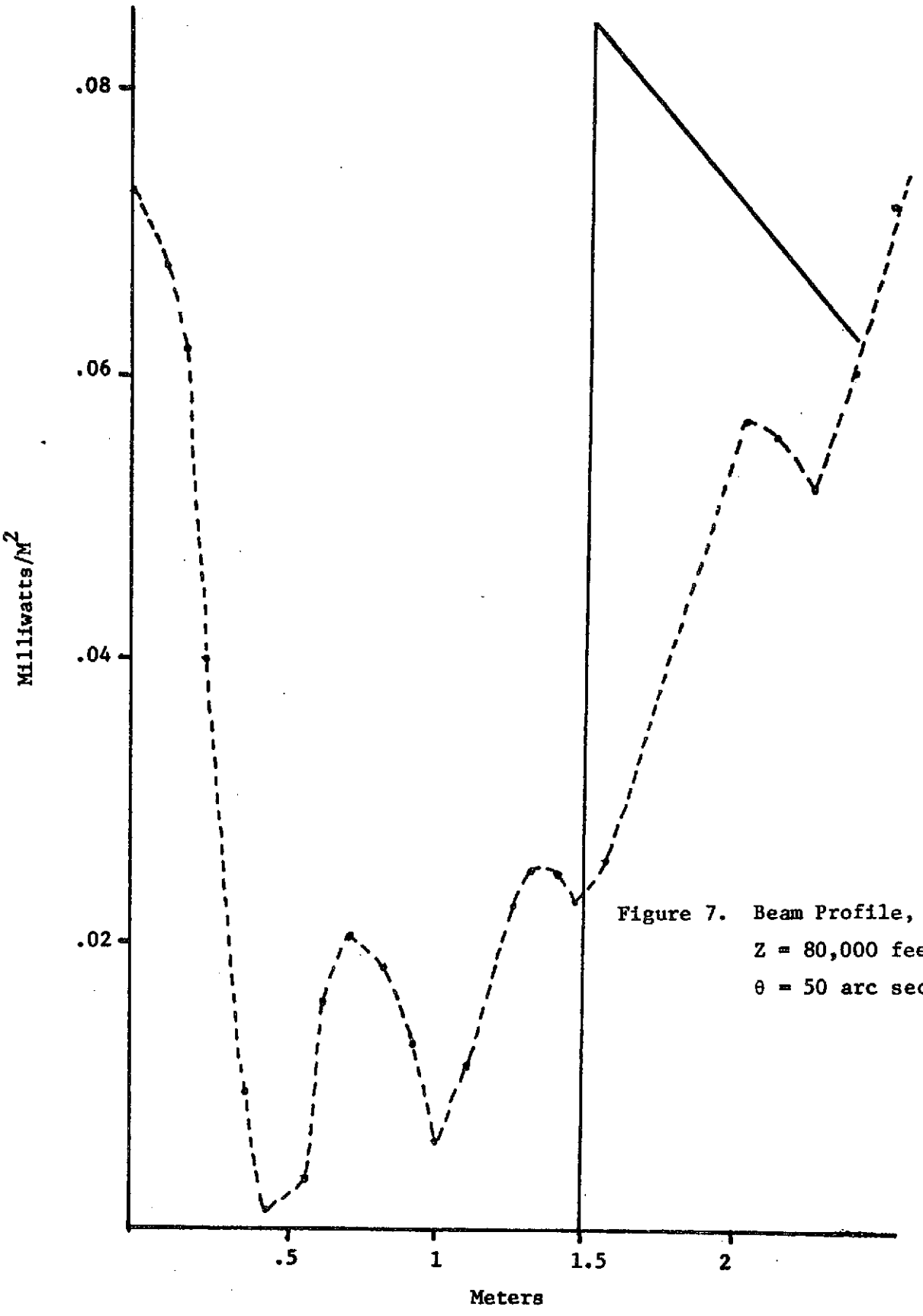

Figure 7. Beam Profile, Downlink.
Z = 80,000 feet
θ = 50 arc sec.

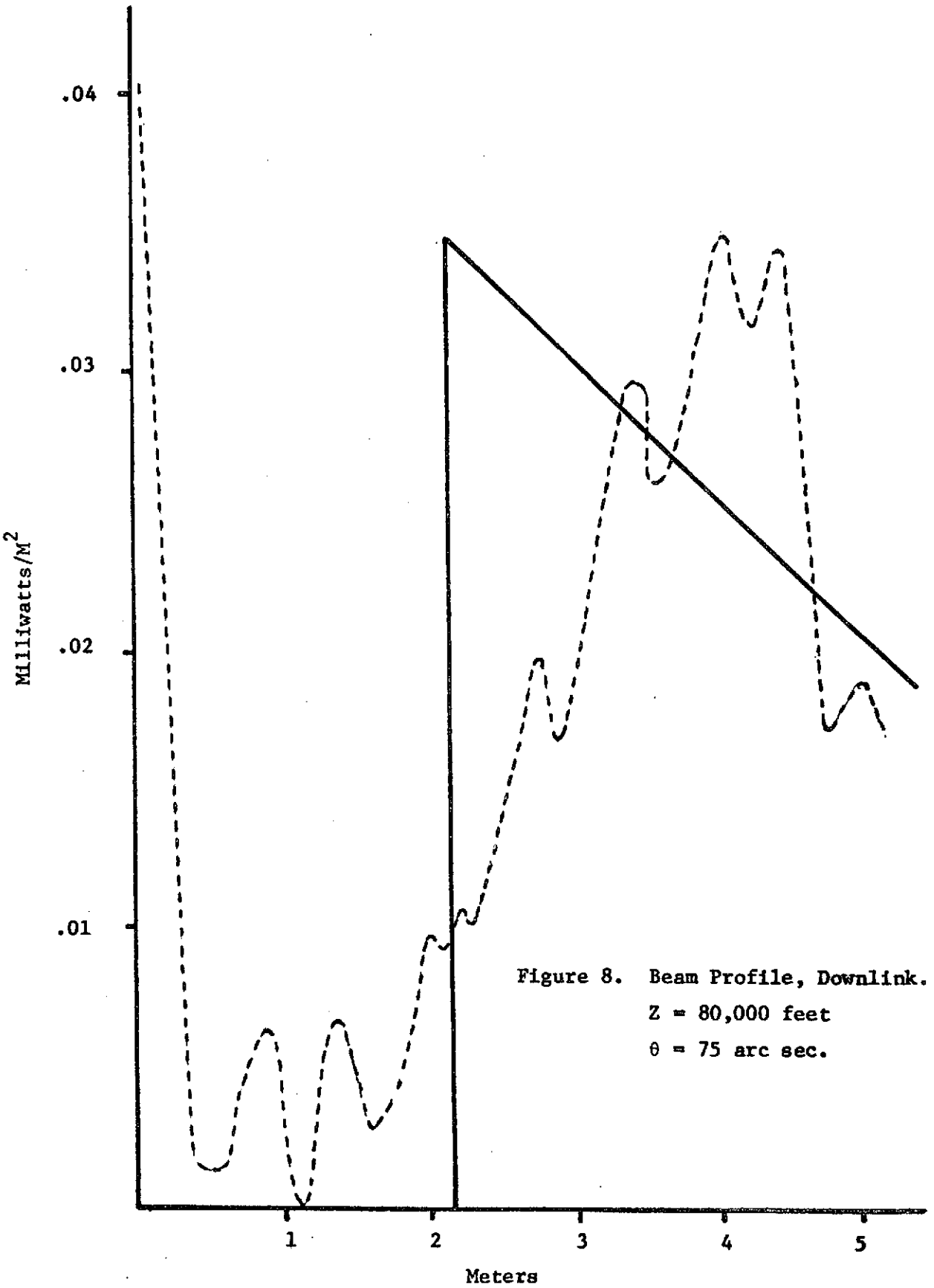

Figure 8. Beam Profile, Downlink.
Z = 80,000 feet
θ = 75 arc sec.

For larger beam divergence angles, the solution tended to oscillate very rapidly in the directly illuminated region. This behavior was also observed at shorter ranges for smaller values of beam divergence. An example of this can be seen in Fig. 3 where the oscillation was so rapid that it could not be plotted. We have therefore indicated the limits of oscillation by the shaded area. This oscillation was at first a cause of considerable concern as we feared that it might be a spurious result due to error buildup in the computer calculations. A number of tests were made, however, which convinced us that the oscillation does correspond to real fluctuations of the Fresnel pattern. These tests included the following:

1) Computing the intensity at very closely spaced points for one case. When this was done it was found that the fluctuations were smooth oscillations rather than random variations which might be expected from error buildups.

2) The number of points used in the Simpson's rule of integration was varied. It was found that the change in computed intensity due to changing the number of field points was much less than the magnitude of the oscillation.

3) A gaussian integration algorithm was used to compute a few field points. These agreed closely with the results of the Simpson's Rule integration.

4) In all cases the magnitude of the oscillation was greatest for shorter distances of axis. This is the region where the integration algorithm should be the most accurate.

5) No oscillation was observed in the shadow.

The rapid oscillation is of no importance as it will be obliviated by atmospheric effects.

For the downlink the situation is somewhat improved. As can be seen from Figures 5-8 the intensity in the shadow oscillates, indicating that at the assumed range one is approaching the Fraunhoffer region. The central maximum has broadened and the intensity levels near the axis have increased. Since the calculated pattern will be further spread by atmospheric effects and by effects such as tracking system jitter it is expected that usable levels of illuminance will be found near the center of the pattern without additional beam spreading or pointing offsets.

Results at ranges other than 80,000 feet were qualitatively similar. As would be expected the filling of the central decreased at shorter ranges and increased somewhat at longer ranges. There was very little significant difference in the shape of the diffraction pattern at any of the distances considered however. Calculations made with plaindromic and displaced gaussian distributions displaced a somewhat different shape radiation pattern in the directly illuminated region but no significant differences in the fields within the shadows.

We have also calculated the transmitter antenna patterns for the 24 inch cassegrainian telescope at a range of 26,400 feet (8.15 Km), corresponding to the length of the Marshall Space Flight Center Optical Range between Madkin and Bradford Mountains. These calculations were made so that MSFC personnel could compare the actual antenna patterns of the ground based transmitter with the predicted pattern. Two representative patterns are shown in Figures 9 and 10. The beam divergences

are 12.5 and 25 arc seconds respectively and a plaindromic gaussian beam was assumed in both cases.

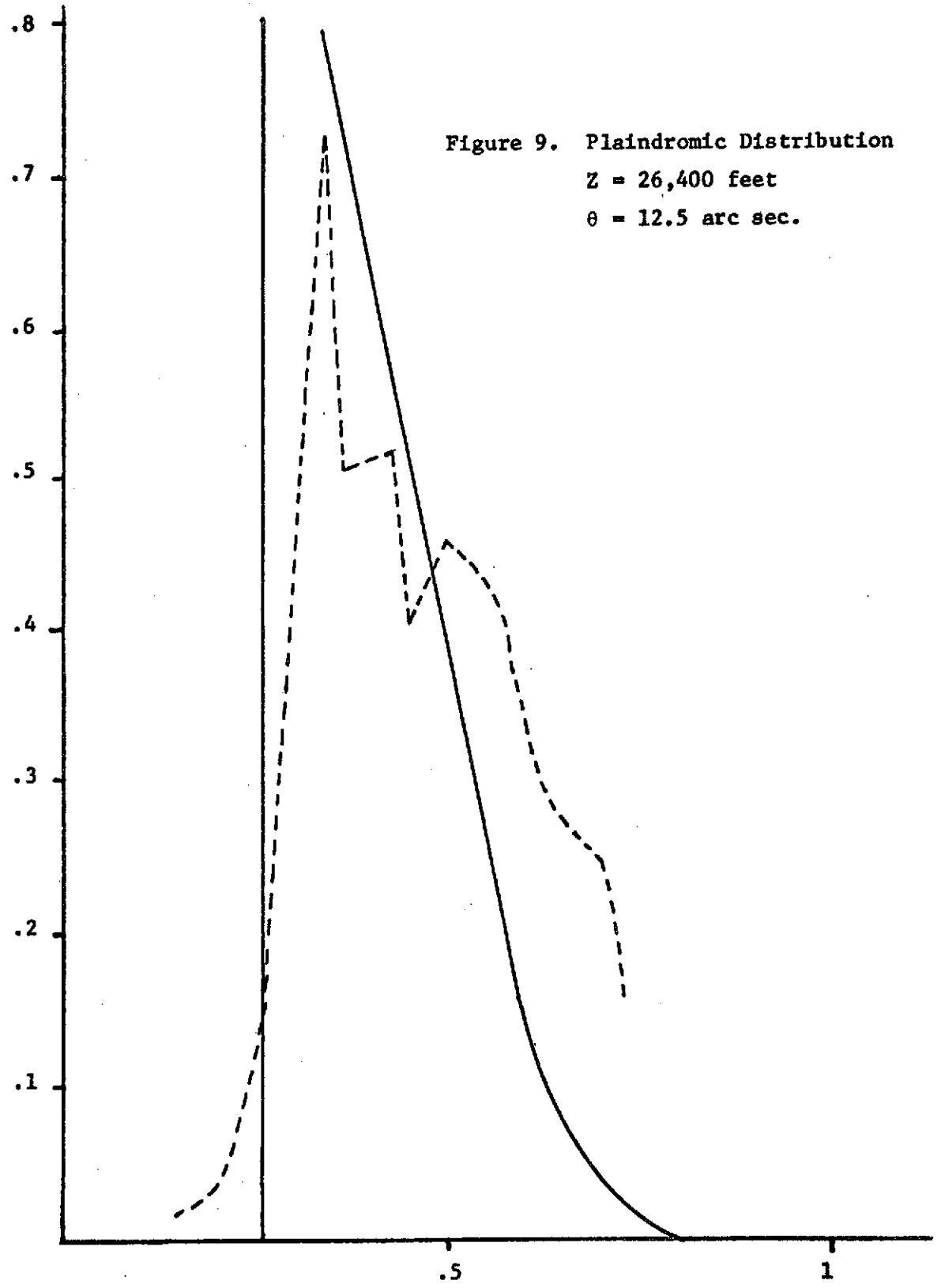

Figure 9. Plaindromic Distribution
Z = 26,400 feet
θ = 12.5 arc sec.

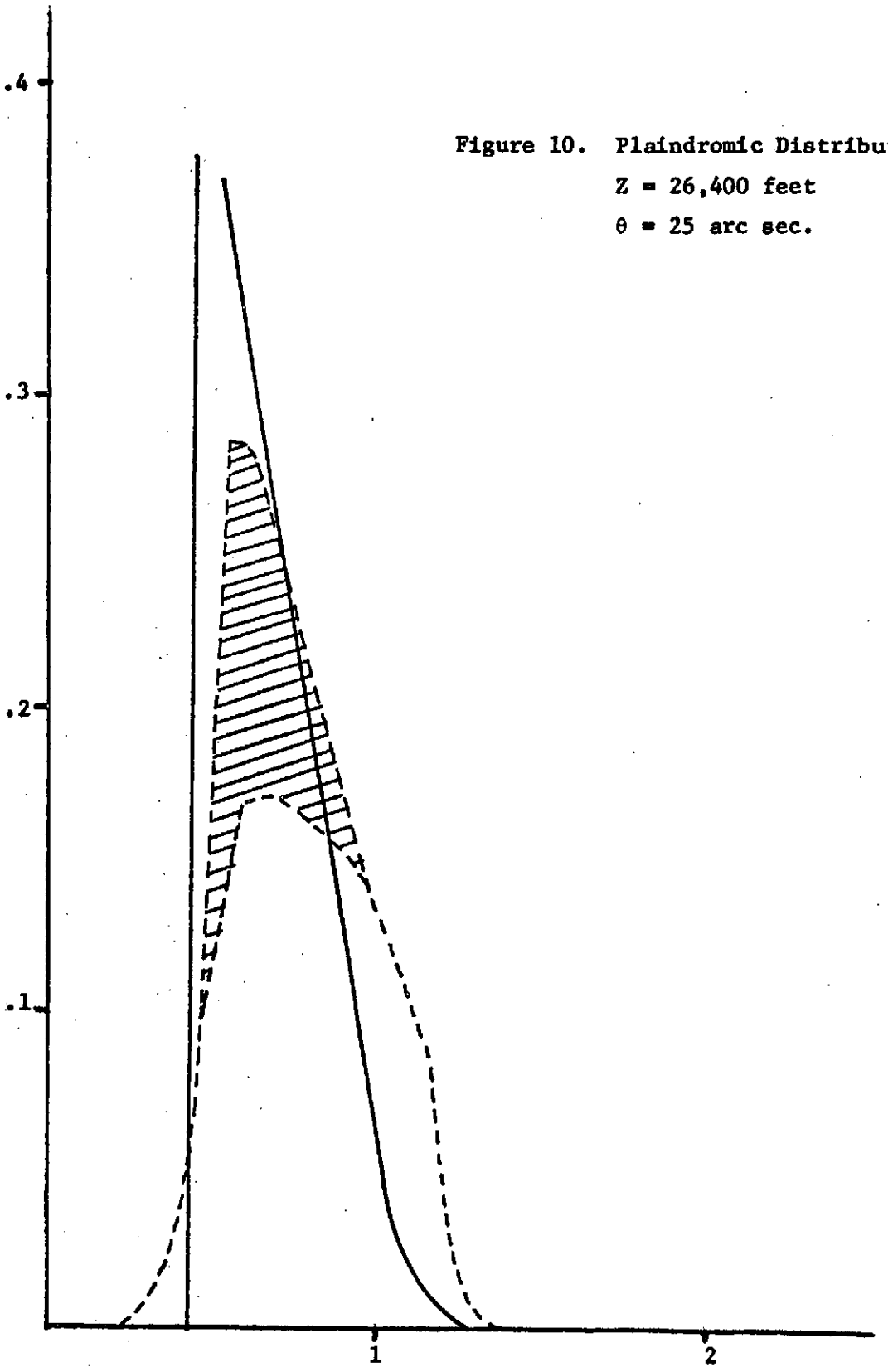

Figure 10. Plaindromic Distribution.
Z = 26,400 feet
θ = 25 arc sec.

ATMOSPHERIC EFFECTS

In a previous section it was suggested that smearing of the transmitted beam by atmospheric turbulence might be sufficient to eliminate the central shadow. In order to estimate the magnitude of the atmospheric effects we may adopt a ray optics approach and consider a differential element of area in the transmitting aperture. A ray leaving this area will satisfy the ray equation

$$d(n\bar{s})/d\ell = \text{grad } n \tag{52}$$

where n is the index of refraction of the atmosphere, $\bar{s}$ is a unit vector tangent to the ray, and $d\ell$ is a differential element of path length along the ray. Integrating equation 52 along the optical path we obtain

$$n'\bar{s}' - n\bar{s} = \int_0^z (\text{grad } n)\, d\ell \tag{53}$$

For large path lengths the deviation of the ray will not depend on the value of the index of refraction at the end points. We may therefore set n and n' equal to unity and obtain

$$s' - s = \int_0^z (\text{grad } n)\, d\ell \tag{54}$$

The angular deviation of the ray is just proportional to the vector difference $s - \bar{s}'$. Following Chernov [9] we may obtain from equation 53, after some algebraic manipulations, the mean square deviation of the ray $\overline{\Delta\theta^2}$.

$$\overline{\Delta\theta^2} = \int_o^z \int_o^z dr_1 dr_2 \; (\text{grad}_1 \; \text{grad}_2 \; B(x_1-x_2, y_1-y_2, z_1-z_2)) \qquad (55)$$

B is the index of refraction correlation function which, for the Kolmogorov atmospheric model, is given by

$$B(r) = \int_{K_o}^{K_m} \frac{\Gamma(8/3) \sin(\pi/3)}{\pi} \; C_N^2 \; \frac{\sin Kr}{r} \; K^{-8/3} \; dK \qquad (56)$$

where C_N^2 is the index of refraction structure constant and K_o, K_m are spatial frequencies corresponding to the outer and inner scales of turbulences (L_o, ℓ_o) respectively. Equation 56 may be substituted into equation 55 and the integrals performed to give [10]

$$\overline{\Delta\theta^2} = 5.7 \; C_N^2 \; Z(\ell_o^{-1/3} - L_o^{-1/3}) \qquad (57)$$

Here C_N^2 and ℓ_o have been assumed to be constants, as would be the case for a horizontal path. For vertical paths the appropriate variation of C_N^2 and ℓ_o with altitude would have to be included. We will use the horizontal path expression and assume the maximum value of C_N^2 and a minimum value of ℓ_o in order to establish an upper limit on the amount of scattering by atmospheric turbulence

which can be expected. Since L_o is much larger than l_o we may drop the last term of equation 57.

$$\overline{\Delta\theta^2} = 5.7\ C_N^2\ Z\ l_o^{-1/3} \tag{58}$$

The energy from a single differential element will be spread over an area whose size is of the order of σ, where σ is obtained directly by taking the product of the mean square scattering angle and the distance from the scattering center to the observation point and integrating over the entire optical path.

$$\sigma^2 = \int_o^z (z - \xi)^2 \left(\frac{d\ \overline{\Delta\theta^2}}{d\xi}\right) d\xi \tag{59}$$

This integration yields

$$\sigma^2 = 1.9\ C_N^2\ z^3\ l_o^{-1/3} \tag{60}$$

Equation 60 expresses the variance of a rays lateral displacement in the plane of the observation point. We now wish to determine the probability that a ray originating at a given point in the transmitter aperture will pass through the observation point. Since the phase fluctuations of a wave passing through the turbulent atmosphere are known to be normally distributed, it is therefore reasonable to assume that the angular deviations of the ray is also normally distributed. This conclusion could also be reached by considering that for propagation distances that are large compared to the inner scale of turbulence, the net angular deviation of a ray is the sum of a large number of

small deviations. Hence appeal to the central limit thereon leads to a normal distribution. The lateral displacement of the ray is just the sum of the individual angular deviations, weighted by the lever arm, i.e., weighted by the distance from the scattering point to the observation point. Therefore, the lateral displacement of the ray is a random variable which is the sum of a number of independent gaussian random variables and hence should be normally distributed. While the foregoing arguments may not be absolutely rigorous they do indicate the reasonableness of a normal distribution. Under any circumstances the error introduced by assuming a normal distribution should not be great.

If we assume a gaussian distribution for the lateral ray displacements the contribution to the intensity at the observation point from a point (x_1,y_1) in the transmitting aperture is just

$$dI_{scatt} = \frac{|U_i(x_1y_1)|^2}{(2\pi)\ \sigma^2}\ \exp\{-\frac{x^2}{2\sigma^2}\}\ dx_1dy_1 \qquad (61)$$

where x is the distance from the observation point to the point where the undeviated ray intersects the observation plane. If x_oy_o are the coordinates of the observation point then x^2 is given by

$$x^2 = (x_o - (1 + \tfrac{z}{R})x_1)^2 + (y_o - (1 + \tfrac{z}{R})y_1)^2 \qquad (62)$$

The total scattered intensity is then given by

$$I_{scat} = \iint \frac{|U_1(x_1y_1)|^2}{(2\pi)\ \sigma^2}\ \exp\{-\frac{1}{2\sigma^2}[(x_o - (1 + \tfrac{z}{R})x_1)^2+(y_o - (1 + \tfrac{z}{R})y_1)^2]\}dx_1dy_1 \qquad (63)$$

where the integration extends over the unobscured portion of the aperture.

To simplify our calculations let us assume an aperture illuminated by a beam of uniform intensity. We will also restrict ourselves to consideration of observation points on the optical axis of the transmitting telescope. With these restrictions equation 63 becomes on changing to polar coordinates

$$I_{scat} = \frac{1}{\sigma^2} \int_a^b \exp\left\{-\frac{1}{2\sigma^2}\left(1 + \frac{z}{R}\right)^2 r_1^2\right\} r_1 dr_1 \tag{64}$$

$$I_{scat} = (R/(z + R))^2 \left[\exp\left\{-\left(1 + \frac{z}{R}\right)^2 \frac{a^2}{2\sigma^2}\right\} - \exp\left\{-\left(1 + \frac{z}{R}\right)^2 \frac{b^2}{2\sigma^2}\right]\right. \tag{65}$$

Equation 65 may be evaluated numerically to give an estimate of the amount of filling of the central shadow. If we assume strong turbulence we may take C_N^2 to be on the order of 10^{-7} meters$^{-1/3}$ and the inner scale of turbulence to be about 1 mm. With these values σ is found to be 1.5 m^2. If we then assume a 25 arc second beam and a range of 20 Km, we find that the intensity on the optical axis is about 2% of the intensity in the transmitting aperture. Thus under the assumed conditions the beam smearing would be appreciable. For weak turbulence, however, C_N might be as small as 10^{-9} meters$^{-1/3}$, in which case the on axis intensity is only

$$\left(\frac{1}{25} e^{-830}\right)$$

times the intensity in the aperture. Clearly for weak turbulence the spreading of the beam is entirely negligible. It should be remembered that these calculations apply only to a horizontal range since the altitude profile of C_N^2 and ℓ_o have been neglected. For vertical paths the beam smearing will be much less since a C_N^2 decreases and ℓ_o increases with altitude.

CONCLUSIONS

The calculated beam profiles indicate that for the ranges and size optics to be used on the MSFC-AVLOC experiment the central shadow of the cassegrainian secondaries will be very dark and hence on axis operation will be impossible unless provisions are made to eliminate the shadow. Diffraction of light into the shadow was found to be negligble and the bright central spot, while present and strong, is far to small to be of any practical use.

Smearing of the beam by atmospheric turbulence has also been considered but it was found that except for very long, horozontal paths and strong turbulence conditions the effect would be small.

REFERENCES

1. "High Altitude Aircraft Experiment Test for Visible Laser Optical Communications" Astrionics Laboratory, Marshall Space Flight Center, Internal Document, August 1970

2. McIntyre, C. M., "Far Field Pattern of Defocused Telescope" Perkin Elmer Engineer Report No. 10798, Norwalk Conn., Sept. 1971

3. Goodman, J. W. "Introduction to Fourier Optics" McGraw Hill, San Francisco, (1968)

4. Watson, G. N. A Treatise on the Theory of Bessel Functions Cambridge University Press. (1966)

5. Abromawitz, M. and I. A. Segun Handbook of Mathmatical Functions Dover, New York.

6. Born, M. and E. Wolf "Principles of Optics" Page 375, Pergamon Press, London (1965)

7. Peters, W. N. and A. M. Ledger Applied Optics 9, Page 1435, (1970)

8. Dey, K. K. and P. Khastgir Comments on the Calculated Radiation Patterns of Truncated Gaussian Aperture Distribution, IEEE Trans, Antenna and Propagation, AP-19, 785 (1971)

9. Chernov, L. A. "Wave Propagation in a Random Medium", McGraw-Hill, New York, 1960.

10. Chiba, T., Spot Dancing of a Laser Beam Propagated Through the Turbulent Atmosphere, Appl. Optics. 10, 2456, 1971

APPENDIX A

COMPUTER PROGRAMS

1. Near Field Diffraction Pattern

This program computes the near field diffraction pattern of a circular aperture or obstructed circular aperture by direct numerical evaluation of the Fresnel diffraction integral. A double precision Simpson's Rule integration is used to evaluate the integral. The program as listed below will allow the aperture to be illuminated with a beam of arbitrary divergence angle and either uniform, gaussian or plaindromic gaussian intensity profile. A later modification will also accept a displaced gaussian beam.

Input to the program consists of three data cards. The first card specifies the type of field distribution which is to be used, i.e., gaussian, plaindromic, or uniform, beginning in column one. The first character is compared with the characters 'G', 'P' and 'U' stored in an array TCLASS and a branching flag is set and passed to the subroutine FRES*8 via the labled common block /TYPE/. If the first character is other than 'G', 'P' or 'U' an error message is generated and execution terminates. The second data card contains the diameter of the obscuration (which may be zero), the diameter of the aperture in inches, the beam power in watts and the wavelength in angstrom units. The card format is 4F10.4. The third data card contains the range, in feet, the beam width parameter in inches, the beam divergence angle

in arc seconds, the distance off axis of the first field point to be computed and the interval at which field points are to be spaced, both in feet, the number of field points to be calculated and the number of points to be used in the Simpson's Rule integration.

The input parameters are printed in the output listing and are then converted to metric units. The number of points specified for the Simpson's Rule algorithm is also checked and if it is even, it is increased by one.

The subroutine DSMPC is called twice to compute the real and imaginary parts of the Fresnel Diffraction integral for the first field point. The intensity is then computed by taking the absolute square of the field. The off axis distance of the field point is then incremented and the intensity at the next field point computed. This process is continued until the specified number of field points have been calculated.

After one profile has been calculated the program reads a new data card which may modify the range, beam width, beam divergence, field point and/or number of points in the integration. Execution continues until all data is exhausted.

```
// EXEC FORTGCLG,PARM.FORT='LIST,NAME=AVGO',
//  COND.GO=ONLY    SUPPRESS GO STEP
//FORT.SYSIN DD *
C     PROGRAM TO COMPUTE FRESNEL DIFFRACTION PATTERN OF A CIRCULAR
C     APERTURE  WITH A CENTRAL OBSCURATION
C     USING A DOUBLE PRECISION SIMPSON RULE WITH CORRECTOR TERMS
C
C
C     A        = DIAMETER OF OBSCURATION  INCHES
C     B        = DIAMETER OF APERTURE     INCHES
C     LAMBDA   = WAVELENGTH               ANGSTROM UNITS
C     W        = WIDTH OF GAUSSIAN BEAM   INCHES
C     POWER    = LASER POWER              WATTS
C     Z        = RANGE                    FEET
C     RHO      = DISTANCE OFF AXIS        FEET
C     THETA    = BEAM DIVERGENCE          ARC SECONDS
C     NPTS     = NUMBER OF POINTS IN INTEGRATION
C
C     T        = TRUNCATION POINT FOR PLAINDROMIC FIELD
C
      EXTERNAL FRES
      COMMON W,K,RHO,PI,TWOPI,R,Z,NTYP
      COMMON/TYPE/PASSA,PASSB,T,WI,IDIST
      DIMENSION LINE (80)
      INTEGER TCLASS(3)/'U','G','P'/,TNUM/3/
      REAL*8 A,B,POWER,LAMBDA,PI,TWOPI,K,Z,W,THETA,R,RHO,RHO1,DRHO,RMAX,
     *SSM,SCM,E1,E2,INT
     *,PASSA,PASSB,T,WI
      PI = 3.141592653589793DO
      TWOPI=2.0D0 * PI
C     READ FIELD DISTRIBUTION TYPE AND SET BRANCHING FLAG
      READ(5,908) LINE
      IDIST=0
      DO 3 KK=1,TNUM
      IF(LINE(1).EQ.TCLASS(KK))  IDIST=KK
    3 CONTINUE
      IF(IDIST.EQ.0)  GO TO 10
      IF(IDIST.NE.3)  GO TO 11
      READ(5,911) T,WI
      WI=1.2700025D-02 * WI
      T=1.2700025D-02 * T
   11 CONTINUE
C     READ PARAMETERS AND CONVERT UNITS
      READ(5,901)  A,B,POWER,LAMBDA
      WRITE(6,902)  A,B,POWER,LAMBDA
      A=1.2700025D-02 * A
      B=1.2700025D-02 * B
      PASSA=B-A
```

```
      PASSB=B
      K=2.0D10 * PI / LAMBDA
    1 READ(5,903,END=800) Z,W,THETA,RHO1,DRHO,NRHO,NPTS
      WRITE(6,904) Z,W,THETA
      WRITE(6,909) LINE
      W=1.2700025D-02 * W
      Z=0.3048006096D0 * Z
      THETA = 4.84814D-06 * THETA
      R = W/THETA
      RHO1 = 0.3048006096D0 * RHO1
      DRHO = 0.3048006096D0 * DRHO
C
C     PARAMETERS HAVE BEEN CONVERTED TO METRIC UNITS
C     NOW CHECK NUMBER OF POINTS *** IT MUST BE ODD
C
      N=MOD(NPTS,2)
      IF(N.EQ.0) NPTS=NPTS+1
      WRITE(6,906) NPTS
      DO 2 J=1,NRHO
      RHO = RHO1 + (J-1)*DRHO
      NTYP=1
      CALL DSMPC(SSM,FRES,E1,NPTS,A,B)
      NTYP=2
      CALL DSMPC(SCM,FRES,E2,NPTS,A,B,)
C     COMPUTE INTENSITY
      INT=((K/Z)**2)*((2.0D0*POWER)/(PI*(W**2))*(SCM**2+SSM**2)
C     PRINT RESULTS
    2 WRITE(6,907) RHO,INT,E1,E2
      GO TO 1
   10 WRITE(6,910)
  800 STOP
  901 FORMAT(4F10.4)
  902 FORMAT('1',25X,'PARAMETER LIST'//10X,'A=',F10.5,'INCHES',5X,'B=',
     *F10.2,' INCHES'/10X,'POWER=',F6.2,' WATTS'/10X,'WAVELENGTH=',F8.2,
     *' ANGSTROMS '      )
  903 FORMAT(5D14.6,2I5)
  904 FORMAT(10X,'RANGE=',F12.2,' FEET'/10X,'BEAM WIDTH=',F10.2,' INCHES
     *'/10X,'BEAM DIVERGENCE=',F10.2,' ARC SECONDS')
  906 FORMAT(10X,'USING A ',I5,' POINT SIMPSONS RULE ')
  907 FORMAT('0',15X,'DISTANCE OFF AXIS =',F10.4,/5X,'INTENSITY =',
     *D24.16/25X,'ERROR TERMS',5X,2D26.16)
  908 FORMAT(80A1)
  909 FORMAT(10X,'TYPE DISTRIBUTION = ',80A1)
  910 FORMAT('  ILLEGAL FIELD DISTRIBUTION SPECIFIED    EXECUTION TERMIN
     *ATED')
  911 FORMAT(2F10.4)
      END
```

The subroutine DSCMP is a double precision Simpson's Rule Algorithm with two correction terms. The correction terms are printed to provide an estimate of the accuracy of the integration routine.

```
      SUBROUTINE DSMPC(SUM,FUN,E,N,FLL,FUL)
      DOUBLE PRECISION SUM,S1,S2,S3,S4,FN,FLL,FUL,DX X,FJ,Y,E,FUN
      S1 = 00.0D0
      S2 = 00.0D0
      S3 = 00.0D0
      S4 = 00.0D0
      FN = N-1
      DX = (FUL-FLL)/FN
      DO 10 I=1,N
      J=I-1
      FJ=J
      X=DX*FJ  +FLL
      Y=FUN(X)
      IF(I.EQ.1.OR.I.EQ.N) GO TO 1
      IF(I.EQ.2.OR.I.EQ.(N-1)) GO TO 2
      K=MOD(I,2)
      IF(K) 3,4,3
    1 S1=S1+Y
      GO TO 10
    2 S2=S2+Y
      GO TO 10
    3 S3=S3+Y
      GO TO 10
    4 S4=S4+Y
   10 CONTINUE
      SUM=(S1+4.0D0*(S2+S4) + 2.0D0*S3) * (DX/3.0D0)
      E=(-4.0D0*S1 + 7.0D0*S2 + 8.0D0*(S4-S3) + FUN(FLL-DX   ) + FUN(
     1 FUL+DX)) * (DX/(-9.0D1))
      SUM=SUM+E
      RETURN
      END
//LKED.SYSLMOD DD DSNAME=UA0L02.EEG00118.PWRFLW(AVLOC2),DISP=SHR,
// UNIT=DISK,VOL=SER=UA0L02,SPACE=
//GO.SYSIN DD *  PROGRAM CHECKOUT DATA

GAUSSIAN
    8.0000   24.0000    1.0000 4880.0000
 80.000000D 03 24.000000D 00  1.500000D 02  1.000000  00  1.000000D 00    1    31
```

The subroutine FRES*8 is called by DSMPC to compute the integrand. Two Bessel function approximations are used; a Jacobi asymptotic expansion and an ascending power series. The program selects the appropriate routine each time depending on the value of the argument.

```
      REAL FUNCTION FRES*8(R)
      REAL*8 W,K,R,RHO,Z,ARG,A,A2,A3,A4,A5,P,Q,PI,TWOPI,RND,ARGJ,JZRO,
     *TRIG,RAD
     *,A6,A7,FAC,XI
     *,U,ARGE,ARGRT,PASSA,PASSB,T
     *,WI
      COMMON W,K,RHO,PI,TWOPI,RAD,Z,NTYP
      COMMON/TYPE/PASSA,PASSB,T,WI,ITYP
C     COMPUTE ZERO ORDER BESSEL FUNCTION FOR LARGE ARGUMENT USING
C         JACOBI ASYMPTOTIC EXPANSION
C
      ARGJ=K*R*RHO/Z
      IF(ARGJ.LT.1.0D01) GO TO 1
      A=8.0D0*ARGJ
      A2=A*A
      A3=A*A2
      A4=A*A3
      A5=A*A4
      A6=A*A5
      A7=A*A6
      P=1.0D0 - 4.5D0/A2 + 4.59375D2/A4 - 1.50077812 D05/A6
      Q=1.0D0/A - 3.75D1/A3 + 7.441875D3/A5 - 3.62 3071875D06/A7
      RND=ARGJ/TWOPI
      NR=RND
      RND=NR
      RND=ARGJ-RND*TWOPI
      RND = RND-PI/4.0D0
      JZRO=DSORT(2.0D0/(PI*ARGJ))*(P*DCOS(RND) + Q*D IN(RND))
    3 CONTINUE
      ARG=0.5D0*K*(1.0D0/RAD + 1.0D0/Z)*(R**2)
      IF(NTYP.EQ.1) TRIG=DSIN(ARG)
      IF(NTYP.EQ.2) TRIG=DCOS(ARG)
      GO TO (11,12,13),ITYP
   11 FRES=TRIG*JZRO*R/1.414213562373095D0
      RETURN
   12 CONTINUE
      FRES = DEXP(-1.0D0*((R/W)**2)) * TRIG * JZRO 8
      RETURN
   13 ARGE=-1.0D0*(((PASSB-R)/PASSA)*(T/WI))
      ARGRT=(PASSB-R)/R
      IF(ARGRT.LE.0.0D0) GO TO 14
      FRES=DEXP(ARGE)*JZRO*R*DSQRT(ARGRT)*TRIG*W*T/( I*PASSA)
      RETURN
```

```
14 FRES=0.0D0
   RETURN
 1 A= -1.0D0 * (ARGJ/2.0D0)**2
   AL=1.0D0
   FAC=1.0D0
   JZRO=1.0D0
   DO 2 I=1,20
   XI=I
   FAC=FAC*XI
   A1=A1*A
   A3=A1/(FAC**2)
   A4=DABS(A3)
   IF(A4.LT.1.0D0-16) GO TO 3
   JZRO=JZRO + A3
 2 CONTINUE
   GO TO 3
   END
```

2. Program for Calculation, Field Intensity on Axis

This program evaluates the Fresnel diffraction integral for field points on the optical axis. In addition, it computes the field distribution from the geometrical optics approximation.

```
   PI=3.14159
 4 READ (5,1) A,B,W,P,WAVE,THETA,Z
   WRITE(6,2) A,B,W,P,WAVE,THETA,Z
   A=0.0127*A
   B=0.0127*B
   W=0.0127*W
   WNUM=2.0E10*PI/WAVE
   Z=0.3048*Z
   R=W/(4.848E-06*THETA)
   C=2.0*P/(PI*(W**2))
   D=(1.0+Z/R)**2 + ((2.0*Z)/(WNUM*(W**2)))**2
   C=C/D
   X=(A/W)**2
   Y=(B/W)**2
   ARG=(WNUM/2.0)*(A*A-B*B)*(1.0/Z+1.0/R)
   PD=C*(EXP(-2.0*X) + EXP(-2.0*Y) - 2.0*EXP(-1.0 (X+Y))*COS(ARG))
   WRITE(6, 3) PD
   WRITE(6,13)
   RAT=(R+Z)/R
   XW=W*RAT
   CO=(2.0*P)/PI*(XW**2))
```

```
      XLO=A*RAT
      XHI=B*RAT
      WRITE(6,11) XLO,XHI
      DX=(XHI-XLO)/10.0
      DO 10 I=1,11
      X=(I-1)*DX + XLO
      PD=CO*EXP(-2.0*(X/XW)**2)
   10 WRITE (6,12) X,PD
   11 FORMAT(10X,'LIMITS OF GEOMETRICAL SHADOW ',25 4.6)
   12 FORMAT(20X,'X= 'E14.6,' INTENSITY= ',E14.6)
   13 FORMAT('0 GEOMETRICAL OPTICS APPROCIMATION')
      GO TO 4
    1 FORMAT(6F10.4,F10.0)
    2 FORMAT('0',10X,6F10.4/11X,F10.0)
    3 FORMAT(10X,'INTENSITY = ',E12.4,' WATTS PER METER SQ ')
      END
```

APPENDIX 3

STUDY OF ATMOSPHERIC EFFECTS ON LASER COMMUNICATIONS SYSTEMS

ABSTRACT

The atmospheric scintillation has been observed at 10.6μm over a 3.2 Km path using a heterodyne optical communications system. The observed probability density functions agreed reasonably well with a log-normal model for small receiving apertures but showed noticable departures from log-normalicy for apertures above 4 cm. The power spectral density of the scintillation has also been computed.

CONTENTS

FIGURES AND TABLES

Figures

Tables

CHAPTER I

INTRODUCTION

The atmosphere is an inhomogeneous non-isotropic media which is usually in a state of turbulence. The atmosphere is characterized by its temperature, wind velocity, and humidity. The variations of these parameters comprise non-stationary random processes and as a result the fluctuation of the index of refraction of the media is also a non-stationary random process. Electromagnetic radiation at optical wave lengths propagating through the atmosphere will be greatly affected by the random fluctuation in the index of refraction. This causes a very complicated scattering to occur which results in amplitude and phase variations of the wave. Clearly, these fluctuations are also of a random nature.

The distortion induced by the atmosphere on the propagating wave is of great concern in the development of optical tracking and communication systems since performance can be seriously degraded due to this effect. For example, amplitude fluctuations cause the signal-to-noise ratio to be reduced in incoherent detection systems. Atmosphere distortion tends to reduce the coherence of the wave which in turn reduces the effective power level of the signal. This will also decrease the signal-to-noise ratio. Loss of coherence is a problem in systems utilizing coherent detection where heterodyne action must be achieved. Wave front tilt due to phase variations of the wave induces errors in optical tracking receivers since they view this tilt as an apparent angle of arrival.

An important aspect in the design of optical systems that is de-

pendent on a knowledge of atmospheric distortion is the size of the optical components. Atmospheric effects can be somewhat overcome by employing large receiving optics which will tend to average out the wave fluctuations. This advantage is limited by the high expense and difficulty in fabrication of such components. The designer must then choose optimum size components which require that he have a thorough knowledge of the atmospheric problem. It is clear that there is a pressing need for an accurate mathematical model of the atmosphere.

Statistical methods must be employed to analyze this problem since the wave fluctuations are random processes. The first step in developing a statistical model is to determine the probability density function of the random process. Theoretical considerations have predicted a log-normal distribution for the amplitude and normal for the phase. This theory has been experimentally verified for visible wave lengths, but results of current investigations in the infrared region of 10.6 microns have been inconsistent.

D. L. Fried[1] has made scintillation measurements at this wave length over a 1 km. range using a point detector. His results do not confirm the hypothesis that intensity scintillation is log-normally distributed. He suggests that this may be a genuine feature of 10.6 micron scintillation but draws no definite conclusion since detector noise and nonlinearity problems in taking measurements could have influenced his results.

Richard Kerr[2] of the Oregon Graduate Research Center has conducted multiwave length laser propagation studies over a mile path and claims confirmation of log-normal statistics for wave lengths of 4880Å and 10.6 microns. In addition Fitzmaurice, Bufton, and Minott[3] have also concluded that scintillation at 10.6 micron fits the log-normal model. Their

work was done over a 2.4 km. path. Both investigators used point source detection.

The effect of the atmosphere on 10.6 micron propagation is important since the popular CO_2 laser emits radiation at this wave length. This type laser is attractive for application in optical systems due to its high efficiency and high output power capability. In addition, the atmospheric effect at this wave length is much less than that at visible wave lengths.

The purpose of this study is experimentally to investigate the statisitical properties of scintillation and the signal-to-noise ratio of heterodyne detection for a CO_2 laser beam propagated over a 3.2 km. path. Both scintillation and heterodyne measurements have been made for a variety of receiving aperture sizes ranging from two to ten cm.

A brief discussion of the theory which is referred to in current literature is presented in Chapter II. The necessary statistical concepts are introduced before a qualitative description of atmospheric turbulence is given. Finally, the physical significance of aperture averaging is discussed.

Chapter III gives a detailed description of the experiment. Described is the equipment, its alignment and check out as well as a discussion on the techniques used to make the measurements.

The handling and reducing of the data is given in Chapter IV. This includes a discussion on the conversion of analog data to digital form for direct use on a digital computer. An outline of the computer program which reduces the data is presented. The theory used to calculate aperture effects is also given.

Chapter V is concerned with interpreting the reduced data to de-

termine if the hypothesis of the log-normal distribution for intensity scintillation is valid for this wave length. This chapter also includes results of calculations for the refractive index structure constant with and without aperture averaging corrections.

Chapter VI contains the summary and conclusions of this study as well as recommendations for further study. A complete documentation for the computer program is given in the Appendix.

CHAPTER II

THEORY

A. Statistical Concepts

It is necessary to give a discussion on pertinent statistical concepts as a prelude to presenting a qualitative discussion on the theoretical aspects of the atmospheric problem.

The random processes are described in terms of parameters which are random variables. The value of any such function at a fixed instant of time is a random variable having definite probability density function. The process may further be described by its auto-covariance function at times t_1 and t_2

$$AC\{f(t_1),\ f(t_2)\} = \left\langle [f(t_1) - \langle f(t_1) \rangle][f(t_2) - \langle f(t_2) \rangle] \right\rangle \qquad 2\text{-}1$$

where $\langle\ \rangle$ indicates an ensemble average. The auto-covariance function reduces to the correlation function

$$B[f(t_1),\ f(t_2)] = \langle f(t_1) f(t_2) \rangle \qquad 2\text{-}2$$

for processes where the mean value is zero. The auto-covariance function characterizes the mutual relation between the fluctuations at different instants of time. The mean value of the random variable can be a constant or can change with time. Similarly, the auto-covariance function can either depend only on the difference between the times t_1 and t_2 or else it can depend on the positions of the points on the time axis. The first case would occur when the statistical relation between the

fluctuations of the variable at different instants of time does not change with time. A random function is called stationary if its mean value does not depend on time and its auto-covariance function depends only on the difference between observation times.

The mean value of the meteorological parameters of the atmosphere such as temperature, wind velocity, and humidity undergo comparatively slow and smooth changes. These variables are non-stationary processes if the definition of stationarity is strictly applied. It is difficult to determine which changes in the fluctuation are to be regarded as slow changes in the mean and which are to be regarded as slow fluctuations of the function.

To avoid this difficulty and to describe random functions which have the above characteristics, the structure function is used instead of the correlation function. This function was first introduced by Kolmogorov[4,5]. The basic idea behind this method is to use the difference function

$$F_\tau(t) = f(t+\tau) - f(t) \qquad 2\text{-}3$$

instead of the non-stationary function f(t). For values of τ which are not too large, slow changes in the function f(t) do not affect the value of the difference function which means that it can be considered a stationary random function. The function f(t) is called a random function with stationary increments. To derive an expression for the structure function consider the transformation of the correlation function for $F_\tau(t_1)$ and $F_\tau(t_2)$:

$$B(t_1, t_2) = \left\langle [F_\tau(t_1)F_\tau(t_2)] \right\rangle \qquad 2\text{-}4$$

$$B(t_1, t_2) = \left\langle [f(t_1+\tau) - f(t_1)][f(t_2+\tau) - f(t_2)] \right\rangle \qquad 2\text{-}5$$

Using the algebraic identity

$$(a-b)(c-d) = \frac{1}{2}\left[(a-d)^2 + (b-c)^2 - (a-c)^2 - (b-d)^2\right] \qquad 2\text{-}6$$

we have

$$B(t_1, t_2) = \frac{1}{2}\left\langle [f(t_1+\tau) - f(t_2)]^2 \right\rangle + \frac{1}{2}\left\langle [f(t_1) - f(t_2+\tau)]^2 \right\rangle$$
$$- \frac{1}{2}\left\langle [f(t_1+\tau) - f(t_2+\tau)]^2 \right\rangle - \frac{1}{2}\left\langle [f(t_1) - f(t_2)]^2 \right\rangle \qquad 2\text{-}7$$

Thus the correlation function is expressed as a linear combination of functions of the form

$$D_f(t_i, t_j) = \left\langle [f(t_i) - f(t_j)]^2 \right\rangle \qquad 2\text{-}8$$

which is called the structure function of the random process. The form of the structure function more commonly used

$$D_f(\tau) = \left\langle [f(t+\tau) - f(t)]^2 \right\rangle \qquad 2\text{-}9$$

is the basic characteristic of a random process with stationary increments. The value of $D(\tau)$ characterizes the intensity of those fluctuations of $f(t)$ which are smaller than or are comparable with τ.

B. Nature of Atmospheric Turbulence

The statistical theory of turbulence was initiated in the works of Friedmann and Keller[6]. This theory was greatly amended in 1941 when A. N. Kolmogorov and A. M. Obukhov[6] established the laws which characterize the basic properties of the microstructure of turbulent

flow at very large Reynolds numbers. The following discussion is drawn from Tatarski's[6] work on the Kolmogorov theory.

Consider the atmosphere to be a viscous fluid in a state of laminar flow. This flow can be characterized by its viscosity ν, velocity v, and the characteristic length L. The quantity L characterizes the dimensions of the flow as a whole and arises from the boundary conditions of the fluid dynamics problem. This laminar flow will be stable if the Reynolds number

$$R = \frac{VL}{\nu} \qquad 2\text{-}10$$

does not exceed a certain critical value.

Suppose that for some reason a velocity fluctuation occurs in a region of size ℓ of the initial laminar flow. The value of Reynolds number will increase and the laminar motion will lose stability. The result of this instability is the formation of a secondary flow or eddies within L which will have their own Reynolds number R_ℓ. As the Reynolds number for the overall flow is increased, R_ℓ will increase causing the secondary flow to break up into smaller scale eddies. These new eddies now give energy to even smaller eddies and the process continues until an eddy with a Reynolds number less than the critical value is formed. The atmospheric turbulence can be considered as consisting of many circulating eddies having different flow characteristics. Eddies are usually described in terms of an inner and outer scale of turbulence. These are measures of the characteristic sizes of the smallest and largest eddies which exist at the time of interest. Figure 1 may aid in visualizing this process. The outer scale is the physical dimension of the largest eddy. The inner scale of turbulence is roughly the size of the smallest

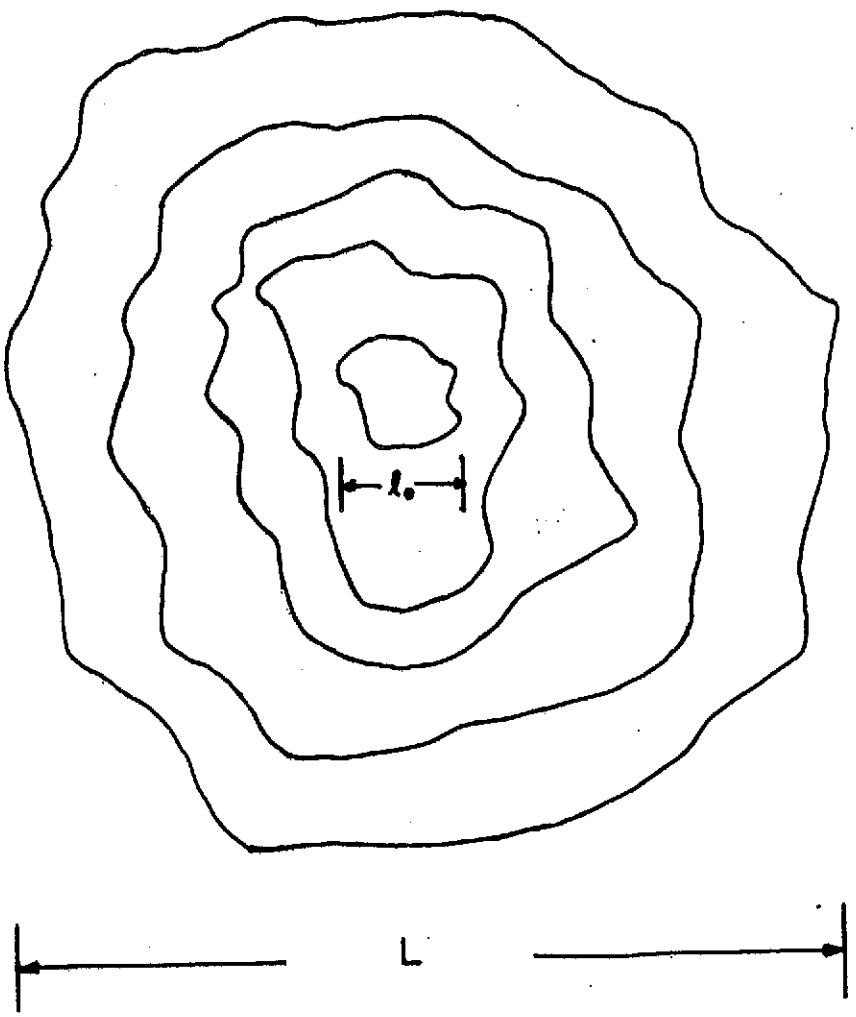

Figure 1. Visualization of Microstructure of Turbulence.

stable eddy. It can be more precisely defined in terms of a characteristic of the longitudinal velocity structure function

$$D_{rr} = \left\langle [V(\bar{r}_1) - V(\bar{r}_2)]^2 \right\rangle \qquad 2\text{-}11$$

where $V(\bar{r}_1)$ is the projection of the velocity at the point $\bar{r}_1$ along the direction of $\bar{r}$, and $V(\bar{r}_2)$ is the same quantity at the point

$$\bar{r}_2 = \bar{r}_1 + \bar{r}$$

For $r \ll \ell_o$ $\qquad D_{rr} = ar^2 \qquad 2\text{-}12$

and for $r \gg \ell_o$ $\qquad D_{rr} = c^2 r^{2/3} \qquad 2\text{-}13$

For r on the order of L the structure function saturates. The inner scale of turbulence ℓ_o is then defined mathematically as the value for D_{rr} where the functions in equations 2-12 and 2-13 intersect.

Each eddy or cell in the field of turbulence can be considered locally isotropic and homogeneous, and as a result it will have a certain index of refraction, which we will assume to be constant throughout the cell. The index of refraction will in general differ from cell to cell. As an electromagnetic wave passes through each cell two things occur: First, the phase of the wave is advanced or retarded in a random manner due to the index of refraction of the cell. Secondly, the wave is scattered due to the interfaces between the cells. This causes the intensity of the beam to be distributed at random after traveling through a large number of cells.

From the model of the atmosphere just developed some insight as to the statistical characteristics of phase and amplitude variation can be

gained. Since the random variations in phase add to each other, the Central Limit Theorem[7] can be applied to predict that the distribution of the phase across the wave front is normal. The amplitude of the wave has a distinctly different character. After each refraction the intensity is the product of the intensity before scattering and the variation due to refraction. The intensity variations are then due to a product of probabilities. If the Central Limit Theorem is applied to the logarithm of the intensities, they will be normally distributed. This leads to a log-normal probability density function for the amplitude distribution. Because of this, it is customary to describe waves propagating through the atmosphere in terms of their phase $\phi(r,t)$ and log-amplitude $L_a(r,t)$, where $L_a(r,t)$ is given by

$$L_a(r,t) = \ln \left\{\frac{A(r,t)}{\bar{A}(r,t)}\right\} \qquad 2\text{-}14$$

or in terms on intensities

$$L_a(r,t) = \frac{1}{2} \ln \left\{\frac{I(r,t)}{\bar{I}(r,t)}\right\} \qquad 2\text{-}15$$

where $\bar{A}$ and $\bar{I}$ are mean values. Using these equations the complex representations of the wave becomes

$$\bar{A}(r,t) \exp [L(r,t) + j\phi(r,t)] \qquad 2\text{-}16$$

C. Aperture Averaging

Collection of light with large aperture optical systems tends to average out atmospherically induced intensity and phase fluctuations. This causes a smaller variance for both and alters the statistical properties of the intensity variation.

Before discussing the principles of aperture averaging it is necessary to define correlation distance r_o. Consider the intensity at two points separated by a distance of r. For r equal zero the correlation function will be unity. As r increases, the correlation function decreases with zero as its lower bound. How rapidly the correlation function decreases with increasing r, is related to the strength of atmospheric turbulence. r_o is defined as the distance at which the intensity variations of the two points are no longer correlated. r_o could also be defined as the distance at which the variations become statistically independent. r_o usually varies from a few millimeters for very strong turbulence to several centimeters for mild turbulence.

Consider the aperture shown in Figure 2 to be the aperture of an optical system which collects and focuses light from a diverging beam. Let the light intensity across the illuminated aperture be divided into n finite circles of radius r_o. The intensity within these circles will be assumed to be highly correlated. The collection and focusing process can be thought of as adding the intensity contribution of each circle on the aperture in the focal plane. Averaging of the intensity fluctuations of each circle across the aperture will occur at the focus if the diameter of the aperture is much larger than r_o such that it contains many circles.

The intensity fluctuation in the circles of radius r_o are log-normally distributed. Since the aperture adds the intensities, it will also add the probability density functions. The Central Limit Theorem can then be applied to predict that the intensity variations at the focus should be normally distributed. In order to apply the Central Limit Theorem, we must assume that the average intensities of the circles are

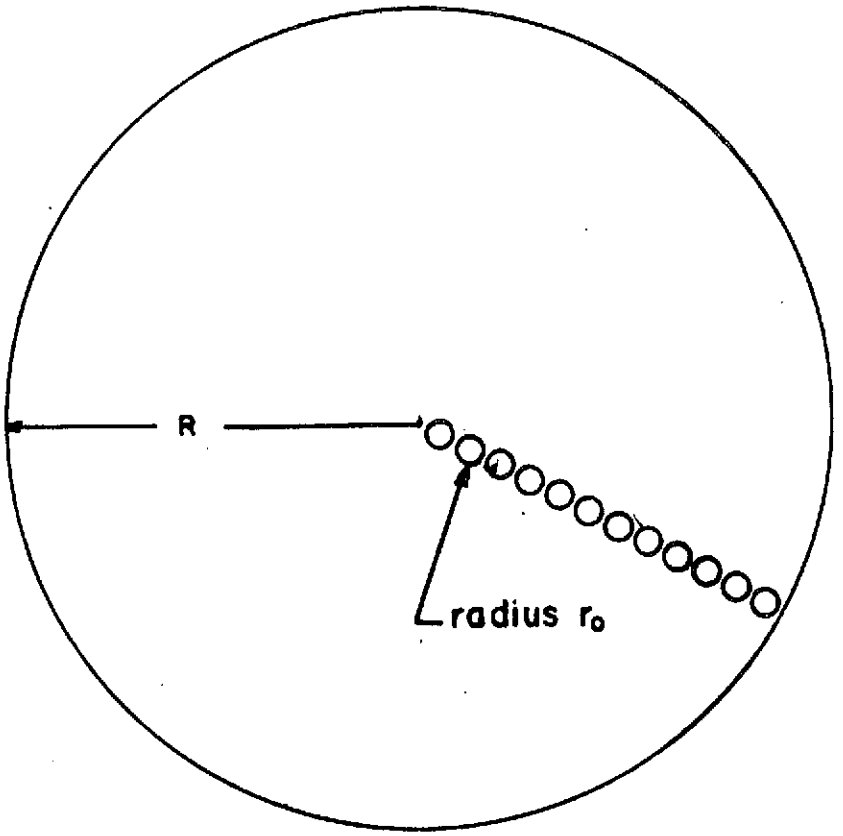

Figure 2. Illustration of the Concept of Aperture Averaging.

of the same order of magnitude across the aperture and that the variance from circle to circle should not change significantly.

CHAPTER III

EXPERIMENTAL

A. Description of Equipment

The experimental measurements were made during the Summer of 1969 at the Marshall Space Flight Center's optical range located on Redstone Arsenal near Huntsville, Alabama.

The transmitting system was located in an astronomical observatory on the crest of Madkin Mountain. The receiving and recording systems were located in the Astrionics Laboratory complex in a special building equipped with a large mirror periscope so that the optical equipment could be conveniently placed on the ground level yet have a clear optical path to the mountain. The height of the periscope was about 15 feet above ground level. The optical path extended in a southwesterly direction for a distance of 3.2 km. The transmitter was about 220 meters above the receiver so that the optical path was at an angle of 4° with the horizontal. Except for a few small buildings and a parking lot paved with bituminous material, the optical path lay mostly over wooded terrain.

The transmitter and receiver were constructed by Minneapolis Honeywell Corporation for Marshall Space Flight Center and have been described in the literature[8]. The transmitter consisted of a 5 watt CO_2 flowing gas laser with a 10 cm. off axis cassegrainian collimator as shown in Figure 3. The laser was designed to have good short and long term frequency stability. This was accomplished in part by constructing the cavity of the low expansion material cervit, which has an expansion

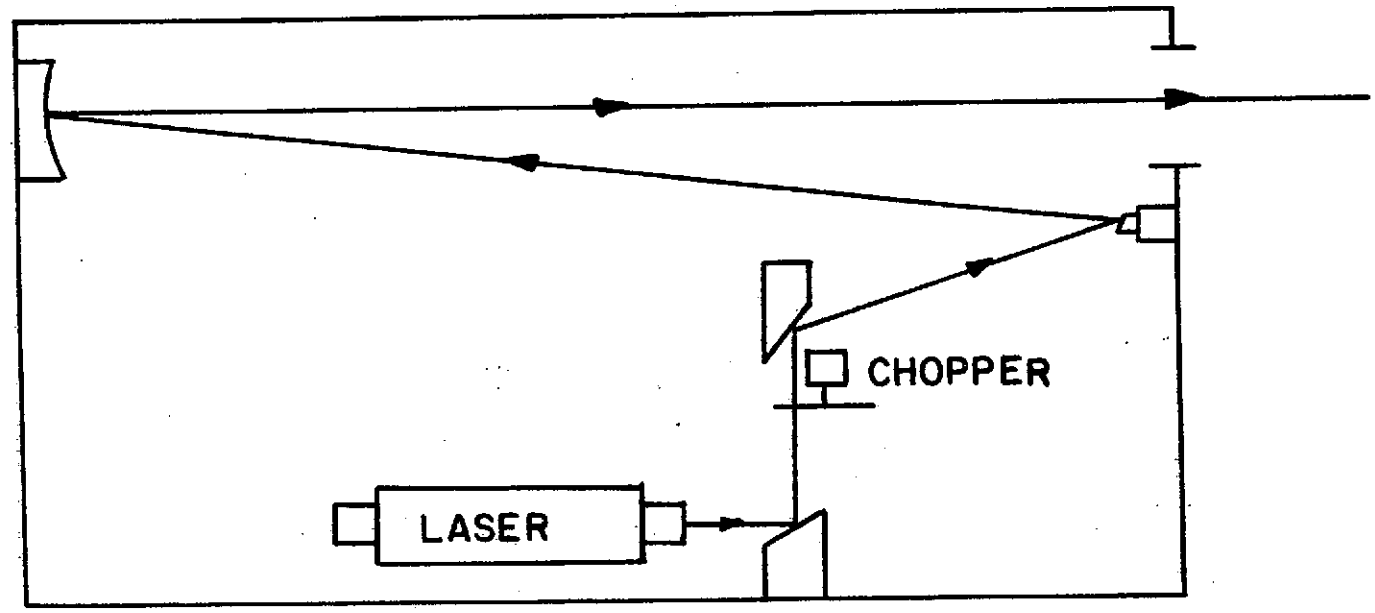

Figure 3. Side View of Transmitter.

coefficient of less than 1×10^{-7} (1/°C). To further stabilize the laser, water held at a constant temperature to better than 0.1°C was continuously circulated through the cervit yoke. The laser in the transmitter was frequency modulated by applying the modulation voltage to a piezoelectric cylinder on which one of the end mirrors was mounted. The other end mirror consisted of an Irtran output coupler that was also attached to a piezoelectric cylinder, which provided laser transition selection. A DC bias was applied to the cylinder to select the desired transition. In addition, the transmitter included a mechanical chopper that was originally intended to be used for alignment purposes. The transmitter unit also contained the necessary electronics to produce a modulation voltage for both carrier or direct modulation. A block diagram of the transmitting unit is given in Figure 4.

The receiving unit was housed in a cabinet identical to that of the transmitter as shown in Figure 5. The receiver consisted of a 10 cm. off axis cassegrainian telescope, a local oscillator laser identical to that of the transmitter, combining optics, and a mercury doped cadmium telluride detector. This is an alloy detector having a spectral response between 8 and 14 microns. The detector was cryogenic and required an operating temperature of 77°K, which was obtained by using liquid nitrogen. The operation of the receiving unit can be described with reference to Figure 6. The transmitter and the local oscillator signal are made spatially colinear by means of a germanium beam splitter and combined on the surface of the mercury doped cadmium telluride detector. The local oscillator frequency is offset by 10 Mhz from the transmitting laser. The 10 Mhz beat frequency produced by the detector is amplified with a 10 Mhz center frequency, intermediate frequency amplifier. This

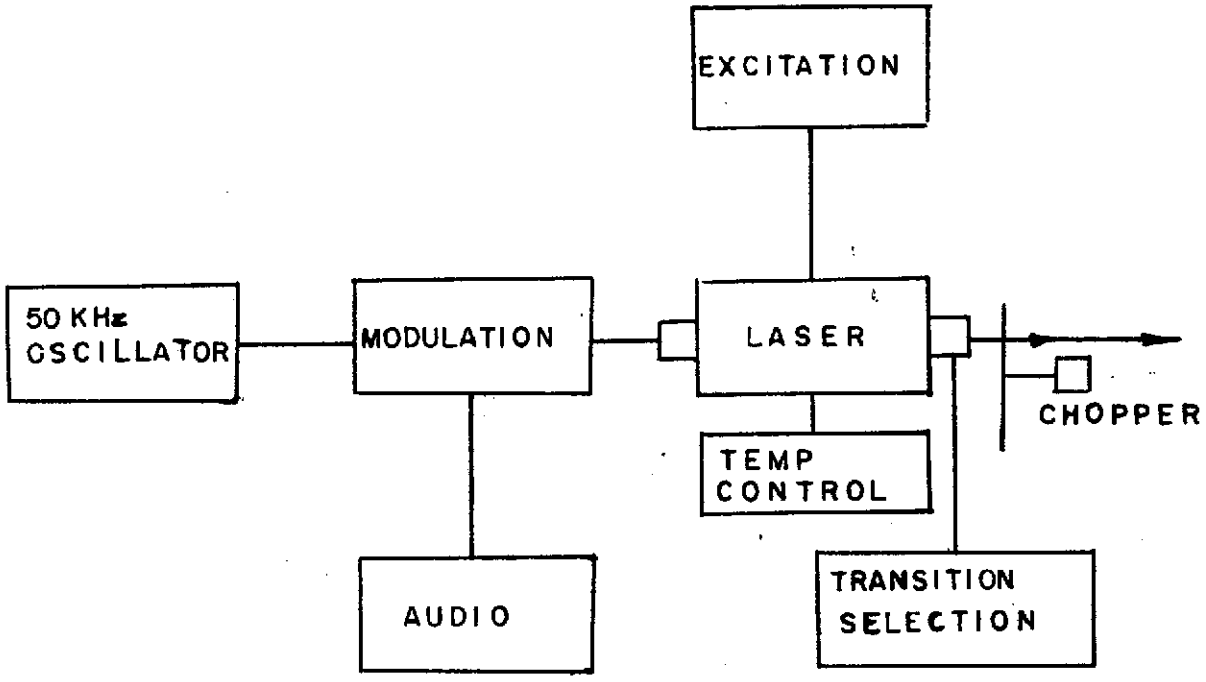

Figure 4. Block Diagram of Transmitter.

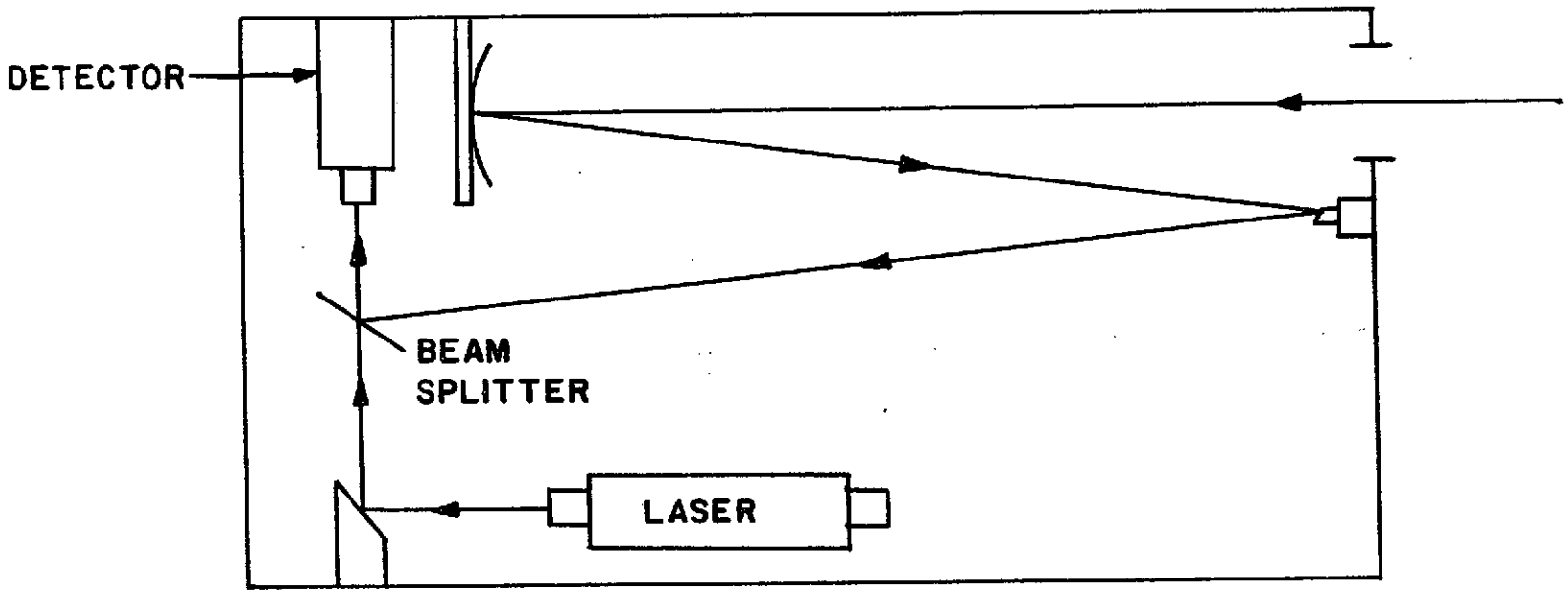

Figure 5. Side View of Receiver.

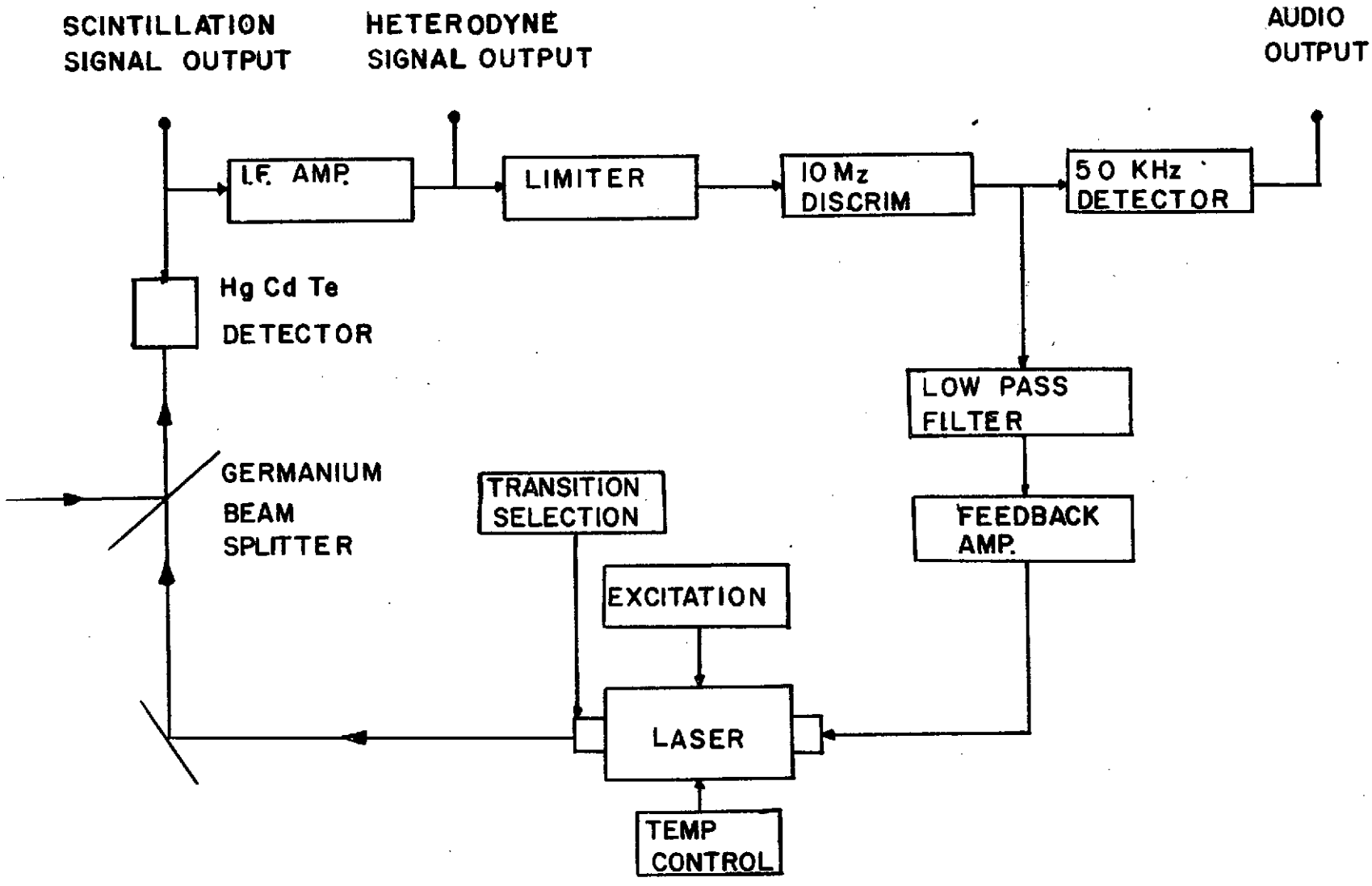

Figure 6. Block Diagram of Receiver.

amplifier has a 2 Mhz bandwidth and a 110 db gain. The intermediate frequency amplifier is followed by a limiter that eliminates amplitude variations. A 10 Mhz discriminator provides an error signal for the local laser feedback loop which consists of a low pass filter and a feedback amplifier. The feedback amplifier drives a piezoelectric cylinder on which one end mirror of the laser is mounted. This provides automatic frequency control of the local oscillator laser.

The data acquisition system was located at the receiver terminal and consisted of an Ampex 14 channel analog F.M. tape recorder, a variable gain AC amplifier with good low frequency response, and two oscilloscopes used for monitoring purposes. Figure 7 gives a block diagram of this system. A spectrum analyzer was also available to check the 10 Mhz beat signal in the receiver.

The monitoring of both the input to the amplifier and the recorder was necessary to insure that they were operating within their linear range. Especially critical was the input level to the recorder, since its linear range for input voltage was ±1 volt. To be safe we operated within ±.5 volt.

B. System Alignment

It was necessary to measure the laser and amplifier noise of the system to insure that it would not have a significant effect on measurements made through the atmosphere. Noise measurements were made with the transmitter and receiver placed a few feet apart with the local laser in the receiver turned off, so that only noise contributions from the transmitter laser, detector and receiver electronics would be present. The system was then operated in the same manner over a 100 meter path through an enclosed tunnel one meter in diameter. The noise

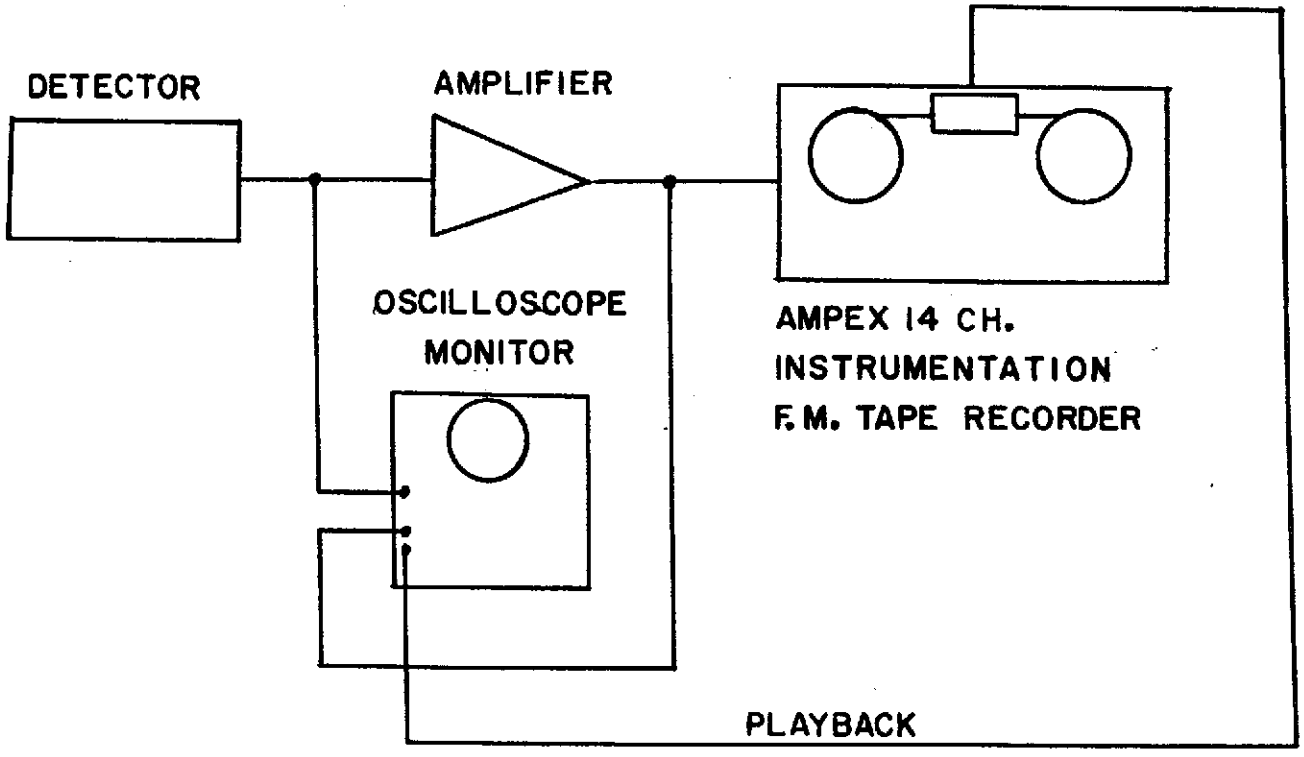

Figure 7. Block Diagram of Data Acquisition System.

of the local oscillator laser was determined by operating it into the detector in the absence of an incoming signal. The noise in all cases was found to be sufficiently low so that it would be negligible compared to the expected variation due to atmospheric scintillation. The linearity of the mercury cadmium telluride detector was determined by noting changes in DC voltage output for different power levels. The laser power was measured on one side of the germanium beam splitter using a Coherent Radiation Laboratories power meter and the DC variation in the detector was measured by a digital voltmeter. For incident power levels less than 300 mw., the detector output was found to be linear.

Alignment of the system over the 3.2 km. path proved to be a difficult task. Our first attempt was to bore sight a 60 power telescope mounted on the transmitter case, with the output beam. The idea was to aim the transmitting unit on the mountain at the laboratory periscope. This method worked over the 100 meter tunnel quite well, but the bore sight became misaligned when the transmitter was transported to the mountain. The second method employed to align the system involved the use of two visible lasers. The transmitter unit, now mounted on the observatory telescope stand on Madkin Mountain, was aligned by placing an argon laser directly in place of the receiving unit in the laboratory. The bright beam could easily be detected by the eye at the transmitting terminal. The position of the argon laser was adjusted until its beam was intercepted by the objective of the transmitter unit. The optical system of the transmitter was then adjusted so that the visible laser was focused onto the output aperture at the transmitter laser. Using heat sensitive paper as a position indicator for the infrared beam, the visible light and the invisible beam were made to coincide at two points in the optical system. Alignment of the receiving unit was accomplished

in a similar manner except that a visible laser could not be mounted in the same position as the now aligned transmitter unit. A small helium neon laser was mounted with a telescope on a tripod and located as near to the transmitter as possible. The telescope was then bore sighted to the helium neon laser. The laser-telescope arrangement was pointed by locating the top periscope mirror at the laboratory. A corner reflector located at this mirror enabled a more precise aim as the reflection of the red light could be seen with the telescope. The visible beam was then focused onto the detector in the receiver. With minor adjustments to the transmitter laser mount, close alignment was attained for the system.

C. Measurement Procedure

Scintillation measurements were made with the receiver laser inoperative so that only light from the transmitter and from the sun's reflection off the observatory dome were intercepted by the receiver. This background light was cause for great concern since accurate measurements of the variations of the laser light could not be made in its presence. Since we could not filter out this unwanted light, it was necessary to record it. To accomplish this scintillation measurements were made by chopping the transmitter beam at 90 Hz by means of the mechanical chopper located in the transmitter. Figure 8 shows a sample of this chopped signal.

Scintillation measurements were made in 90 second segments. A written log was kept on each data run giving the date and time of day, analog tape number, the channel number, aperture size, and weather conditions such as temperature, wind velocity and humidity. The intensity signal for each data run was read on the analog tape into marked time slots. One

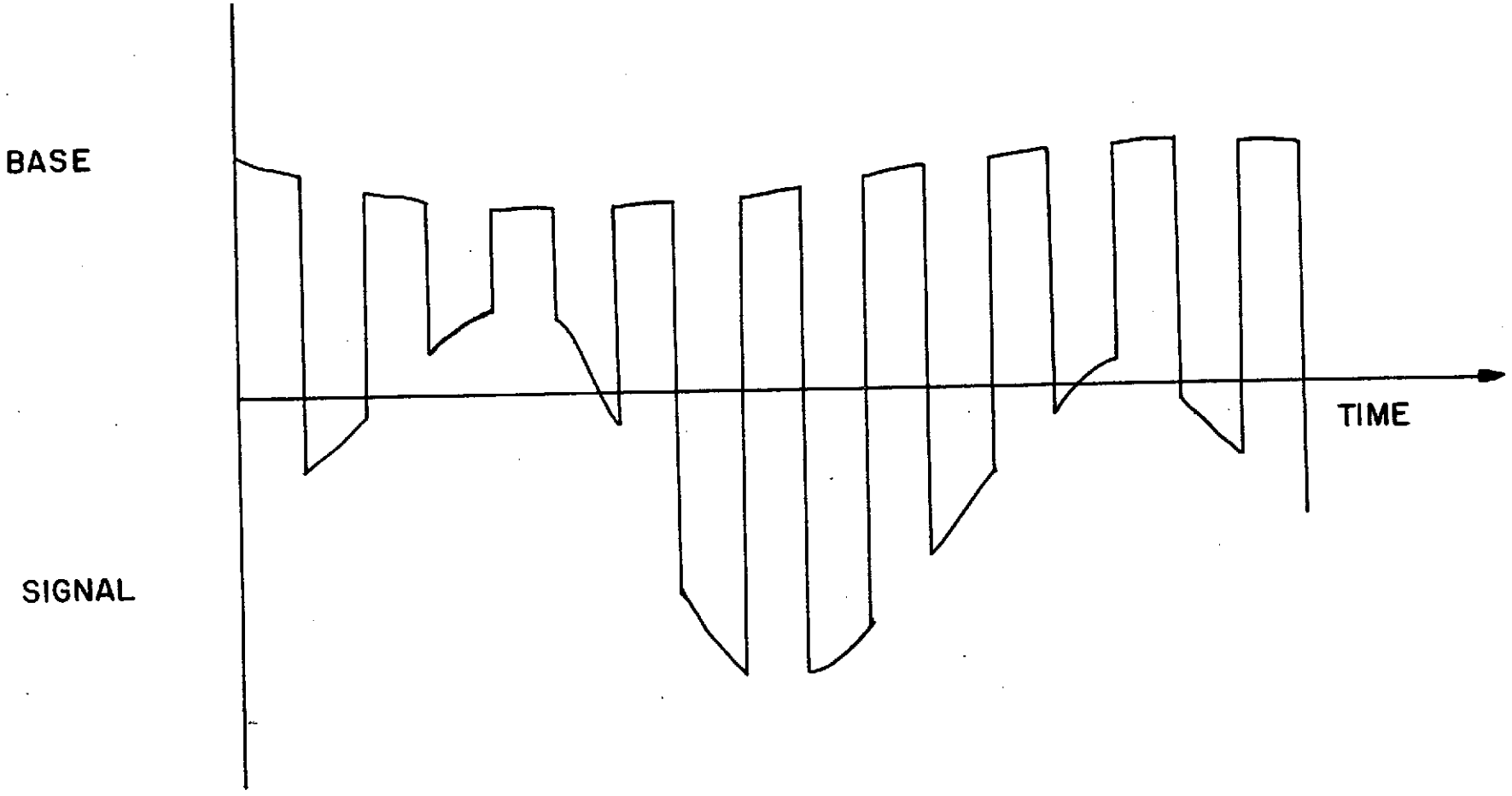

Figure 8. Waveform of Signal Recorded for Scintillation Measurements.

of the channels was marked every 90 seconds with an audio tone code so that approximately 33 slots were available on each data channel. When sufficient signal was being received, data runs were made in succession using five different size apertures. The aperture size varied from two to ten cm. in diameter. The runs were made in succession to insure that atmospheric conditions remained constant over each set of five runs.

Since the signal level for small aperture sizes was below that for the larger apertures, it was necessary to adjust the AC amplifier from one run to another using the monitor oscilloscope. Also, it was important to keep the dewar on the detector filled with liquid nitrogen so that the detector temperature would remain constant.

Measurements of the signal to noise ratio and distortion were made on the communication system operating over the optical range. The signal-to-noise ratio of the heterodyne action was measured at the receiver by extracting the 10 Mhz beat note between the received signal and the local oscillator after it had passed through one stage of amplification. The signal was detected with a simple diode circuit and the resulting voltage recorded by the data acquisition system. These measurements were also made for different aperture sizes.

CHAPTER IV

DATA REDUCTION

A. Analog-to-Digital Conversion

All measurements were recorded on analog tape. In order to process this data it was necessary to convert it to a digital form suitable for computer input. The very large quantity of data collected necessitated electronic conversion to digital magnetic tape which could then be read directly into the computer.

The first step in the conversion from analog-to-digital form consisted of recording a timing signal on a reserved channel of the analog tape. Eight standard time signals are broadcast by Marshall Space Flight Center's Computation Laboratory on a frequency of 226.5 Mhz. The time signals are subcarrier multiplexed with pilot frequencies between 2.3 KHz and 70.0 KHz. The signal chosen was a rectangular pulse with a one-second repetition rate broadcast on a subcarrier frequency of 52.5 KHz. This signal is designated as 100/1000 AMR-D-5, and is coded with the time of day in Greenwich Mean Time by pulse width modulation. This timing signal had no relation to the actual time the data was recorded.

The analog tapes were then read into a cathode-ray-oscillograph. Four data channels, the timing channel and the marker channel were recorded simultaneously. The oscillograms were inspected and the sections of the tape to be digitized were selected. At this time bad data was identified and eliminated. The starting and stopping time for each time interval selected was read from the timing channel and recorded on the Computation Laboratories instruction forms. The analog-to-digital converter system was set to convert only those time intervals selected by

reading the timing channel. Approximately 30 one-minute segments were selected from each channel. As the running time for the analog tape was about 45 minutes, about two-thirds of the total data recorded on a tape channel was converted.

The analog-to-digital conversion was performed by Marshall Space Flight Center's Computation Laboratory using an Astrodata type converter. Five data channels were digitized simultaneously. The five channels were sampled alternately at a rate of 5000 samples per second which amounted to sampling each channel at 1000 samples per second. The resulting binary coding was recorded on seven channel digital tape in a multiplexed format.

The digital tape format consisted of a ten bit binary word so that 2048 levels were available to represent analog signal levels between -.5 volts and +.5 volts. Since seven track tape was used, each sample required two tape characters consisting of a ten bit word plus the sign bit, blank bit and two parity bits. The data was recorded in records of 2004 tape characters. The first four tape characters contained the time as read from the timing channel at which the first sample was taken. The remaining 2000 characters contained 1000 sample points, 200 from each channel, alternating between channels. Subsequent records were written until the segment was completed, at which time an end of file mark was written; therefore, each file on the digital tape contained one time slice or data run from the analog tape. In addition, the first record of each file was an identification record of 24 tape characters which contained the tape number and other information.

B. Description of Computer Program

A program was written for an IBM-360-50 computer to reduce the data

stored on magnetic tapes. This program reads data from the tape, changes the binary format to a fortran compatible form, then calls its various subroutines to perform the analysis. The principle problems which were encountered in writing this program concerned formatting the data for the computer and extracting the actual light intensity signal from the modulated square wave. When the signal was extracted it was either stored for spectral analysis or is used to construct a histogram. A Fourier transform subroutine or statistical subroutine was then called to analyze the signal.

Development of a routine to extract the desired signal proved to be somewhat difficult since the sampling rate during digitization could not be accurately synchronized with the period of the square wave. The sampling rate of 1 KHz and the chopping rate of 90 Hz should yield approximately 10 samples per cycle of the square wave. In actuality, the number of samples per cycle varied between ten and twelve due to the sampling rate not being an integral multiple of the square wave frequency. The routine was designed to determine whether a particular data sample was a base point (i.e., from the part of the square wave when the laser beam was blocked by the chopper) or a signal point (when power was being received from the laser beam). The problem was further complicated by the fact that the rise and fall times of the square wave were non-negligible so that about one percent of the data points were sampled during the switching transient and should be neglected. In addition, some of the data contained an occasional noise spike which should be eliminated. It was decided that the elimination of these spikes would not adversely effect the validity of the analysis so provisions for eliminating them were also included in the program.

The extraction routine operates basically as follows: A pre-processing routine reads the data from the magnetic tape and stores a record containing 200 data points into a common array. To begin the analysis twenty data points from the array are selected and their maximum and minimum value computed. Two limits, L_1 and L_2 are then set by the relations

$$L_1 = A_{max} - P_1(A_{max} - A_{min}) \qquad 4\text{-}1$$

$$L_2 = A_{min} - P_2(A_{max} - A_{min}) \qquad 4\text{-}2$$

where A_{max} and A_{min} are the maximum and minimum values of the first twenty points, and P_1 and P_2 are constants between zero and one half. Since the signal was inverted when it was recorded on the analog tape, the base line is greater than the signal, hence a particular point greater than L_1 is considered a base point, if it is less than L_2 it is considered a signal point. Points lying between L_1 and L_2 are assumed to be from the transient portion of the wave form and are neglected. The routine takes each point successively and determines if it is a base point, a signal point or neither. As a preliminary to processing, the first twenty points are scanned and the beginning of a base line segment of the wave form is found. Then new limits are set on the next 15 points and they are scanned and grouped into three arrays, a base line segment, a signal segment and a second base line segment. Each array may contain up to ten points. At this time another routine is used to compute the signal amplitude of the square wave for the group of signal points (as will be described later). The second group of base points is transferred into the first array, new limits are set using the next ten data points,

and a new group of signal points and base points are found to fill the second and third arrays, and finally their amplitudes computed. This process is continued until the 200 points from the first record have been used. At this time the routine pauses while the next record is read in. Processing then continues until the number of records called for (up to 300) have been processed.

This routine also contains several checks to handle possible irregularities in the data. During the search for either base or signal points if more than ten consecutive points are found, the routine will request that the next record be read in, which means the remainder of the bad record is discarded. Also if the number of unsuccessful scans while in the base or signal search phase exceeds ten, the routine will enter an error recycle phase. In this phase the routine skips 20 points and resumes processing as if it were at the beginning of a new run. If the error recycle phase is entered five times in a given record, a request for the next record will be executed. When a new record is requested due to an irregularity in the record being processed the routine again treats it as it does the first record of a new run. In addition to the above, if three or less base or signal points are found in a given search, the error recycle phase is entered.

During processing, a record is kept of each irregularity encountered and this information is printed in tabular form when the processing of a run is completed. If an excessive number of irregularities occurs in a given run, the results of that run must be suspected.

The three arrays containing base and signal points found by the extraction routine are passed into a routine that determines the actual amplitude of the signal. Three methods for computing the amplitude were

tried: The first method took to base line for a group of signal points as the average of all the points in the group of base points preceding it and the ones following it. This is equivalent to considering the background light during the time when the laser beam intensity was being recorded to be the average of the background light recorded during the half-cycle immediately preceding the signal and the half-cycle immediately following it. The difference between the signal point and the average base line was taken as the amplitude of the laser beam at that instance.

The second method of amplitude calculation considered was to reconstruct the base line by fitting a least-mean-square curve to the base points. This method produced erratic results and also required additional computer time and was abandoned.

In the third approach, the difference in the first signal point in a group and the last base point preceding it is taken as the signal amplitude. The difference in the last signal point in the group and the first base point following it gives a second amplitude. This method yields only two amplitudes per cycle but has the advantage that they are evenly spaced. Since the difference in time between signal and base points is very small, this method eliminates the problem of the unknown base line over the signal interval.

The computer program contained both the first and third methods of signal amplitudes calculations. The method to be used was selected by a parameter read during execution. The values computed by this routine were either stored in an array to be used in the spectral analysis, or used to construct a histogram. Histograms are sometimes referred to as being the probability density function for discrete variables.

The final segment of the program consists of the analysis routines.

The statistical routines accept the histogram for the intensity fluctuation which has been generated and computes the scintillation statistics. The routine computes and lists the corresponding value of the log-amplitude as defined by

$$L_i = \frac{1}{2} \ln [I_i/\bar{I}] \qquad 4\text{-}3$$

where L and I_i are the log-amplitude and the intensity for the ith class interval and $\bar{I}$ is the mean intensity. The frequency for each class and the cumulative probability are also listed. The routine also calculates the mean, standard deviation, skewness, and kurtosis for both the intensity and log-amplitude distribution. A chi-square test that checks the intensity distribution for a normal fit and the log-amplitude for a log-normal fit is also included. Appendix A includes a typical computer print out of the statistical analysis.

The program includes routines to perform a spectral analysis on the intensity scintillation. In calculating the scintillation spectrum 2^8 (8192) values of the beam intensity were extracted from the raw data using the preprocessing routines described previously. These values represent the intensity fluctuations of the beam sampled at 180 Hz rate. The spectrum of the sampled data was computed using the Cooley-Tukey algorithm[9] for fast Fourier transforms. The resulting spectra were displayed by means of a plot routine. In cases where data points are discarded due to irregularities in the extraction routine, the omitted points were replaced with zero values. The purpose of this was to preserve the phase relationship of the signal, which is important in the integration operation of the Fourier transform.

C. Program Check and Parameter Adjustment

To test the program several records were read from a magnetic tape and printed out for inspection. Each sample was classified either as a signal point, or a base point, or as a point from the transient portion of the waveform. This classification was purely subjective, yet in inspecting the data there was usually no questions as to how a point should be categorized. The same data was then read into the computer. A print out of all the pertinent variables at each decision branch of the extraction routine was obtained. The program was then run several times varying the parameters P_1 and P_2 in equations 4-1 and 4-2 between runs and the results compared with the subjective analysis. Data having irregularities was also processed and the results compared to determine whether or not a segment should be omitted. Using these comparisons as a criteria, the parameters P_1 and P_2 were set at 0.05 and 0.10 respectively. Therefore a point within 5% of the maximum base point or 10% of the minimum signal point would be retained while points between these limits were discarded.

The statistical routines were checked out with sets of numbers which had a known probability distribution function. A routine readily available in the IBM Scientific Subroutine Package for the IBM 360 computer was used to generate a large set of normally distributed numbers. These numbers were then processed by the statistics routines in the same manner as the intensity fluctions were to be processed. The part of the routine which tests for the normal distribution fit gave very positive results, and that for the log-normal fit gave negative results. The test routine was then altered to generate numbers with a log-normal distribution. The results of the statistical analysis of this data strongly indicated a

log-normal fit. A description of the log-normal generator is given in Appendix B.

D. Atmospheric Structure Constant and Aperture Averaging

An important parameter in the statistical model for atmospheric studies used in current literature is the refractive index structure constant C_n^2, defined as a constant of proportionality in the relation

$$D_n = \left\langle [n_1(r_1) - n_2(r_2)]^2 \right\rangle = C_n^2 \, r^{2/3}$$

$$r = r_2 - r_1 \qquad 4\text{-}4$$

where D_n is called the structure function and is a measure of the deviation of the index of refraction at two points separated by a distance r. C_n is actually a measure of the strength of the turbulence. Fried[10] gives a relation involving C_n for an infinite spherical wave propagating a distance z in a turbulent atmosphere. The relation is

$$C_\ell(0) = .124 \, K^{7/6} \, Z^{11/6} \, C_n^2 \qquad 4\text{-}5$$

where $C_\ell(0)$ is the log-amplitude variance. Equation 4-5 can be used directly to obtain C_n^2 by noting that the standard deviation of the log-amplitude distribution which we have computed is the square root of $C_\ell(0)$.

A finite receiving aperture has the effect of averaging the intensity fluctuating from various parts of the wave front thereby reducing the variance of the scintillation.

The effect of aperture averaging can be allowed for by using relations developed by Fried[11,12] viz.

$$\sigma_s^2 = [\frac{\pi}{4} D^2]^2 \theta C_I(0) \qquad 4\text{-}6$$

Where σ_s is the signal variance which corresponds to the square of the standard deviation of the intensity fluctuation, D is the diameter of the receiving aperture, and θ is an aperture averaging factor given by:

$$\theta = \frac{16}{\pi D^2} \int_0^D \rho d\rho \frac{\exp[4C_\ell(\rho)]-1}{\exp[4C_\ell(0)]-1} H(\rho/D) \qquad 4\text{-}7$$

$H(\rho/D)$ is the optical transfer function of a circular aperture

$$H(\rho/D) = \cos^{-1}(\rho/D) - \rho/D\ [1-(\rho/D)^2]^{1/2} \qquad 4\text{-}8$$

and $C_\ell(\rho)$ is log-amplitude covariance given by:

$$C_\ell(\rho) = C_\ell(0) \sum_{n=0}^{\infty} [a_n + b_n \left(\frac{k\rho^2}{4z}\right)][\left(\frac{k\rho^2}{4z}\right)/(2n)!]$$

$$- 7.53034 \left\{\frac{k\rho^2}{4z}\right\}^{5/6} \qquad 4\text{-}9$$

In the last expression a_n and b_n are the expansion coefficients for the modified confluent hypergeometric function and are given by the recursion relations

$$a_n = -a_{n-1} \{(2n - 23/6)(2n - 17/6)/(2n-1)(2n)\}$$

$$b_n = -b_{n-1} \{(2n - 11/6)(2n - 17/6)(2n-1)/(2n)(2n+1)^2\} \qquad 4\text{-}10$$

where

$$a_o = 1 \qquad b_o = 6.84209$$

The intensity variance $C_I(0)$ can be related to the log-variance by:

$$C_I(0) = I_o^2 \left[\exp(4C_\ell(0)) - 1\right] \tag{4-11}$$

Equation 4-11 specifies $C_\ell(0)$ in terms of σ_s^2 and I_o^2. I_o and σ_s are the mean and standard deviation of the recorded intensity. Combining the above equations we have:

$$\left(\frac{\sigma_s}{I_o}\right)^2 = \pi D^2 \left[\exp[4C_\ell(0)] - 1\right] \times \int_o^D \rho d\rho \, \frac{\exp[4f(\frac{k\rho}{4z})\, C_\ell(0)]-1}{\exp[4C_\ell(0)]-1} \, H(\rho D) \tag{4-12}$$

where $f(k\rho/4z)$ is the summation given in equation 4-9. Since σ_s/I_o is an experimentally determined constant, equation 4-12 is an integral equation for $C_\ell(0)$. A special computer program was written to solve equation 4-12. The technique used is to evaluate the integral in equation 4-12 for a number of trial values of $C_\ell(0)$ using a fourth order Runga-Kutta integration. This gives a table of $\frac{\sigma_s}{I_o}$ as a function of $C_\ell(0)$. From this table the value of $C_\ell(0)$ corresponding to the measured value of $\frac{\sigma_s}{I_o}$ is determined using Lagrange-Hermite interpolation formula.

CHAPTER V

RESULTS

A. Probability Density Function for Intensity Scintillation

It has been customary in the literature to test the hypothesis of log-normality of scintillation data by plotting the cumulative probability function of the log-amplitude against a "probability scale" such that if the data is log-normal the resulting curve will be a straight line. The same method can be applied when testing the intensity amplitude for a normal distribution. Since this test would require considerable time if it were applied to every run, it was necessary to use a test that could be incorporated into a computer program in an efficient manner in order to determine which distribution each run more closely fit.

The necessary statistical parameters to make this test were calculated as described in Chapter III and were available on punched data cards. The skewness coefficient was chosen as the parameter to indicate the type of distribution. The skewness coefficient will ideally have zero value for perfectly normal or log-normally distributed data; however, for real data we expected a small value but somewhat greater than zero.

We have chosen the skewness coefficient as the measure of closeness of fit in preference to the chi-square test since the chi-square depends upon the number of class intervals in the sample while the skewness does not. To use the chi-square on a comparative basis would require the generation of a table of chi-square for all possible number of class intervals and would lend to undesirable complexities in the computer program.

In order to use the skewness as a criteria for categorizing the data it was necessary to set bounds on its value. Since the lower bound is zero, it was only necessary to determine the largest value that the skewness could attain which would represent a suitable fit. This was accomplished by plotting several graphs of the cumulative probability for runs with values of skewness ranging from .02 to .79. The chi-square test made on each run was examined to insure that the overall results of the analysis were consistent. A selected number of these graphs are given in Figures 9-17. An inspection of these plots will show that the cumulative probability curve becomes nonlinear with increasing values of skewness. An inspection of many such plots indicated that the curve deviated from linearity much faster when values of skewness became greater than 0.15. For values from 0.0 to 0.15 the curve remained approximately linear.

The results of the statistical analysis of each run was categorized in the following manner: If the skewness for the log-amplitude data is less than or equal to 0.15, the run was categorized as being log-normally distributed. If the value of the skewness meets the above requirement for the intensity data the run was considered to be normally distributed. If both skewness coefficients were greater than 0.15, the run was put in a "neither" category. In addition we have had to include a category for those distributions which were sufficiently close to both a normal and a log-normal distribution that we could not distinguish between them. These runs which have approximately the same skewness for both distributions have been designated as "both".

The results of the categorization for 196 runs are shown in Table I. Only runs with a small number of preprocessing irregularities have

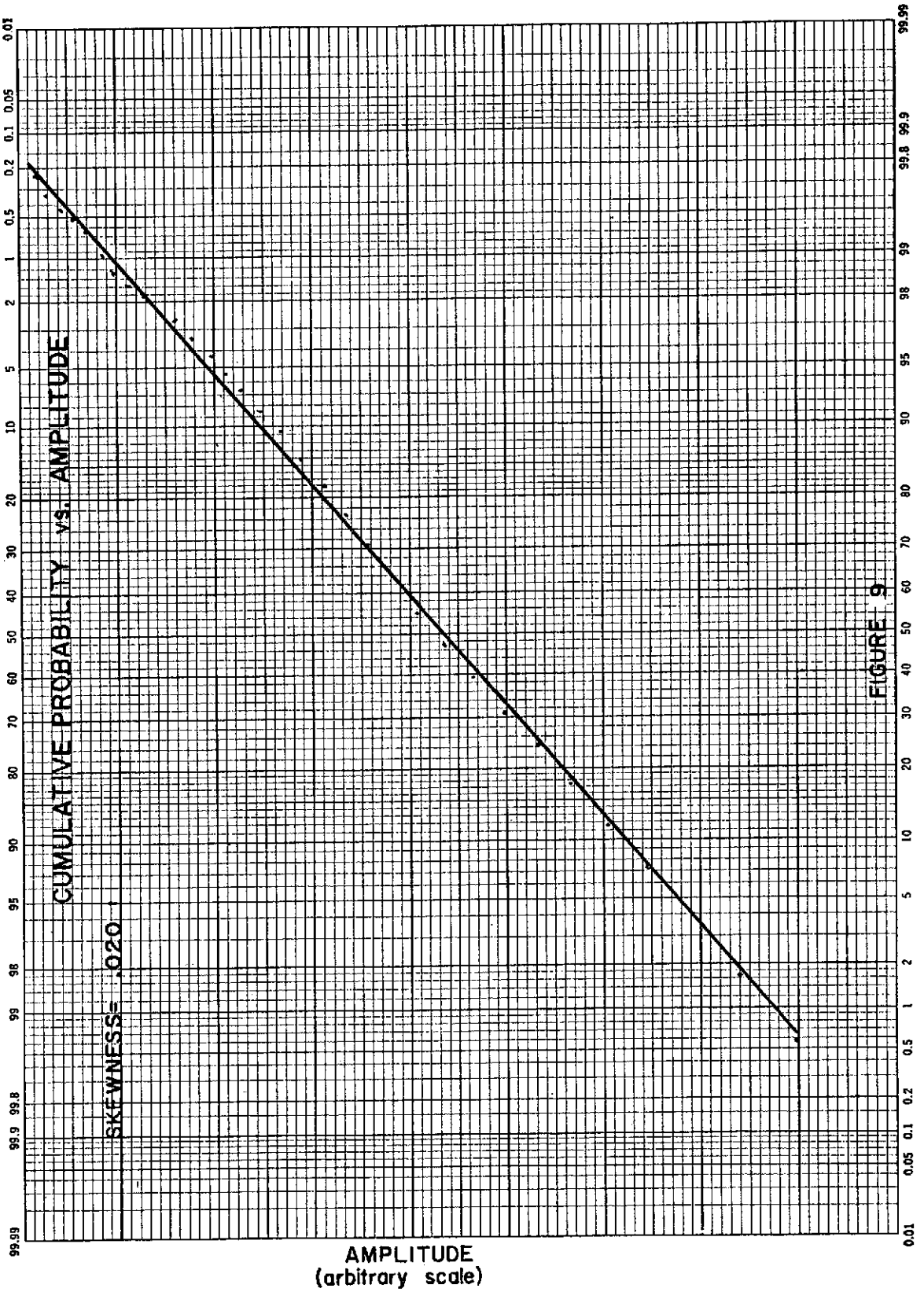
CUMULATIVE PROBABILITY vs. AMPLITUDE
SKEWNESS= .020
AMPLITUDE
(arbitrary scale)
0.01 0.05 0.1 0.2 0.5 1 2 5 10 20 30 40 50 60 70 80 90 95 98 99 99.8 99.9 99.99

FIGURE 9

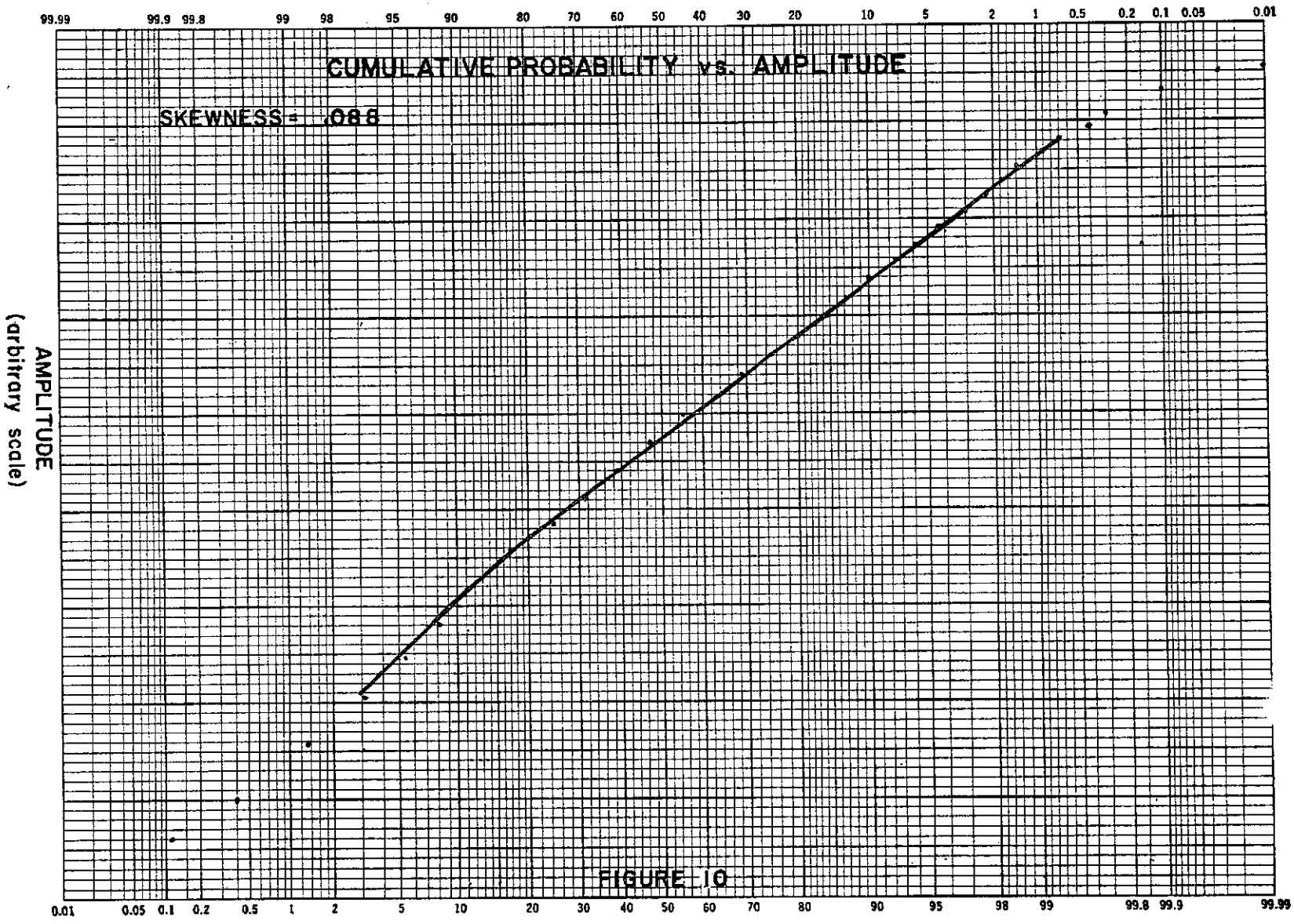
CUMULATIVE PROBABILITY vs. AMPLITUDE
SKEWNESS = .086
99.99 99.9 99.8 99 98 95 90 80 70 60 50 40 30 20 10 5 2 1 0.5 0.2 0.1 0.05 0.01
0.01 0.05 0.1 0.2 0.5 1 2 5 10 20 30 40 50 60 70 80 90 95 98 99 99.8 99.9 99.99
AMPLITUDE (arbitrary scale)

FIGURE 10

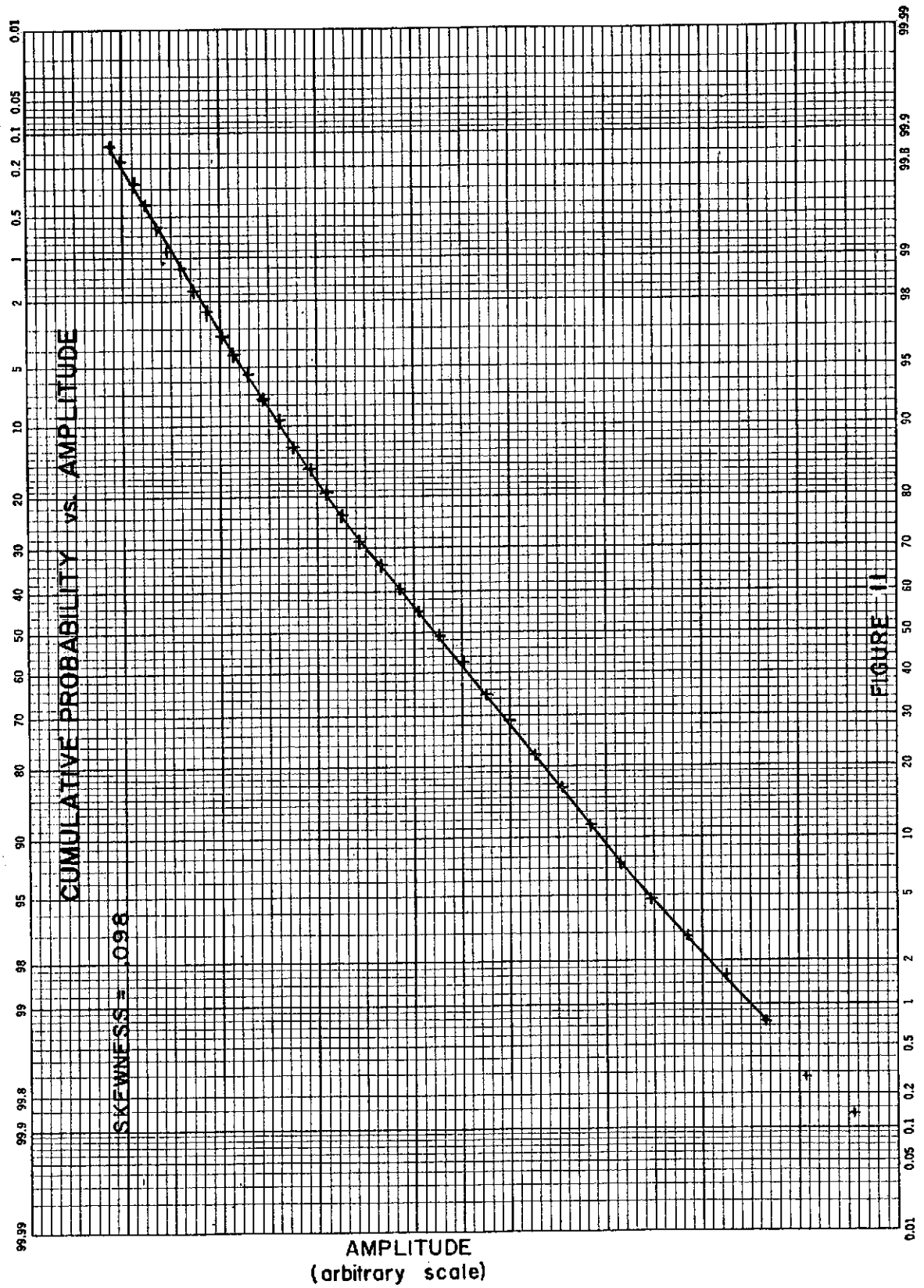
CUMULATIVE PROBABILITY vs. AMPLITUDE
SKEWNESS = .098
AMPLITUDE
(arbitrary scale)
0.01
0.05
0.1
0.2
0.5
1
2
5
10
20
30
40
50
60
70
80
90
95
98
99
99.8
99.9
99.99

FIGURE 11

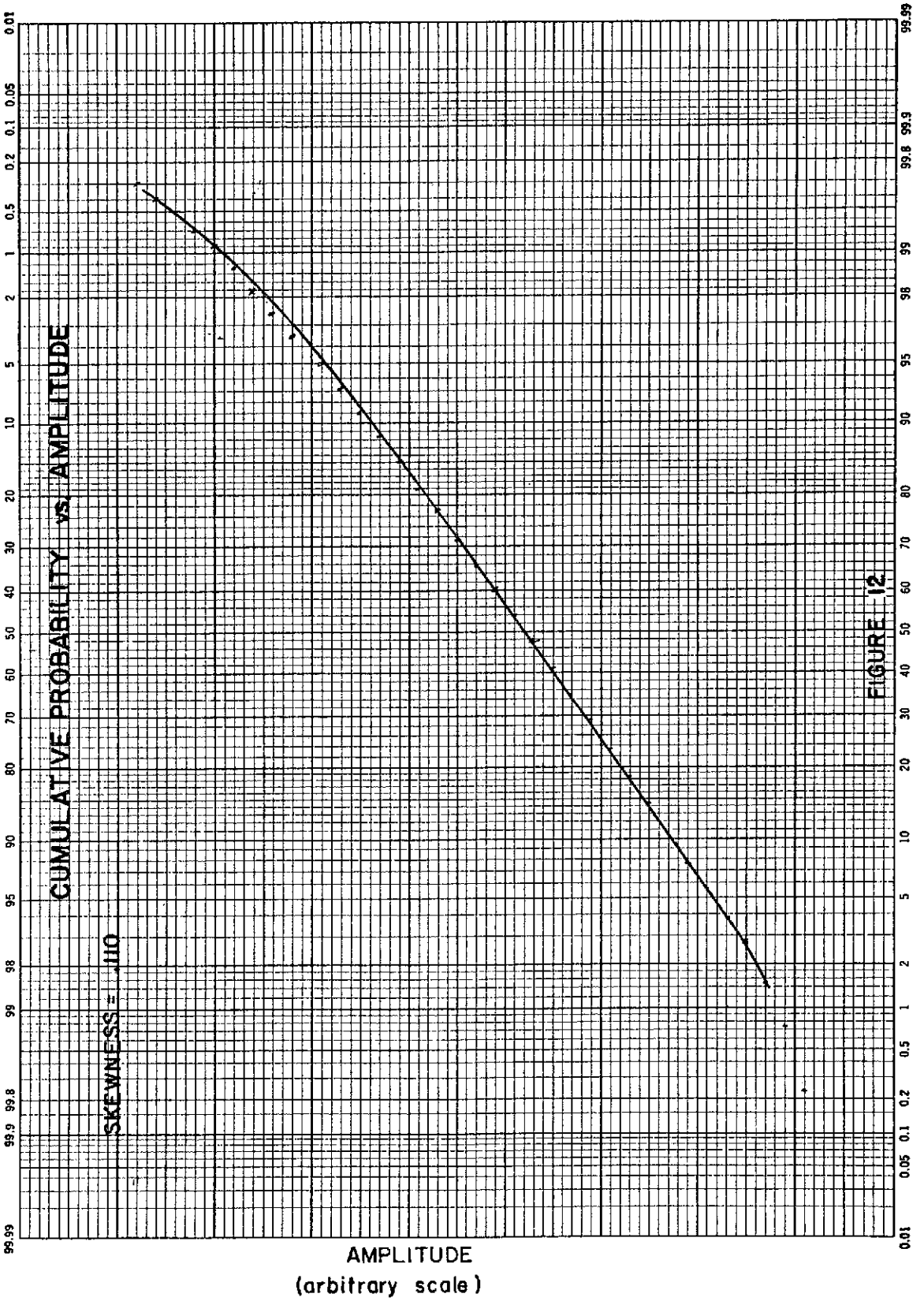
CUMULATIVE PROBABILITY vs. AMPLITUDE
SKEWNESS = .110
99.99 0.01
99.9 0.1
99.8 0.2
99 1
98 2
95 5
90 10
80 20
70 30
60 40
50 50
40 60
30 70
20 80
10 90
5 95
2 98
1 99
0.5 99
0.2 99.8
0.1 99.9
0.05 99.9
0.01 99.99
AMPLITUDE
(arbitrary scale)

FIGURE 12

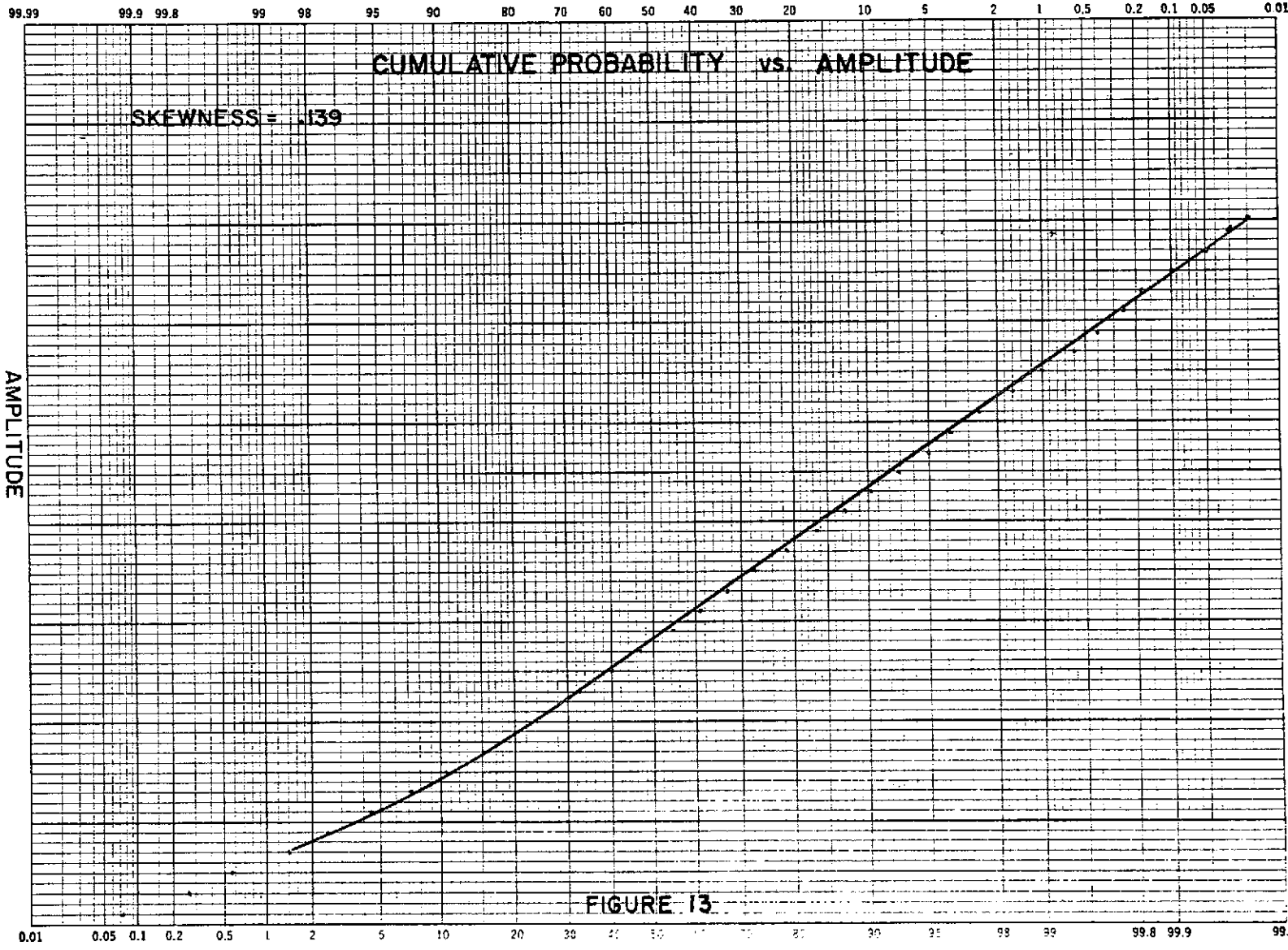
CUMULATIVE PROBABILITY vs. AMPLITUDE
SKEWNESS = .139
99.99 99.9 99.8 99 98 95 90 80 70 60 50 40 30 20 10 5 2 1 0.5 0.2 0.1 0.05 0.01
0.01 0.05 0.1 0.2 0.5 1 2 5 10 20 30 99 99.8 99.9 99.99
AMPLITUDE (arbitrary scale)

FIGURE 13

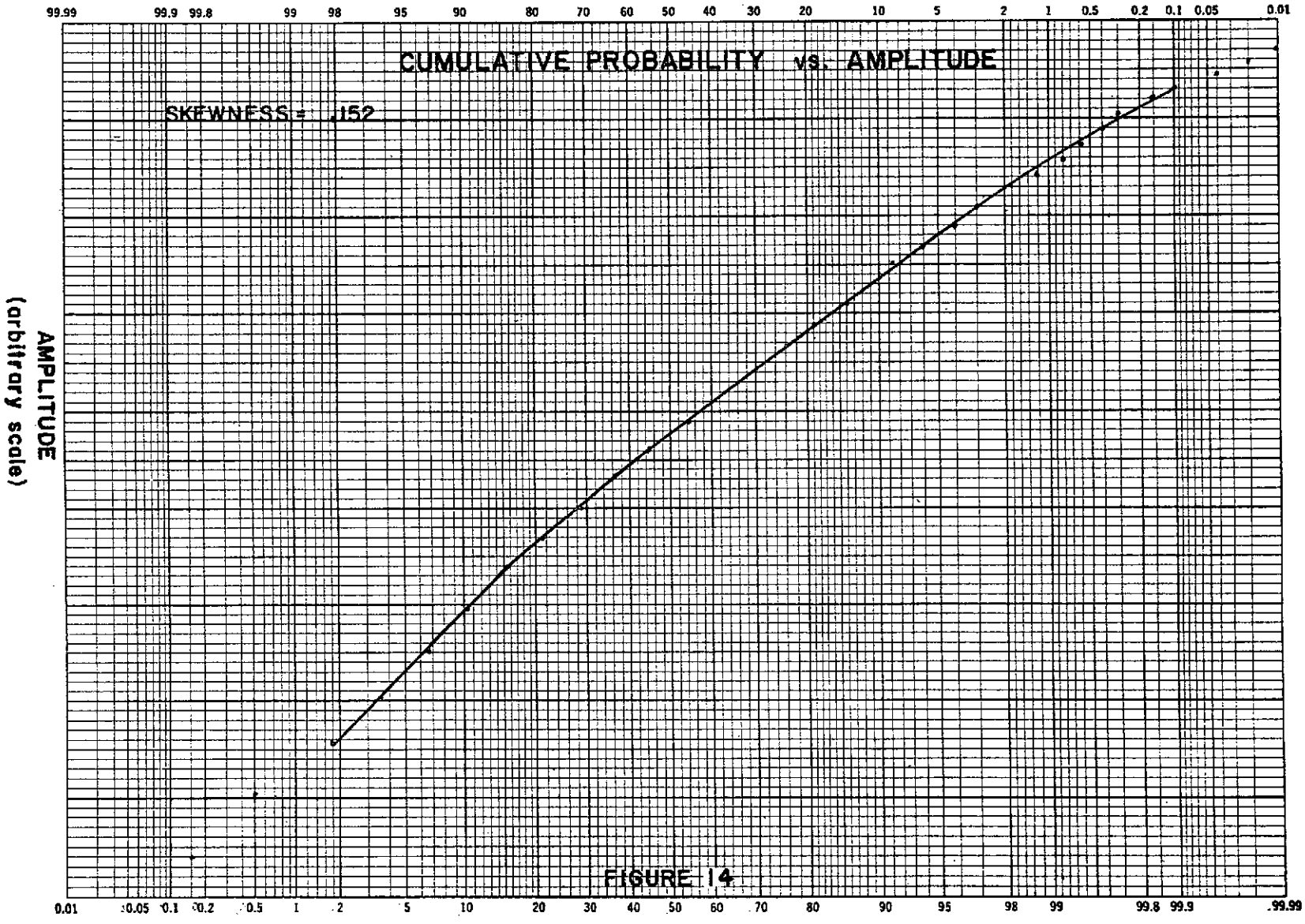
CUMULATIVE PROBABILITY vs. AMPLITUDE
SKEWNESS = .152
AMPLITUDE
(arbitrary scale)
99.99 99.9 99.8 99 98 95 90 80 70 60 50 40 30 20 10 5 2 1 0.5 0.2 0.1 0.05 0.01
0.01 0.05 0.1 0.2 0.5 1 2 5 10 20 30 40 50 60 70 80 90 95 98 99 99.8 99.9 99.99

FIGURE 14

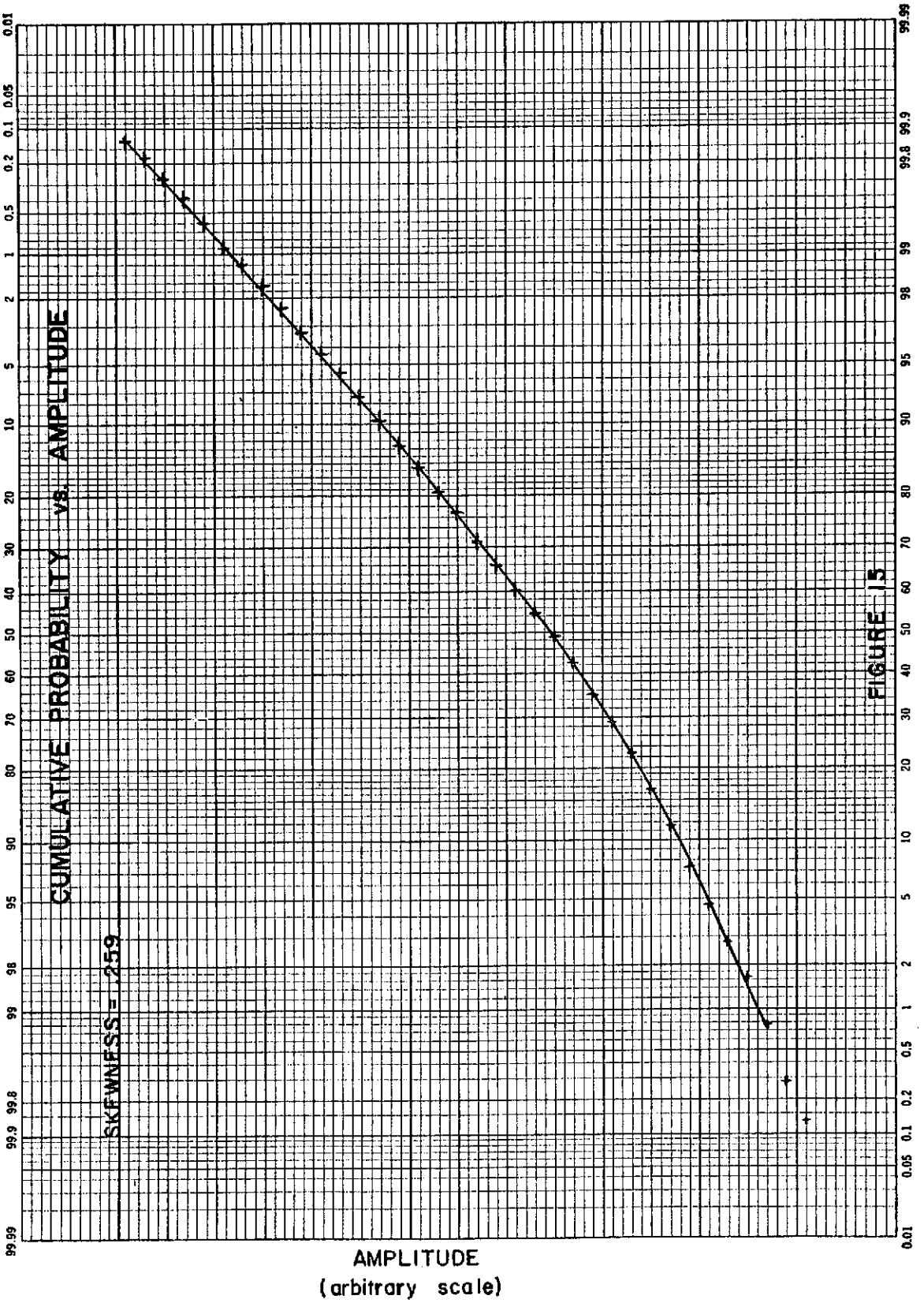
CUMULATIVE PROBABILITY vs. AMPLITUDE
SKEWNESS = .259
AMPLITUDE
(arbitrary scale)
0.01
0.05
0.1
0.2
0.5
1
2
5
10
20
30
40
50
60
70
80
90
95
98
99
99.8
99.9
99.99

FIGURE 15

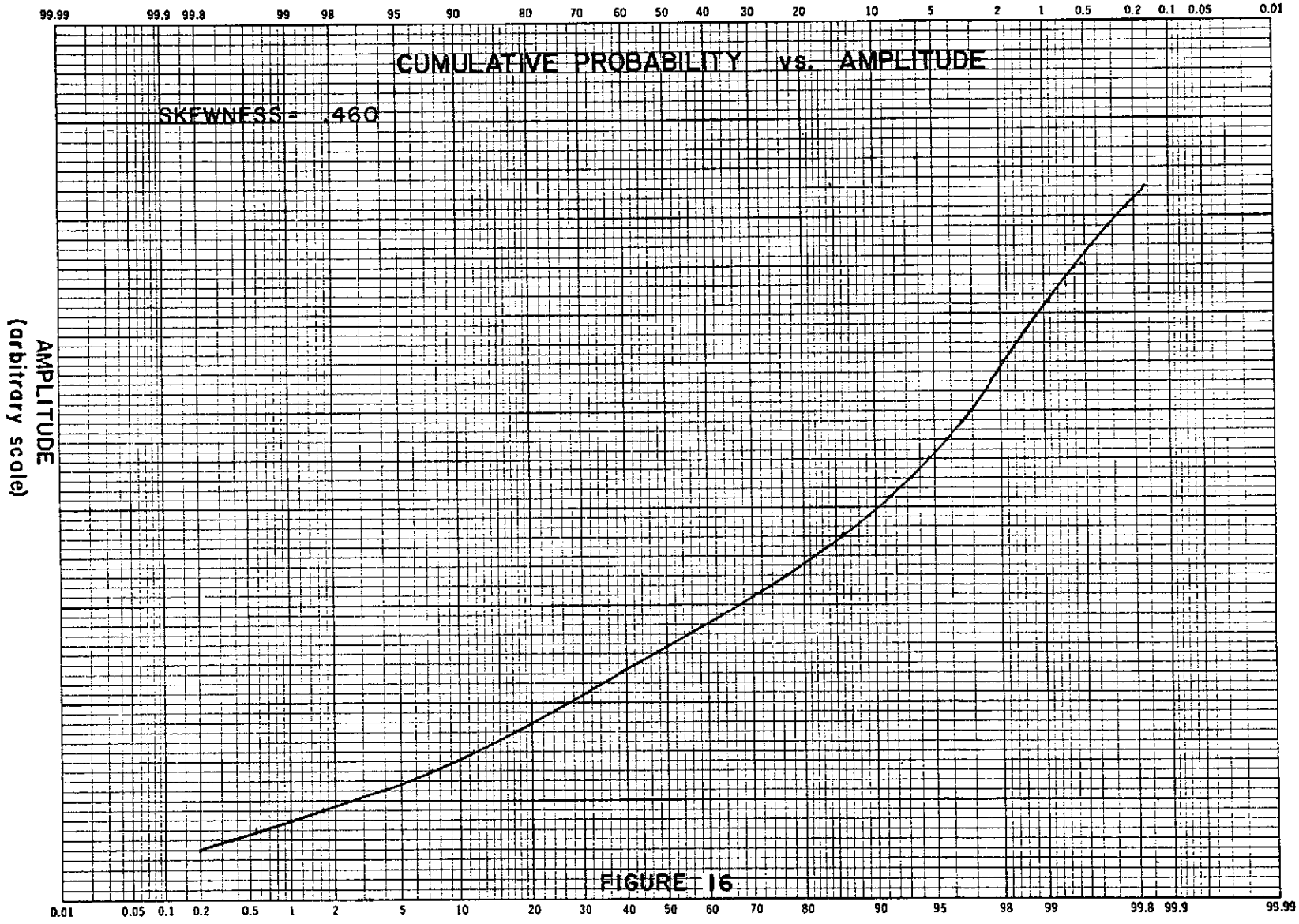
CUMULATIVE PROBABILITY vs. AMPLITUDE
SKEWNESS= .460
AMPLITUDE (arbitrary scale)
99.99 99.9 99.8 99 98 95 90 80 70 60 50 40 30 20 10 5 2 1 0.5 0.2 0.1 0.05 0.01
0.01 0.05 0.1 0.2 0.5 1 2 5 10 20 30 40 50 60 70 80 90 95 98 99 99.8 99.9 99.99

FIGURE 16

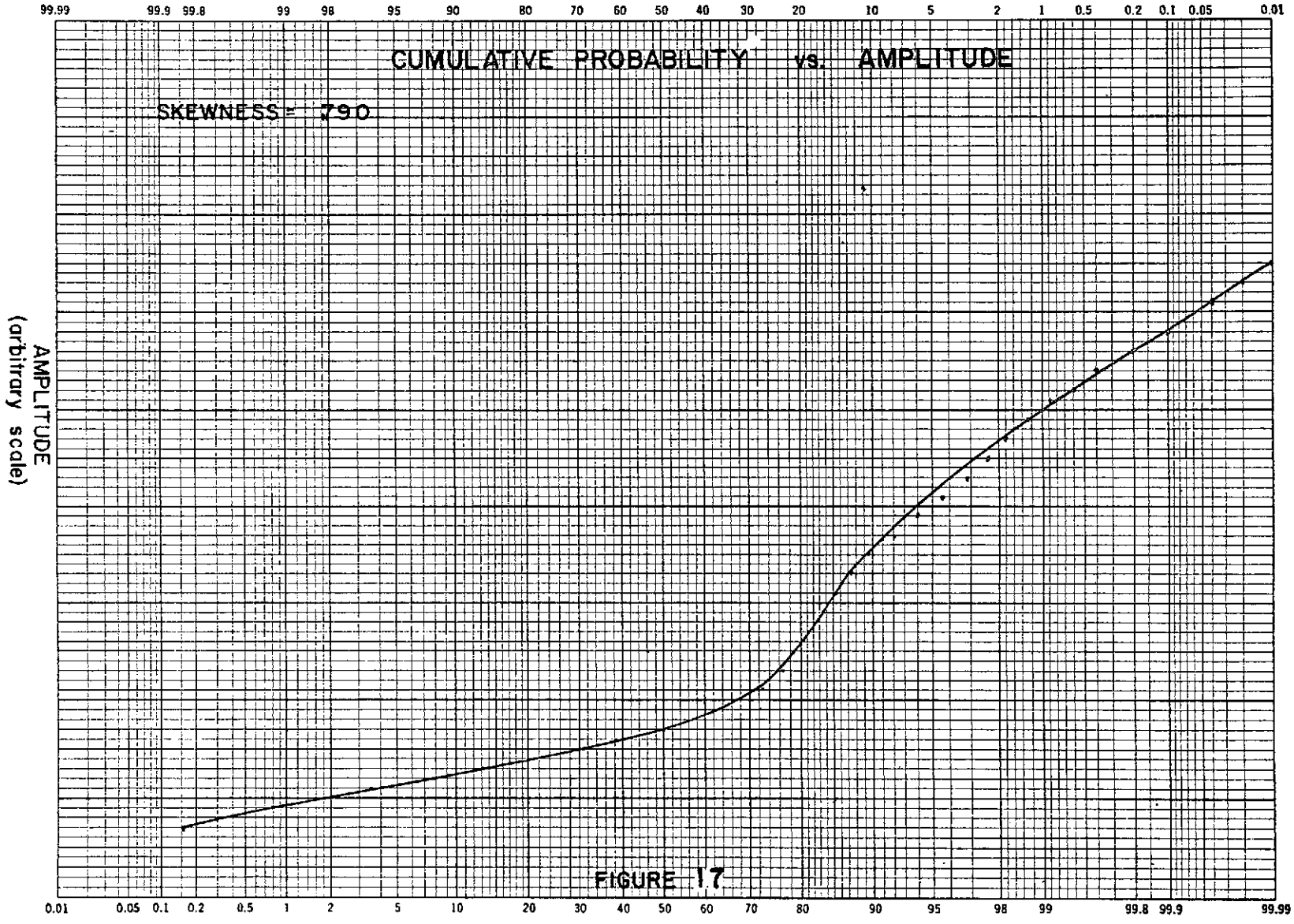
CUMULATIVE PROBABILITY vs. AMPLITUDE
SKEWNESS = .790
AMPLITUDE (arbitrary scale)
99.99 99.9 99.8 99 98 95 90 80 70 60 50 40 30 20 10 5 2 1 0.5 0.2 0.1 0.05 0.01
0.01 0.05 0.1 0.2 0.5 1 2 5 10 20 30 40 50 60 70 80 90 95 98 99 99.8 99.9 99.99

FIGURE 17

APERTURE SIZE (CM)	NUMBER OF RUNS				
	TOTAL	LOG NORMAL	NORMAL	NEITHER	BOTH
2	4	2	2	0	0
4	17	13	2	1	1
6	30	10	6	13	1
8	43	12	14	11	6
10	102	33	23	37	9

Table 1. Results of Statistical Analysis of Scintillation Measurements.

been tabulated. From this table we see that the two cm. aperture runs were divided equally between normal and log-normal distributions. The results for this aperture size are not considered significant since there were only four runs with small irregularities, and these were taken with a very weak signal. The four cm. runs, which had a reasonably small aperture, yet the recorded signal was strong, show a strong tendency toward log-normality. As the aperture increases the number of runs which differ from log-normal also increases. This behavior may be due to the effect of aperture averaging. Since this process is additive in nature, it would cause the distribution to tend toward a normal curve according to the Central Limit Theorem. This combined with the difficulty in distinguishing normal data from log-normal data could lead to results of the type exhibited by the larger aperture runs.

B. Calculation of Atmospheric Structure Constant

The refractive index structure constant was calculated using equation 4-5 and taking the measured value of the log-amplitude variance $C_\ell(0)$. This equation does not allow for aperture averaging effects. Values of C_n obtained ranged between $1.6 \times 10^{-8}\ M^{1/3}$ and $8.7 \times 10^{-8}\ M^{1/3}$ for a group of runs where the aperture was varied rapidly from two to ten cm. The structure constant computed from two cm. aperture data was usually larger than that computed from ten cm. aperture data by a factor of from two to four. The time required to collect the data for such a group of runs was less than ten minutes. As a comparison, several groups of runs were made in a similar time period holding the aperture constant. The observed variation in the structure constant for these runs was usually about ten percent. This clearly indicates that the observed variation in the structure constant was due to aperture

averaging effects and not to changes in the strength of turbulence between runs.

Using the techniques described in Chapter III, section D, calculations for the structure constant have been refined, allowing for the effects of aperture averaging. For the 212 segments of data which were analyzed, the values of the corrected structure constant ranged from $5.8 \times 10^{-7} M^{1/3}$ to $9.0 \times 10^{-7} M^{1/3}$. These values are characteristic of very strong atmospheric turbulence, which agree with our subjective observations of the scintillation while the data was being taken.

Table II shows four typical sets of runs for various aperture sizes. As can be seen, the variation in the structure constant is significantly reduced when the effects of aperture averaging are included.

It should be noted that the inclusion of aperture averaging effects has a tendency to overcorrect the structure constant variation. This could be an indication of a systematic error in recording the data. Another possibility is that the deep scintillation conditions under which the experimental data was collected produced saturation effects which have not been considered. On the other hand the validity of the basic approach to the problem of aperture averaging in terms of the structure function has been questioned[13]. Therefore it is possible that the aperture correction we have used is not valid. In any case, this method of compensating for aperture averaging effects is a good approximation since the structure constant is far more consistent when corrected than when aperture averaging effects are neglected.

C. Scintillation Frequency Spectrum

The frequency spectrum has been computed using the Fast Fourier

APERTURE SIZE (C M)	RUN 1		RUN 2		RUN 3		RUN 4	
	UNCOR C N	COR C N	UNCOR C N	COR C N	UNCOR C N	COR C N	UNCOR C N	COR C N
10	.878	7.50	.178	5.88	.179	5.88	.885	7.47
8	.686	7.50	.217	6.40	.241	6.48	.709	7.53
6	.547	7.61	.326	7.15	.425	7.35	.635	7.73
4	.563	8.05	.451	7.90	.617	8.10	.590	8.09
2			.550	8.77	.590	8.82	.565	8.79
MEAN	.662	7.67	.344	7.22	.410	733	679	7.92
%VARIATION	51.7	12.9	109	40	100	40.2	47.2	16.7

(C_N) IN $(\text{METERS})^{1/3} \times 10^{-7}$

Table 2. Comparison of Structure Constant Corrected for Aperture Averaging Effects with its Uncorrected Value.

Transform techniques described above. This calculation was performed only on selected data runs due to the time required for such a calculation. Also the computed spectra were very consistent so it was felt that analysis of additional runs would yield little additional information.

The computed spectra cover a range of frequencies from DC to 90 Hz, the upper limit being set by the 180 sample per second sampling rate. A typical spectrum is shown in Figure 18. Although the computer plotted frequency components out to 90 Hz only components out to 20 Hz are shown in the figure for the sake of clarity. Above 20 Hz the spectrum continued to decrease linearly so that no appreciable frequency components above 40 Hz were observed.

D. Heterodyne Detection

The effect of atmospheric turbulence on the performance of the equipment operating as a heterodyne communication system was investigated. This was accomplished by recording the amplitude of the 10 Mhz heterodyne signal at the output of the I. F. amplifier. Also the transmitter was modulated with a 1 Khz signal which was recorded at the output of the receiver's F. M. descriminator. It was found that neither signal showed any effect attributable to atmospheric turbulence large enough to be accurately measured. Even under conditions of deep scintillation encountered during the course of this experiment, the atmospherically induced noise was of the same magnitude or smaller than system noise. It was also found that clear voice communications were possible over this range under the worst conditions of scintillation encountered.

While these results clearly indicate the feasibility of using a

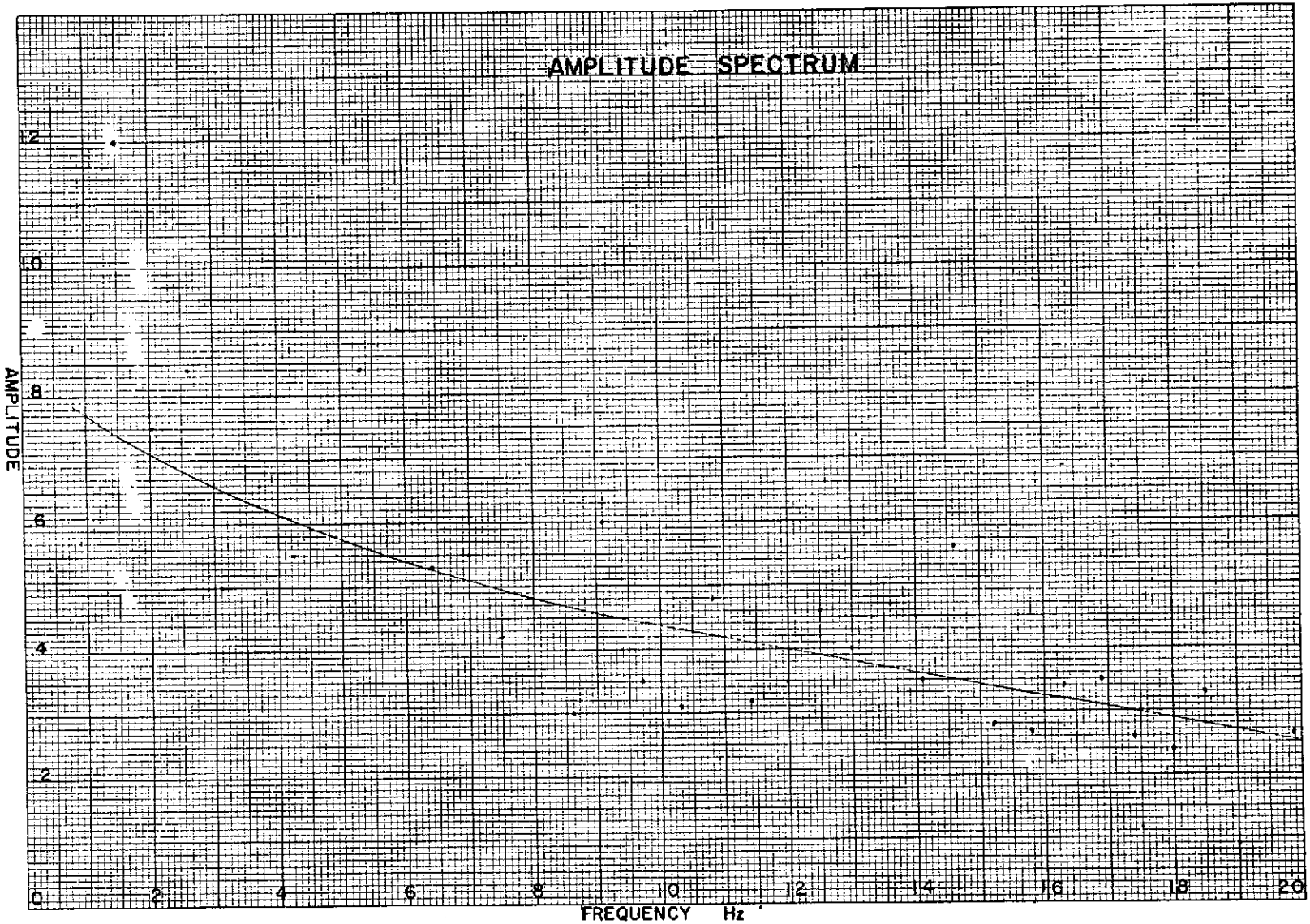
AMPLITUDE SPECTRUM
AMPLITUDE
12
10
8
6
4
2
0
2
4
6
8
10
12
14
16
18
20
FREQUENCY Hz

FIGURE 18

heterodyne CO_2 laser system to communicate through the earth atmosphere, they were somewhat disappointing since they did not permit a quantitative measurement of noise induced by atmospheric turbulence.

CHAPTER VI

SUMMARY AND CONCLUSION

The results of the scintillation measurements made on the 10.6 micron wave length laser beam tend to confirm the log-normal model for small receiver apertures. The data for the larger apertures did not seem to fit the log-normal or normal models with any consistency. One possible explanation for this could be aperture averaging. It is possible that the larger aperture sizes were not large enough with respect to the correlation distance to cause the distribution to be normal, but yet large enough to cause the distribution to deviate from log-normally. This in addition to the difficulty in distinguishing between the two distributions could have caused the results to be inconclusive.

The value of the refractive index structure constant computed was found to lie within the range of values for this constant as calculated by Fried. The value of this constant was found to decrease with increasing aperture size. Equations developed by Fried were used to correct the structure constant for aperture effects. This technique seemed to give a slightly larger value of the aperture averaging effect than was observed. Although this may indicate an inaccuracy in the theoretical expression, a systematic error in the experimental measurements cannot be firmly ruled out. These calculations were significant in that they indicated in a quantitative manner the nature of aperture averaging.

The spectral analysis indicated that low frequency components of the scintillation were predominant. The magnitude of the scintillation decreases linearly with increasing frequency. Above 20 Hz the

scintillation is negligible.

The feasibility of optical heterodyne communication at 10 microns through extreme turbulence was demonstrated. To our knowledge, this was the first system of this kind to be operated through the atmosphere at this path length. We feel that the successful operation of the communications system under extreme scintillation conditions was a significant result.

It would be a great advantage in this type experiment to reduce the data immediately after it is taken. Information gained from the speedy reduction should give the experimenter a knowledge of how the system is performing and aid in making better measurements.

As a result of performing this experiment and surveying the results of other investigations, it is clear that the atmospheric problem is far from being completely solved. The log-normal model needs to be further verified for other wave lengths. The variance and the structure constant should be investigated under as wide a variety of weather conditions as possible and should be correlated to the variations of the meterological parameters.

After having carried out this type experiment, the need for several refinements in the procedure was realized. Before any data is taken, a thorough analysis of system noise should be made. Sensitive noise measuring instruments should be employed. The noise of the transmitting laser should be recorded simultaneously with scintillation measurements. The background light effect should be further studied and perhaps a method other than signal chopping used to handle the problem. Mechanical stability of equipment is a problem that needs investigation since even very small vibrations could cause the beam to shift out of alignment

with the receiver.

Aperture averaging effects need to be investigated with many different size apertures for all wave lengths. The relationship between correlation distance and aperture size needs to be determined. The determination of correlation distance in itself would be an interesting experiment.

APPENDIX A

Introduction

This appendix further describes the computer program employed to reduce the atmospheric data. The program is written in Fortran IV language for the IBM-360 Model 50 computer at the University of Alabama. The program operates in the following manner: The MAIN or supervisory routine accepts instructional and operating data for the program. It reads the atmospheric data from the magnetic tape and calls subroutine EXT to extract the intensity signal. EXT calls on subroutines LIMIT, FILL, HIST, and AMPX to perform the extration. When a file of data has been processed MAIN calls subroutine PRINT to print a table of the irregularities that occurred during extraction. MAIN then calls subroutine STAT and/or FFT to perform the statistical and spectral analysis. STAT calls on subroutine CHI to perform the chi-square test which in turn calls on a Simpsons rule integration subroutine SIMP. FFT calls on two package subroutines FOURT and PLOT which perform and plot the spectral analysis.

Routine Main

Routine MAIN's first step is to read the identification record from the magnetic tape. This is done by calling subroutine RID. RID actually does the reading and stores the data in a common array to be printed by MAIN in the next step. The numerical instructions and operating constants are then read in as data on punched cards. These are read in as variable names and are used in the various subroutines and are discussed as part of the description of these subroutines.

Processing actually begins when MAIN reads in 4 additional instructional constants on punched cards. These are given according to their variable name as

NAME	FUNCTION
FILES	The number of the data file to be processed.
ISTART	The record number within the file from which data will start being taken.
ICHNO	The channel number of the magnetic tape to be processed.
IRCEND	The record number at which processing is to stop.

The values of these numerical constants enable the user to process any record or segment of records within a data file on any of the five channels. Each time a new file is to be processed these variables must be read in for the new file. The read statement for these variables is in a loop so that when processing of a file is completed the program returns to this statement to get instructions for processing the next file. After the last file has been processed the program is stopped by entering a negative number for the variable FILES.

The program now moves the tape to the desired file and record by calling subroutine REDREC. When the first record to be processed is found, it is stored in a common array IBUF. MAIN then transfers the data in IBUF into a work array P. REDREC is called again to read the next record which is transferred by MAIN into an auxilary array AUX. This is done in order to have the next record available in an array since it is sometimes necessary for the program to "look" into the following record before processing in a record is completed.

The record of data in array P is now processed by calling sub-

```
FORTRAN IV G LEVEL 1, MOD 4            MAIN              DATE = 70122          02/35/57

0001                INTEGER FILES,FILCK
0002                COMMON P(1000),AUX(1000),INDO(10),NCNT(300),JOVF,JUNF,
                   *BASE(2,10),SIG(10),IBLOC(2,10),KK,MM,XL90,XL10
                   *, DUMMY(2700)
0003                COMMON/AAA/IPRINT
0004                COMMON/AP/AMP(10000),NDATA
0005                COMMON/RLC/IRTN
0006                COMMON/RAT/IRCEND
0007                COMMON/GO/N1,N3,N4,FM,IDO
0008                COMMON/NPTS8/N8
0009                COMMON/PR/IE(7,300)
0010                COMMON/UUU/NPNCH
0011                DIMENSION IBUF(1000)
0012                DIMENSION IA(3),IB(5)
0013                CALL RID(I1,I2,IB)
0014                IF(I1) 155,150,155
0015          155   PRINT 157,FILCK
0016          157   FORMAT(' ***  END OF FILE  ***',I8)
0017           150  IF(I2) 158,161,158
0018          158   PRINT 159
0019          159   FORMAT('  ***  READ ERROR  ***')
0020           161  CONTINUE
0021                NTAPE=IB(1)
0022                PRINT 160,IB
0023          160   FORMAT('  TAPE NUMBER=',1A4,
                   1'  IDCAL=',1A4,
                   1'  BASE=',1A4,
                   1'  NUMBER OF CHANNELS=',1A4,
                   1'  NUMBER OF SCANS=',1A4)
0024                FILCK=1
0025                READ(5,9921) FMAX,DT,FM,N1,N3,N4,IDO,ISSB
0026          9921  FORMAT(3E10.0,5I10)
0027                READ(5,3350)IPRINT,NPNCH
0028          3350  FORMAT(2I10)
              C     READ INSTRUCTIONS AND TOLERANCES
0029                READ(5,360)  IBTYP,IFLAG,NCI,NOSCAN,NOCHAN,L1,L2
0030          360   FORMAT(7I10)
0031                READ(5,1991) TOL1,TOL2,TOL3
0032          1991  FORMAT(3E10.0)
0033                PRINT 361,IBTYP,IFLAG,NCI,NOSCAN,NOCHAN,TOL1,TOL2,TOL3,L1,L2
0034          361   FORMAT('  TYPE BASE CALCULATION  **********************************
                   ******  ***** IBTYP     *****     'I10/,
                   *'  TYPE STATISTICS CALLED FOR  **********************************
                   ****** IFLAG     *****     ',I10/,
                   *'  NUMBER OF CLASS INTERVALS  **********************************
                   ****** NCI       *****     ',I10/,
                   *'  NUMBER OF SCANS PER RECORD  *********************************
                   ****** NOSCAN    *****     ',I10/,
                   *'  NUMBER OF CHANNELS ON TAPE  *********************************
                   ****** NOCHAN    *****     ',I10/,
                   *'  TOLERANCE ON BASE LIMITS  ***********************************
                   ****** TOL1      *****     ',F10.3/,
                   *'  TOLERANCE ON SIGNAL LIMITS  *********************************
                   ****** TOL2      *****     ',F10.3/,
                   *'  NUMBER OF SIGNAL AND BASE POINTS REQUIRED PER CYCLE  ********
                   ****** TOL3      *****     ',F10.3/,
```

```
FORTRAN IV G LEVEL 1, MOD 4            MAIN              DATE = 70122          02/35/57

                *'  NUMBER OF PASSES REQUIRED TO ABORT CYCLE  ********************
                ****** L1        *****      ',I10/,
                *'  NUMBER OF BASE POINTS REQUIRED FOR SIGNAL POINT SEARCH  *****
                ****** L2        *****      ',I10)
0035             PRINT 9111,NPNCH,IPRINT,ISSB,FMAX,DT,FM,N1,N3,N4,IDO
0036           9111 FORMAT('  PUNCHED OUTPUT FLAG  ************************************
                ******  ***** NPNCH     *****      ',I10/,
                *'  PRINT ERROR TABLE FLAG  ************************************
                ****** IPRINT     *****      ',I10/,
                *'  TYPE ANALYSIS ROUTINE WANTED  ********************************
                ****** ISSB       *****      ',I10/,
                *'  INFORMATION FOR FFT ROUTINE  *********************************
                ****** FMAX       *****      ',F10.3/,65X,'***** DT          *****
                *',F10.3/,65X,'***** FM          *****      ',F10.3/,65X,'***** N1
                *    *****      ',I10/,65X,'***** N3         *****      ',I10/,65X,'**
                **** N4         *****      ',I10/,65X,'***** IDO        *****      ',I1
                *0/)
              C      READ DATA FOR TAPE PROCESSING
0037                 LFILE=0
0038             511 READ(5,882)FILES,ISTART,ICHNO,IRCEND
0039                 N8=0
0040                 NDATA=0.0
0041                 DO 8892 LJ=1,7
0042                 DO 8892 JI=1,300
0043            8892 IE(IJ,JI)=0
0044                 IRECNT=ISTART-1
0045                 IEXIT=0
0046                 IF(FILES-LFILE)22,22,987
0047            987  IREC=0
0048            22   CONTINUE
0049                 LFILE=FILES
0050            882  FORMAT(4I3)
0051                 PRINT 901,FILES,ICHNO,ISTART,IRCEND
0052            901  FORMAT(1H1,'     PROCESSING FILE **********',I5/,
                *'     CHANNEL *****************************',I5/,
                *'     BEGIN AT RECORD **********************',I5/,
                *'     STOP PROCESSING AT RECORD ************',I5)
0053                  IRTN=1
0054                 IF(FILES)991,9,9
0055            991  PRINT 992
0056            992  FORMAT(10X,'******  PROGRAM STOP *****')
0057                 STOP
0058            9    CALL REDREC(FILES,IREC,FILCK,IBUF,TIME,N,NOSCAN,NOCHAN,ICHNO)
              C      MOVE TAPE TO DESIRED FILE
0059                 IF(FILCK-FILES)9,887,887
              C      READ RECORD, STORE RECORD IN ARRAY IBUF
0060            887  CALL REDREC(FILES,IREC,FILCK,IBUF,TIME,N,NOSCAN,NOCHAN,ICHNO)
              C      MOVE TAPE TO DESIRED RECORD
0061                 IF(IREC-ISTART)887,889,889
              C      STORE CONTENTS OF IBUF INTO MAIN ARRAY P
0062            889  DO 888 L=1,N
0063            888  P(L)=IBUF(L)
              C      READ NEXT RECORD INTO IBUF
0064                 CALL RED REC(FILES,IREC,FILCK,IBUF,TIME,N,NOSCAN,NOCHAN,ICHNO)
              C      STORE CONTENTS OF IBUF INTO AUXILIARY ARRAY AUX
0065                 DO 500 L=1,N
```

```
FORTRAN IV G LEVEL 1, MOD 4            MAIN              DATE = 70122          02/35/57

0066          500  AUX(L)=IBUF(L)
0067               GO TO 501
0068          502  DO 503 L=1,N
0069          503  P(L)=AUX(L)
0070               CALL RED REC(FILES,IREC,FILCK,IBUF,TIME,N,NOSCAN,NOCHAN,ICHNO)
              C    STORE IBUF INTO AUX
0071               DO 504 L=1,N
0072          504  AUX(L)=IBUF(L)
0073          501  CALL EXT(N,L1,L2,IRECNT,TOL1,TOL2,TOL3,NCI,IBTYP)
              C    STOP PROCESSING ON DESIRED RECORD
0074               IF(IEXIT) 1000,1000,507
0075         1000  IF(NDATA.EQ.10000) GO TO 507
0076          661  IF(IREC-IRCEND) 502,221,221
0077          221  DO 2293 I=1,N
0078          2293 P(I)=AUX(I)
0079               IEXIT=1
0080               GO TO 501
              C    PRINT ERROR TABLE
0081            507 CALL PRINT(1)
0082               IF(ISSB.EQ.2) GO TO 2514
0083                     CALL FFT(N,DT,PMAX)
0084               IF(ISSB.EQ.1) GO TO 511
0085          2514 CALL STAT.(NTAPE,ICHNO,FILES,NCI,IFLAG)
0086               GO TO 511
0087               END
```

routine EXT. When EXT completes the processing it returns program control to MAIN. The program checks the variable IEXIT to see if the record just processed is the last record in the file. If it is not, the program checks to see if the next record is the last. If this record is not the last, the program calls in the next record and continues processing. However, if it is the last record in the file to be processed, the program transfers the contents of the AUX array (which contains the last record) into work array P. IEXIT is set to 1 and EXT called to process the last record. When EXT returns program control to MAIN, IEXIT indicates that processing of this file has been completed.

The program then calls subroutine PRINT to print the irregularity table. The analysis of the extracted signal continues by calling the statistical analysis subroutine STAT or the spectral analysis subroutine FFT. When the analysis is completed for this file of data, control is returned to MAIN which loops back to read the instructions for the next file to be processed.

Subroutines

A description of the subroutines called in the program is given in this section. The only subroutines not listed are FOURT and PLOT, since they were used in a package furnished by the computer department. A Fortran list is included after the description of each subroutine.

SUBROUTINE RID (13, 14, IC)

This subroutine reads the identification file which is the first file on the tape. This routine uses 3 subroutines that are especially written for the University of Alabama IBM-360 Model 50 computer. The first, NTRAN, actually reads the tape and stores the data into an array.

The data is then transferred from this array and decoded for system compatibility using utility subroutines MOVE and TRNSL. This routine would probably require modification or rewriting if it were used on another machine.

SUBROUTINE REDREC (FILES, IREC, FLICK, IBUF, TIME, N, NOSCAN, NOCHNO, ICHNO)

Subroutine REDREC is called by MAIN to read and reformat the data from the magnetic tape. REDREC calls on the special utility subroutine, NTRAN to read the tape. Utility subroutines MOVE and TRNSL are called to convert the 7 track tape output into the byte system. REDREC must unpack from the multiplexed data the desired channel and convert the binary code to conventional base ten numbers. It must also keep up with the record and file number that it is reading. Provisions were made in REDREC to indicate read errors that might occur in NTRAN. This subroutine would probably require modification if used on another machine.

Argument Variables

FILES - Number of files to be processed.

IREC - Record number as counted by REDREC.

FLICK - File number as counted by REDREC.

IBUF - Array containing raw data.

TIME - Not used.

N - Number of data points per record (either 200 or 1000).

NOSCAN - Number of scans per record per channel (either 200 or 1000).

NOCHAN - Number of channels multiplexed on the tape.

ICHNO - Channel number to be processed.

```
FORTRAN IV G LEVEL 1, MOD 4            RID                DATE = 70122          02/35/57

0001                SUBROUTINE RID(I3,I4,IC)
0002                INTEGER IB(5),IA(3), BUF(501),FLCNT,TTB(3),BLK,FILES,FILCK,
                   *IBUF(1),IC(1)
0003                M=1
0004                I1=0
0005                I2=0
0006           5    CALL NTRAN(1,2,3,IA,K,2,-2004,BUF,L,22)
0007           2    IF(K+1) 1,2,3
0008           3    CALL MOVE(IB,1,IA,1,4)
0009                CALL TRNSL(IB,4,TTB)
0010                DATA TTB/'0123456789'/
0011                DATA BLK /' '/
0012                IB(2)=BLK
0013                CALL MOVE(IB(2),1,IA,5,1)
0014                CALL TRNSL(IB(2),1,TTB)
0015                IB(3)=BLK
0016                CALL MOVE(IB(3),1,IA,6,1)
0017                CALL TRNSL(IB(3),1,TTB)
0018                IB(4)=BLK
0019                CALL MOVE(IB(4),1,IA,7,2)
0020                CALL TRNSL(IB(4),2,TTB)
0021                CALL MOVE(IB(5),1,IA,9,4)
0022                CALL TRNSL(IB(5),4,TTB)
0023                GO TO (6,7), M
0024           6    DO 14 I=1,5
0025          14    IC(I)=IB(I)
0026                I3=I1
0027                I4=I2
0028                RETURN
0029           1    IF(K.EQ.-2) GO TO 4
0030                I2=1
0031                CALL NTRAN(1,22)
0032                GO TO (6,7),M
0033           4    I1=1
0034                CALL NTRAN(1,22)
0035                GO TO (6,7),M
0036                ENTRY REDREC(FILES,IREC,FILCK,IBUF,TIME,N,NOSCAN,NOCHAN,ICHNO)
0037                M=2
0038          13    IREC=IREC+1
0039                CALL NTRAN(1,22)
0040           9    IF(L+1)8,9,10
0041          10    TIME=BUF(1)
0042                N=(L-4)/(2*NOCHAN)
0043                K=3+2*ICHNO
0044                DO 11 I=1,N
0045                IBUF(I)=0
0046                J=0
0047                CALL MOVE(J,4,BUF(1),K,1)
0048                CALL MOVE(IBUF(I),4,BUF(1),K+1,1)
0049                IBUF(I)=IBUF(I) + 64*J
0050                IF(IBUF(I).GE.1024) IBUF(I)=1024-IBUF(I)
0051          11    K=K+2*NOCHAN
0052                CALL NTRAN(1,2,-2004,BUF,L)
0053                RETURN
0054           8    IF(L.EQ.-2) GO TO 12
0055                PRINT 100
```

```
FORTRAN IV G LEVEL 1, MOD 4            RID                DATE = 70122        02/35/57

0056          100  FORMAT('0******  READ ERROR  ******')
0057               CALL NTRAN(1,22)
0058               CALL NTRAN(1,2,-2004,BUF,L)
0059               GO TO 13
0060          12   CONTINUE
0061               FILCK=FILCK+1
0062               CALL NTRAN(1,22)
0063               GO TO 5
0064          7    CONTINUE
0065               IREC=0
0066               GO TO 13
0067               END
```

SUBROUTINE EXT (NK, L1, L2, IREC, TOL1, TOL2, TOL3, NCI, IBTYP)

This subroutine is by far the most complex routine in the program. It extracts the intensity amplitudes from the chopped data. A written explanation of EXT will not be given due to its complexity. Included instead is a flow diagram. It is hoped that the interested reader can use the description given in the text along with the flow chart to understand the operation of this routine. As an additional aid, the important variable names are given a brief description.

Argument Variables

NK - Number of data points per record.

L1 - Number of sequential searches for base and signal points allowed before cycle is aborted.

L2 - Number of base points required for projected signal point search.

IREC - Record number being processed.

TOL1 - Sets tolerance on base limits for base point selection.

TOL2 - Sets tolerance on signal limits for signal point selection.

TOL3 - Number of signal and base points required for a normal cycle.

NCI - Number of class intervals. See subroutine HIST.

IBTYP - Type base calculation. See subroutine HIST.

Common Block Variables

P - Work array containing record of data points being processed.

AUX - Auxillary array containing the next record to be processed.

INDO - Array containing position in the data array from which the signal points came.

JOVF - Number of overflows in HIST. Variable is initialized in EXT.

JUNF - Number of underflows in HIST. Variable is initialized in EXT.

BASE - Array containing both groups of base points.

SIG - Array containing signal points .

I BLOC - Array containing position in the data array P from which each group of base points came.

L, M - When EXT calls subroutine LIMIT, it gives it the initial position L and the final position M LIMIT is to scan in the data array.

XL90 - This is the result of calling LIMIT and is the criteria for selecting base points.

XL10 - Also the result of LIMIT and is the criteria for selecting signal points.

Labeled Common Variables

IPRINT - If IPRINT is other than 0, EXT will print the record if any irregularities occur while the record is being processed. If IPRINT = 0 it will avoid printing.

IRTN - Place keeper for subroutine EXT. The subroutine may be in any part of its cycle when it completes a record since data is continuous from record to record. IRTN is set to a number corresponding to the exit point in the routine when it returns to the MAIN routine for a new record. When subroutine EXT is recalled, a computed GO TO statement keyed to IRTN returns control to the phase EXT was previously in.

IE - Array passed to subroutine print which contains the errors accumulated for each record.

IBCNT - Array containing the number of base points in each group.

ISCT - Number of signal points.

Important Internal Variables

IRUN - IRUN = 1 indicates routine in start up cycle. Converse for IRUN = 0.

INDX - The value of this variable indicates the position (1-200) in the record being processed.

IDINX - The number of positions subroutine FILL must place zeros due to irregularities which cause data points to be skipped.

NP - Count of unsuccessful passes through signal and base search cycle.

IBC - Indicates which group of base points are being searched for.

LC - Indicates loop condition. LC = 0 means routine is the base point search phase; LC = 1 indicates signal point search.

INP - Counts the times the error recycle phase is entered.

SUBROUTINES HIST (BA, IDUM, NCI, IBTYP, IRUN)

This routine is called by EXT to compute the amplitude of the chopped wave and constructs a histogram with the results. The routine is designed to use numbers between 0 - 1000 but can be easily modified to handle a larger range. The histogram is stored in a common array to be used by the statistical analysis subroutine STAT.

Argument Variables

BA - Average of the base points.

NCI - Number of class intervals for histogram.

IBTYP - Determines the method to be used to calculate the amplitude. If IBTYP = 0, amplitudes are calculated by taking the difference between the signal points and the average of the base points in both groups. If IBTYP = 1, calculation will be the difference between the first signal point and the last base point of group 1, and the difference between the last signal point and the first base point of group 2. If IBTYP = 3, calculation is performed only on the last base point of group 1 and the first signal point.

IRUN - If equal to 1, indicates that EXT is in its first cycle.

Common Block Variables

NCNT - Array containing frequency for each class interval.

JOVF - Number of overflows or excessively large numbers resulting from classifications of amplitudes.

JUNF - Number of underflows or very small numbers resulting from classification of amplitudes.

BASE - Array containing two groups of base points.

SIG - Array containing signal points.

```
FORTRAN IV G LEVEL 1, MOD 4            EXT                DATE = 70122          02/35/57

0001                SUBROUTINE EXT(NK,L1,L2,IREC,TOL1,TOL2,TOL3,NCI,IBTYP)
0002                COMMON P(1000),AUX(1000),INDO(10),NCNT(300),JOVF,JUNF,
                   *BASE(2,10),SIG(10),IBLOC(2,10),L,M,XL90,XL10
0003                COMMON/AAA/IPRINT
0004                COMMON/BLC/IRTN
0005                COMMON/PR/IE(7,300)
0006                COMMON/CBA/IBCNT(2),ISCT
0007                IREC=IREC+1
0008                IST=IST + 1
0009                INP=0
0010                INO=1
0011                INDX=1
0012                GO TO (150,11,12,150,776),IRTN
0013             150  IRUN=1
0014                IRP=0
0015                IST=0
0016                L=1
0017                M=20
0018                IF(IRTN.EQ.4)  GO TO 209
0019                DO 1050 I=1,300
0020            1050  NCNT(I)=0
0021                JOVF=0
0022                JUNF=0
0023                NDATA=0
0024             209  CALL LIMIT(TOL1,TOL2,NK)
                C       SEARCH FOR FIRST BASE POINT- HOLD VALUE OF INDX
0025             776  DO 1 I=L,M
0026                IF(I.GT.NK) GO TO 2000
0027                IF(P(I)-XL90) 1,3,3
0028             3     INDX=I
0029                GO TO 4
0030             1     CONTINUE
0031                IE(1,IREC)=IE(1,IREC)+1
0032                IRTN=4
                C       RETURN TO DRIVER FOR NEXT RECORD
0033                RETURN
0034             2000 L=1
0035                M=M-NK
0036                IRTN=5
0037                RETURN
0038                4 M=INDX+15
0039                L=INDX
0040                CALL LIMIT(TOL1,TOL2,NK)
0041                IDINX=IABS(INDX-INO)
0042                CALL FILL(IDINX)
0043                INO=INDX
0044                IBC=1
0045                IBCNT(1)=0
0046                IBCNT(2)=0
0047                ISCT=0
0048             10   LC=0
0049                NP=0
                C       BASE POINT SEARCH
0050             11   IF(P(INDX)-XL90)  12,13,13
0051             13   IBCNT(IBC)=IBCNT(IBC)  +1
0052                I=IBCNT(IBC)
```

```
FORTRAN IV G LEVEL 1, MOD 4            EXT              DATE = 70122        02/35/57

              C      STORE BASE POINT
0053                 BASE(IBC,I)=P(INDX)
0054                 IBLOC(IBC,I)=INDX
0055                 IF(IBCNT(IBC)-10) 14,401,401
0056           401   IRTN=4
0057                 IE(2,IREC)=IE(2,IREC)+1
0058                 IDINX=NK-INDX
0059                 CALL FILL(IDINX)
0060                 RETURN
0061           14    INDX=INDX + 1
0062                 INO=INDX
0063                 IF(INDX-NK) 11,11,158
0064           158   IRTN=2
              C      NORMAL RETURN TO DRIVER FOR NEXT RECORD
0065                 RETURN
              C      SIGNAL POINT SEARCH
0066           12    IF(P(INDX)-XL10) 20,20,15
0067           15    IF(LC) 16,16,21
0068           16    NP=NP+1
              C      CHECK NUMBER OF UNSUCESSFUL PASSES
0069                 IF(NP-L1) 1944, 1944, 208
0070           1944  IF(ISCT.EQ.0) GO TO 14
0071                 GO TO 70
0072           21    IF(P(INDX)-XL90) 22,30,30
0073             30  IF(IRUN)10,10,31
              C      SET BASE COUNT INDX CONDITION
0074           31    IF(IBC-1)34,33,34
0075           33    IBC=2
0076                 GO TO 10
0077           34    IBC=1
0078           20    IF(IRUN) 23,23,24
              C      CHECK LOOP CONDITION
0079           23    IF(LC) 40,40,29
0080           24    IF(IBC-1) 25,25,40
0081           25    LC=1
0082                 NP=0
0083           29    ISCT=ISCT + 1
              C      STORE SIGNAL POINT
0084                 SIG(ISCT)=P(INDX)
0085                 INDO(ISCT)=INDX
0086                 IF(ISCT-10) 26,501,501
0087           501   IRTN=4
0088                 IE(3,IREC)=IE(3,IREC)+1
0089                 IDINX=NK-INDX
0090                 CALL FILL(IDINX)
0091                 RETURN
0092           26    INDX=INDX+1
0093                 INO=INDX
0094                 IF(INDX-NK) 12,12,162
0095           162   IRTN=3
              C      NORMAL RETURN TO DRIVER FOR NEXT RECORD
0096                 RETURN
0097           22    NP=NP+1
0098                 IF(NP-L1) 26,26,208
              C      CHECK NUMBER OF BASE AND SIGNAL POINTS
0099           40    IF(IBCNT(1).LT.TOL3) GO TO 222
```

```
0100              IF(IBCNT(2).LT.TOL3) GO TO 222
0101              IF(ISCT.LT.TOL3) GO TO 224
0102              GO TO 100
0103           222 IE(4,IREC)=IE(4,IREC)+1
0104              GO TO 555
0105           224 IE(5,IREC)=IE(5,IREC)+1
0106              GO TO 555
                C     ENTER ERROR RECYCLE
0107           208 IE(6,IREC)=IE(6,IREC)+1
0108           555 L=INDX
0109              M=INDX+20
0110              IRUN=1
0111              IF(IPRINT.EQ.0) GO TO 742
0112              PRINT 666,IREC,INDX
0113           666 FORMAT(1X,'IREC=',I10,10X,'INDX=',I10)
0114              IF(IREC.EQ.IRP) GO TO 742
0115              PRINT 333,(P(I),I=1,NK)
0116           333 FORMAT(1X,/,(1X,10F10.3))
0117              IRP=IREC
0118           742 CONTINUE
0119              INP=INP+1
0120              IF(INP-5)209,921,921
0121           921 IE(7,IREC)=IE(7,IREC)+1
0122              IBTN  = 4
0123              IDINX=NK-INDX
0124              CALL FILL(IDINX)
0125              RETURN
                C     POINT SEARCH CYCLE COMPLETE
0126           100 SUM1=0.0
0127              SUM2=0.0
0128              I=IBCNT(1)
                C     PREPROSSING FOR HISTOGRAM FOLLOWS
0129              DO 101 J=1,I
0130           101 SUM1=SUM1+ BASE(1,J)
0131              I=IBCNT(2)
0132              DO 102 J=1,I
0133           102 SUM2=SUM2 +BASE(2,J)
0134              BA=(SUM1+SUM2)/(IBCNT(1) +IBCNT(2))
0135              CALL AMPX(IRUN)
0136              CALL HIST(BA,NK,NCI,IBTYP,IRUN)
0137           43  IF(IBC-1) 44,45,44
0138           45  IBC=2
0139              GO TO 46
0140           44  IBC=1
0141           46  ISCT=0
0142              IBCNT(IBC)=0
0143              LC=1
0144              NP=0
0145              IRUN=0
0146              INDX2=INDX+9
0147              L=INDX
0148              M=INDX2
0149              CALL LIMIT(TOL1,TOL2,NK)
0150              GO TO 12
                C     LOOK INTO NEXT RECORD FOR SIGNAL POINT
0151           70  IF(IBCNT(IBC)-L2) 14,72,72
```

```
0152          72    L=INDX
0153                N=INDX + 9
0154                CALL LIMIT(TOL1,TOL2,NK)
0155                IF(P(INDX)-XL10) 20,20,14
0156                END
```

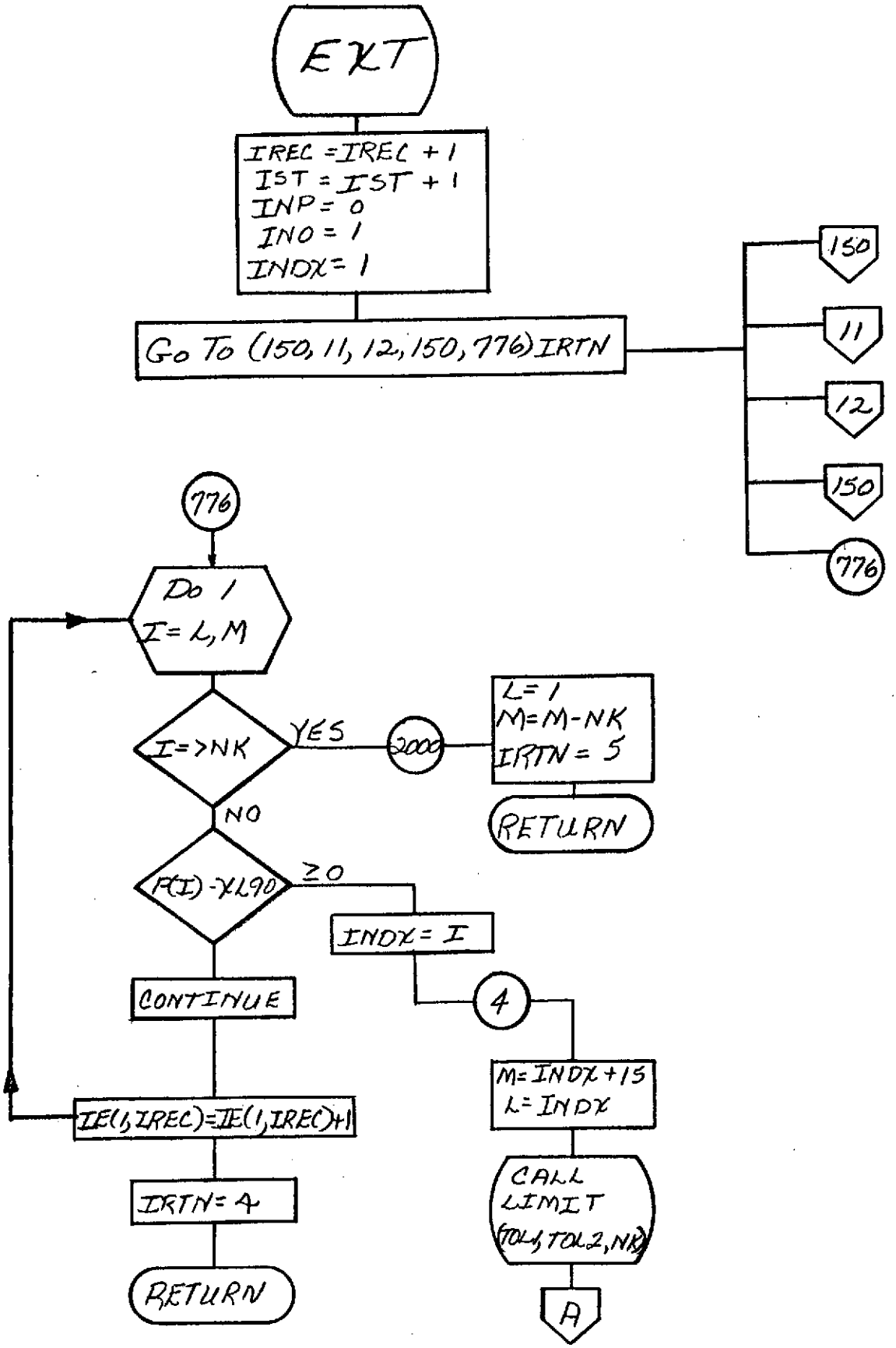

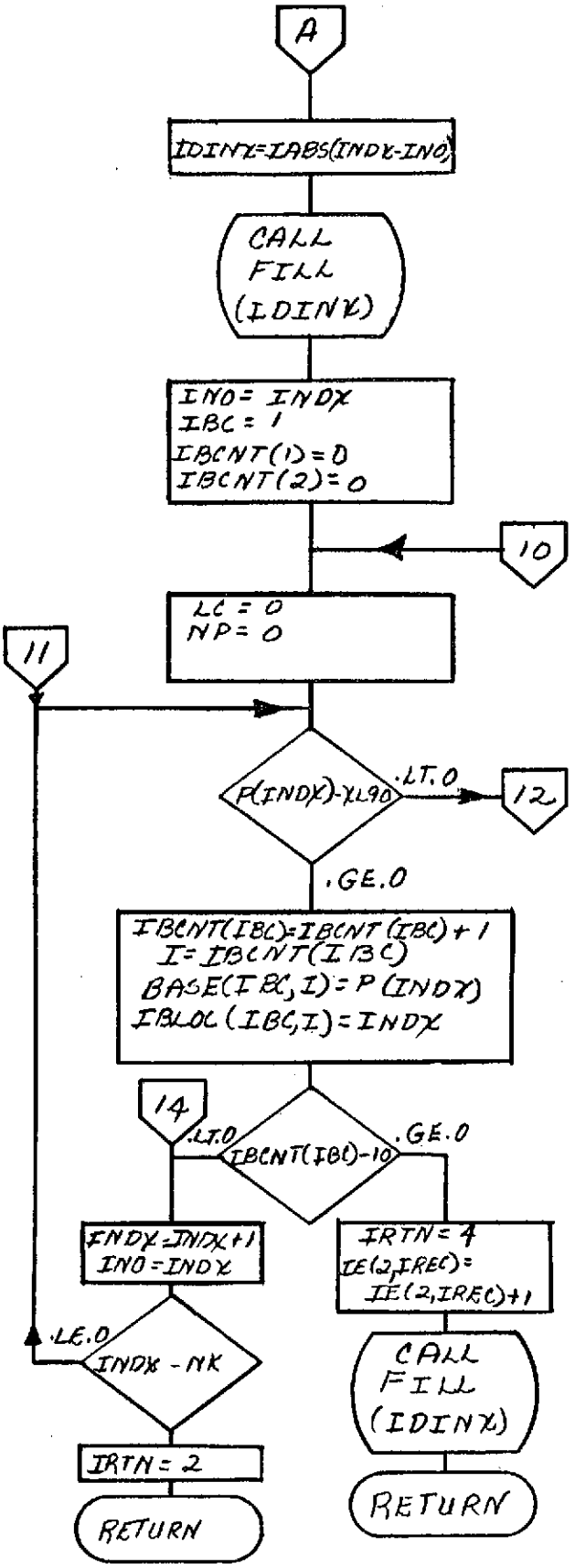

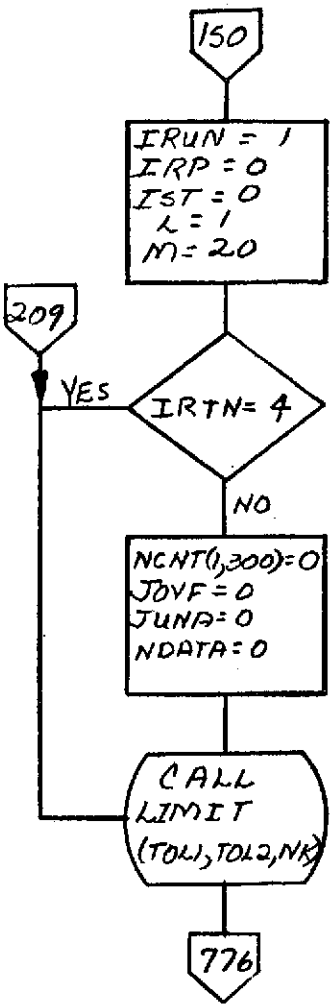

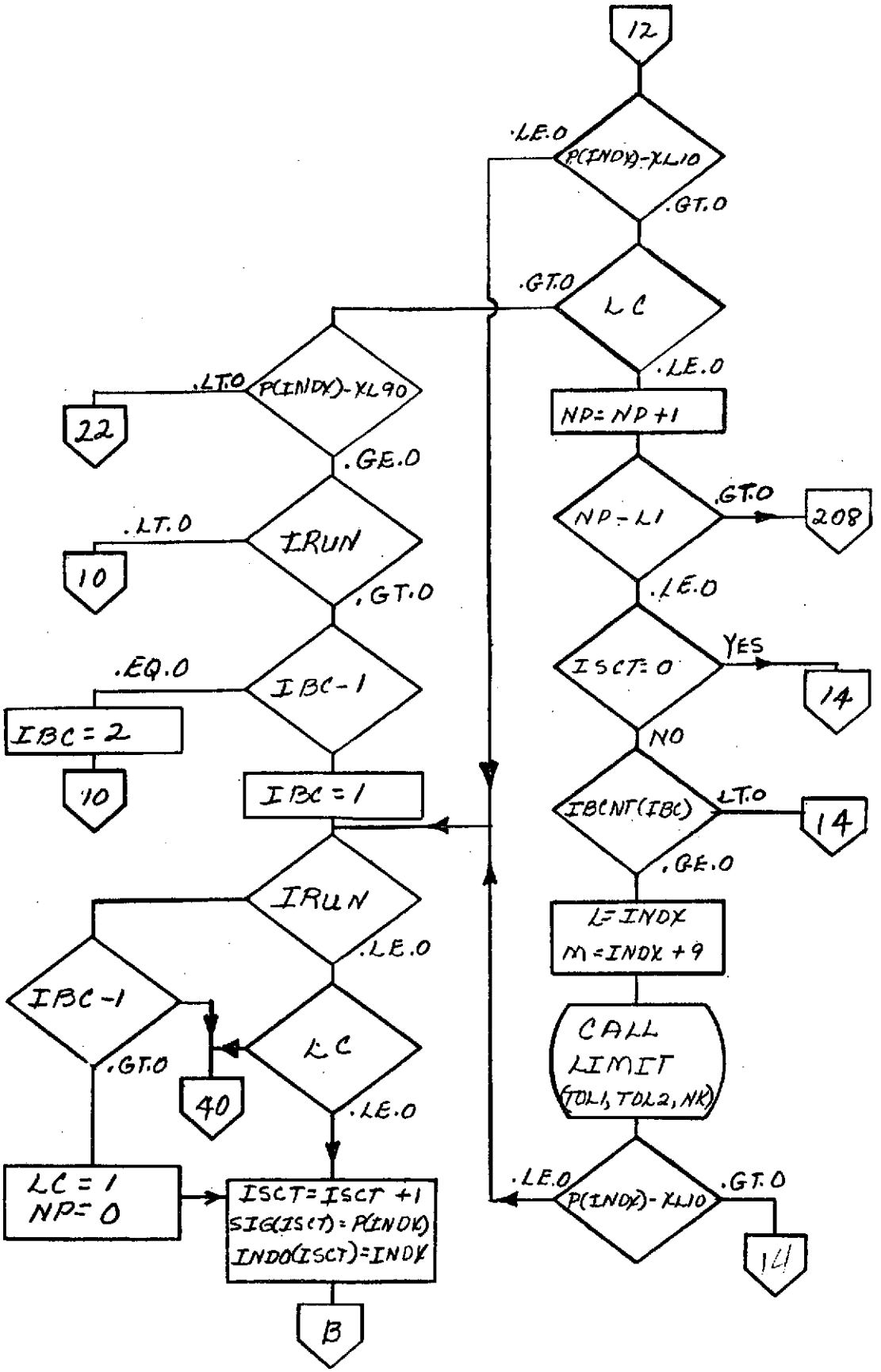

ORIGINAL PAGE IS
OF POOR QUALITY

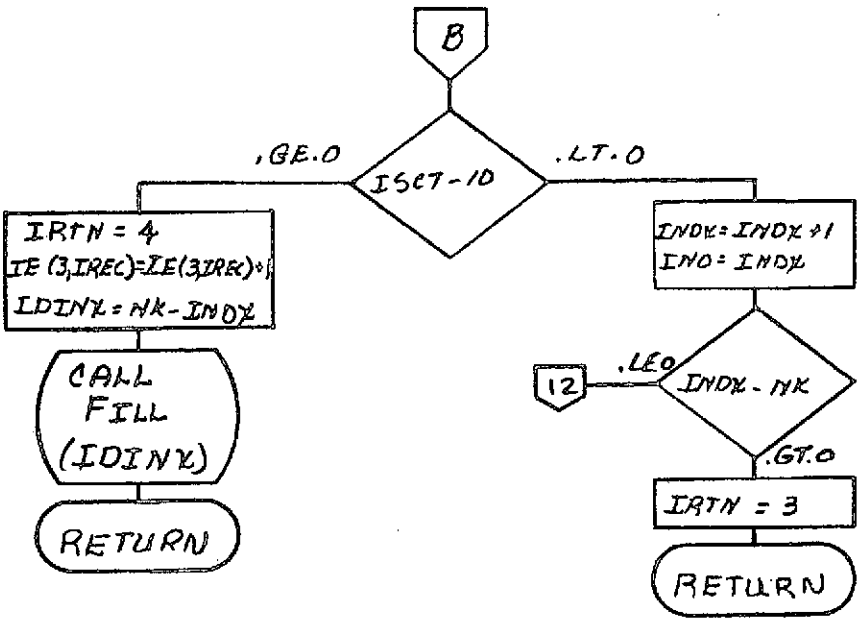

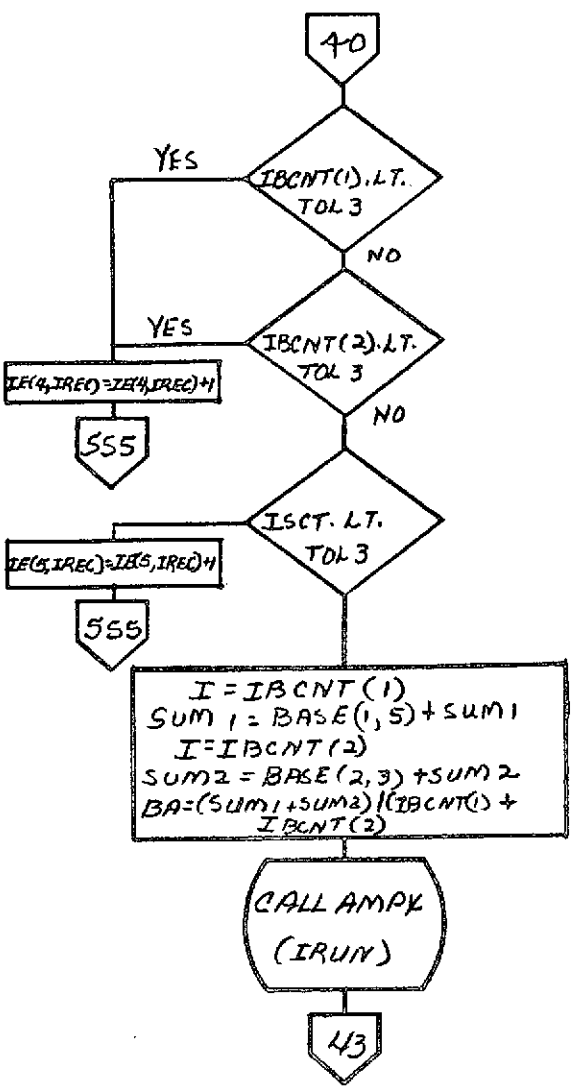

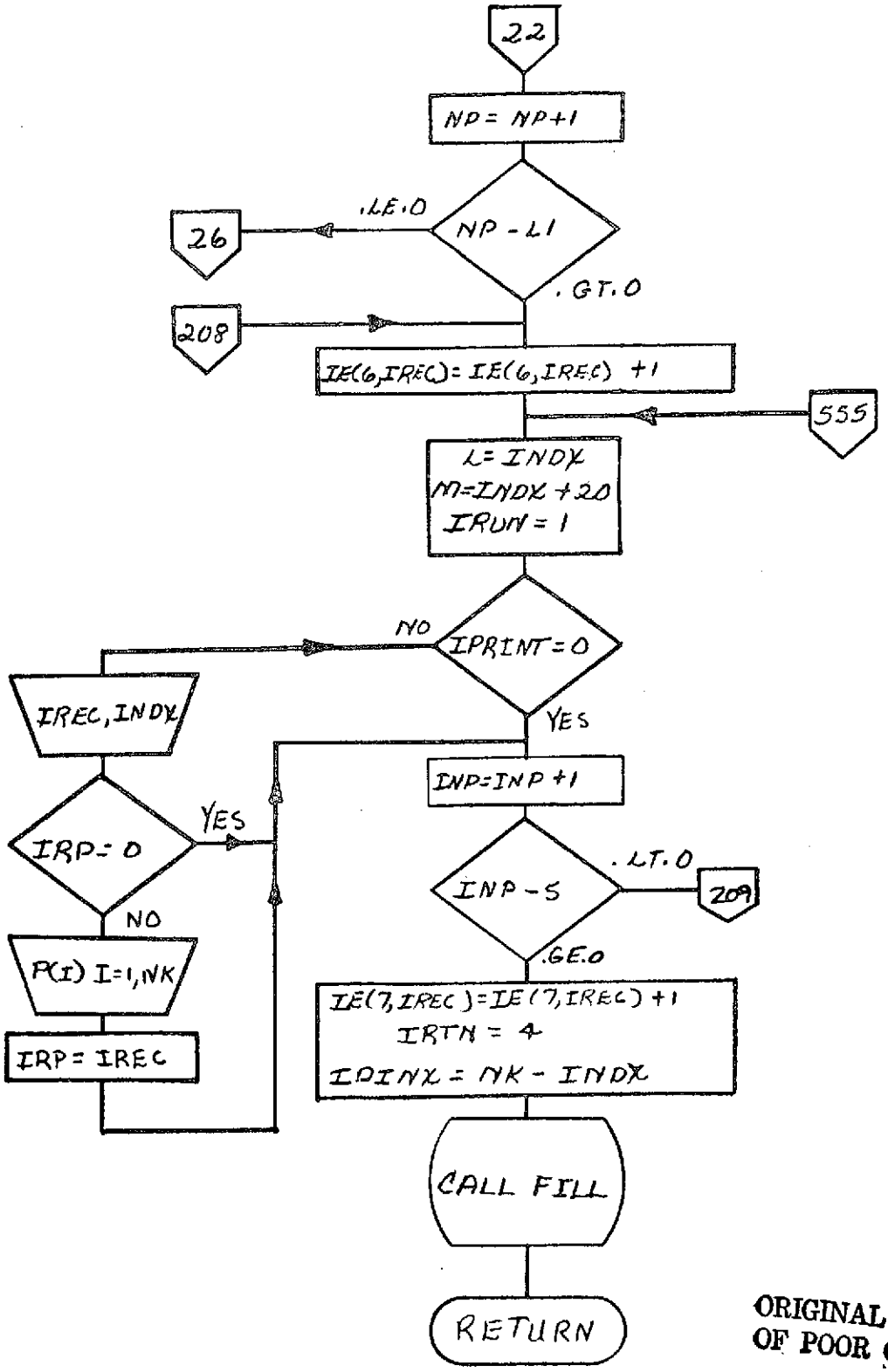

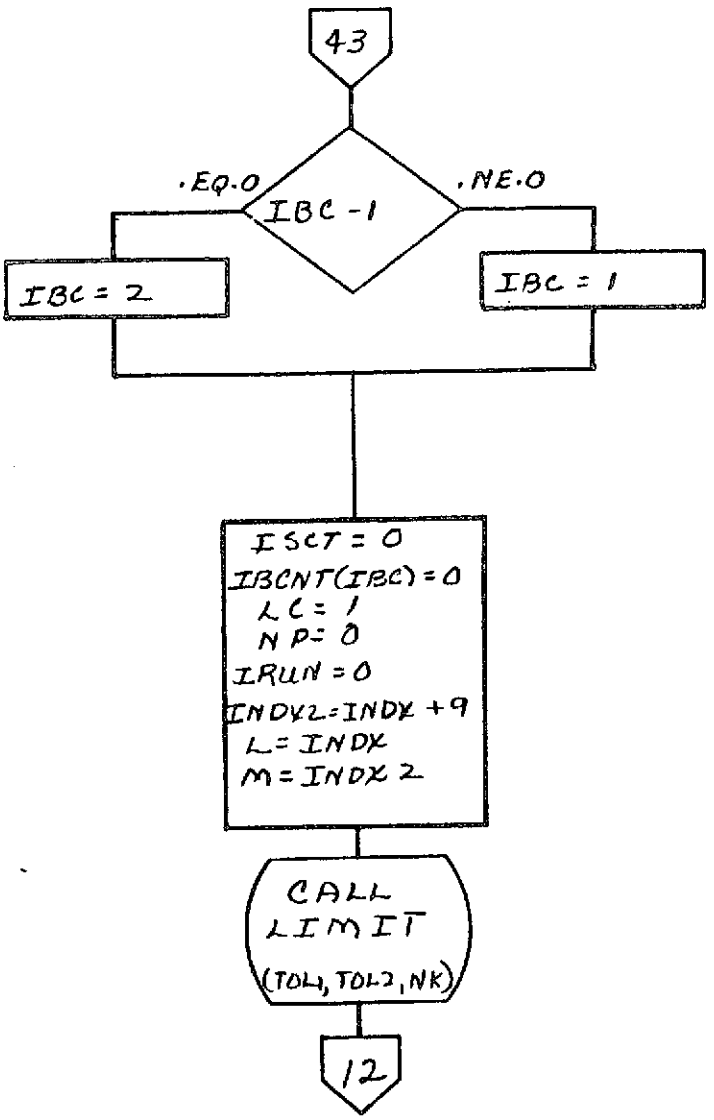

```
FORTRAN IV G LEVEL 1, MOD 4            HIST              DATE = 70122          02/35/57

0001                  SUBROUTINE HIST(BA,IDUM,NCI,IBTYP,IRUN)
0002                  COMMON P(1000),AUX(1000),INDO(10),NCNT(300),JOVF,JUNF,
                     *BASE(2,10),SIG(10),IBLOC(2,10),KK,MM,XL90,XL10
0003                  DIMENSION Y(40), X(40), LOC(40), A(15), V(15), B(200)
0004                  COMMON/CBA/IBCNT(2),N
                C     COMBINE BASE 1 AND BASE 2
0005                  IF(IBTYP) 100,100,200
0006                200 IF(IRUN.EQ.1) MMM=1
0007                  KKK=1
0008                  LLL=1
0009                  IF(MMM.EQ.1) LLL=2
0010                  IF(MMM.EQ.0) KKK=2
0011                100 IJ=N
0012                  DO 1 I=1,N
0013                  IF(IBTYP.EQ.0) GO TO 202
0014                400 IF(I-1) 402,401,402
0015                401 NTEMP=IBCNT(KKK)
0016                  BA=BASE(KKK,NTEMP)
0017                  GO TO 202
0018                402 IF(I-IJ) 1,403,1
0019                403 BA=BASE(LLL,1)
0020                202 J=BA-SIG(I)
0021                  J=(NCI*J)/1000     +1
0022                  IF(J-1) 2,3,3
0023                2     JUNF=JUNF+1
0024                  GO TO 1
0025                3     IF(J-300) 5,5,4
0026                4     JOVF=JOVF+1
0027                  GO TO 1
0028                5     NDATA=NDATA+1
0029                  NCNT(J)=NCNT(J)+1
0030                  IF(IBTYP.EQ.3) GO TO 50
0031                  1 CONTINUE
0032                  IF(MMM.EQ.0) MMM=1
0033                  IF(MMM.EQ.1) MMM=0
0034                 50 RETURN
0035                  END
```

SUBROUTINE STAT (NTAPE, NCH, NFILE, NCI, IFLAG)

STAT performs the statistical analysis by using the intensity histogram constructed by HIST. A log-amplitude histogram is generated from the intensity histogram to perform log-normal tests. The mean, standard deviation, skewness and kurtosis are calculated for both the intensity and log-amplitude data. In addition, the cumulative probability is calculated and a chi-square test made on both sets of data.

Argument Variables

NTAPE - Tape number.

NCH - Channel number.

NFILE - File number.

NCI - Number of class intervals.

IFLAG - Indicates type statistical calculations.

Common Block Variables

NCNT - Array contains histogram.

JOF - Number of overflows.

JUF - Number of underflows.

SUBROUTINE LIMIT (TOL1, TOL2, NK)

This routine is called by subroutine EXT to calculate the criteria for determining if a data point is a base point or a signal point or neither. LIMIT has the capability of looking into the next record if it is called near the end of the record being processed.

Argument Variables

TOL1 - Experimentally determined constant.

TOL2 - Experimentally determined constant.

NK - Number of data points in record.

```
FORTRAN IV G LEVEL 1, MOD 4            STAT              DATE = 70122          02/35/57

0001                  SUBROUTINE STAT(NTAPE,NCH,NFILE,NCI,IFLAG)
                C      IFLAG = 1    NO CHI SQUARE TEST
                C              2    CHI SQUARE TEST ON NORMAL DISTRIBUTION
                C              3   CHI SQUARE TEST ON LOG NORMLL DISTRIBUTION
                C              4   CHI SQUARE TEST ON BOTH
0002                  COMMON P(1000),AUX(1000),INDO(10),NCNT1(300),JOF,JUF,BASE(2,10),
                     *PIG(10),IBLOC(2,10),KK,MM,XL90,XL10
0003                  COMMON/UUU/NPNCH
0004                  DIMENSION Y(300),XLN(300),Q(4),R(4)
0005                  DIMENSION NCNT(300)
0006                  DO 60 I=1,300
0007                60 NCNT(I)=NCNT1(I)
0008                  C=1000/NCI
                C       FIND THE HIGHEST  AND LOWEST CLASS INTERVAL
0009                  DO 1 I=1,NCI
0010                  IF(NCNT(I)) 1,1,2
0011                 2 ILO=I
0012                  GO TO 3
0013                 1 CONTINUE
0014                 3 DO 4 I= ILO,NCI
0015                   IF(NCNT(I))4,4,5
0016                 5 IHI=I
0017                 4 CONTINUE
                C       FIND NUMBER OF POINTS AND FLOAT NCNT
0018                  N=0
0019                  DO 6 I=ILO,IHI
0020                  Y(I)=NCNT(I)
0021                 6 N=N+NCNT(I)
                C       PRINT HEADINGS
0022                  WRITE(6,101) NTAPE,NCH,NFILE
0023                  WRITE(6,102)
                C       DEFALT DUE TO TOO FEW CLASS INTERVALS
0024                  NN= IHI-ILO
0025                  IF(NN-10) 50,50,51
0026                50 WRITE(6,110)
0027                  RETURN
                C       FIND AVERAGE AMPLITUDE
0028                51 XN=N
0029                  AVE=0.00
0030                  DO 8 I=ILO,IHI
0031                  XI=I
0032                 8 AVE=AVE+Y(I)*(XI-0.5)*C
0033                  AVE=AVE/XN
                C       COMPUTE CUMULATIVE PROBABILITIEC AND LOG AMPLITUDES
0034                  SUM=0.00
0035                  DO 10 I=ILO,IHI
0036                  XI=I
0037                  XI=(XI-0.5)*C
0038                  XLN(I)=0.5*ALOG(XI/AVE)
0039                  SUM=SUM+Y(I)
0040                  CP=SUM/XN
0041                10 WRITE(6,103)  XI,XLN(I),Y(I),CP
0042                  WRITE(6,111) JOF, JUF
                C       COMPUTE MOMENTS ABOUT THE MEAN
0043                  XLA=0.00
0044                  DO 20 I=ILO,IHI
```

```
FORTRAN IV G LEVEL 1, MOD 4            STAT            DATE = 70122          02/35/57

0045            20 XLA=XLA+Y(I)*XLN(I)
0046               XLA=XLA/XN
0047               DO 21 I=2,4
0048               Q(I)=0.00
0049            21 R(I)=0.00
0050               DO 22 I=ILO,IHI
0051               XI=I
0052               DO 22 J=2,4
0053               Q(J)=Q(J)+Y(I)*((XI-0.5)*C-AVE)**J
0054            22 R(J)=R(J)+Y(I)*(XLN(I)-XLA)**J
0055               DO 23 J=2,4
0056               Q(J)=Q(J)/XN
0057            23 R(J)=R(J)/XN
0058               NT=IHI-ILO+1
0059               WRITE(6,104) NT
0060               SIG=SQRT(Q(2))
0061               SIGL=SQRT(R(2))
0062               SKEW=0.5*Q(3)/(SIG**3)
0063               SKL = 0.5*R(3)/(SIGL**3)
0064               XKUR=((Q(4)/(Q(2)**2))-3.0)/2.0
0065               XKURL = ((R(4)/(R(2)**2))-3.0)/2.0
                C       PRINT MOMENTS
0066               WRITE(6,105) AVE,SIG,SKEW,XKUR,XLA,SIGL,SKL,XKURL,N
0067               IF(NPNCH .EQ. 0) GO TO 810
0068               PUNCH 800,NTAPE,NCH,NFILE,AVE,SIG,SIGL,XLA
0069            800 FORMAT(A4,I2,I4,4E14.4)
0070            810 CONTINUE
0071               GO TO (31,32,42,32) ,IFLAG
0072            31 RETURN
                C       NO CHI SQUARE TEST REQUESTED
                C
                C       CHI SQUARE TEST
0073            32 CALL CHI(CSQ,Y,ILO,IHI,C,NUSE,AVE,XLA,SIG ,XN,0,SIG)
0074               XN=CSQ
0075               WRITE(6,106) CSQ,NUSE
                C       PRINT CHI SQUARE      NORMAL
0076               GO TO (31,31,42,42)     ,IFLAG
0077            42 CALL CHI(CSQ,Y,ILO,IHI,C,NUSE,AVE,XLA,SIG ,XN,1,SIGL)
0078               AXLN=CSQ
0079               WRITE(6,106) CSQ,NUSE
                C       PRINT CHI SQUARE      LOG NORMAL
0080               PUNCH 999,NTAPE,NCH,NFILE,SIGL,SKEW,SKL,XN,AXLN
0081            999 FORMAT(A4,I1,I2,5E13.6)
0082               RETURN
0083              101 FORMAT('1',5X,'TAPE NUMBER  ',A4,5X,'TRACK',I3,5X,'FILE',I3)
0084              102 FORMAT('0',16X,'AMPLITUDE',10X,'LOG AMPLITUDE',12X,'COUNT',
                     1  8X,'CUMULATIVE PROBABILITY'/)
0085              103 FORMAT(7X,4E21.6)
0086              104 FORMAT('0',10X,'NUMBER OF CLASS INTERVALS =',I6)
0087              105 FORMAT('0',17X,'AVERAGE',9X,'STANDARD DEVIATION',8X,'SKEWNESS',
                     *13X,'KURTOSIS'/7X,4E21.6/7X,4E21.6/'0',10X,'NUMBER OF DATA POINTS'
                     *,I10)
0088              106 FORMAT('0',10X,'CHI SQUARE=',E14.6/11X'NUMBER OF CLASS INTERVALS
                     1USED =',I5)
0089              110 FORMAT('0',5X,'TOO FEW CLASS INTERVALS  '/
                     1 '0',5X,'  EXECUTION OF STATISTICS CALCULATION SUSPENDED')
```

```
FORTRAN IV G LEVEL 1, MOD 4            STAT            DATE = 70122        02/35/57

 0090          111  FORMAT('0',5X,'NUMBER OF OVERFLOWS',I6/
                    *6X,'NUMBER OF UNDERFLOWS',I5)
 0091                END
```

Common Block Variables

KK - Gives the position (value of INDX) in the record at the time LIMIT is called.

MM - This variable is the sum of KK and the number of points LIMIT is to scan.

XL90 - The resulting criteria for base point selection.

XL10 - The resulting criteria for signal point selection.

SUBROUTINE AMPX (IRUN)

This routine takes the signal and base points extracted by EXT and computes the amplitude of the square wave for the spectral analysis. The amplitudes are calculated by taking the difference between the last base point in the first group and the first signal point, and the difference between the last signal point and the first base point in the second group. This produces two signal points per group. The points are stored in array AMP for use by the spectral analysis routines.

Argument Variables

IRUN - Indicates if EXT in startup cycle.

Common Block Variables

BASE - Array containing both groups of base points.

SIG - Array containing signal points.

Labeled Common Variables

IBCNT - Array containing number of base points in each group.

N - Number of signal points

SUBROUTINE CHI (CSQ, Y1, ILO, IHI, C, NUSE, AVE, XLA, SD, XN, NTYP, SX)

This routine is called by the statistics subroutine to perform the chi-square test for normal and log-normal distributions.

```
FORTRAN IV G LEVEL 1, MOD 4            LIMIT              DATE = 70122          02/35/57

0001                SUBROUTINE LIMIT(TOL1,TOL2,NK)
0002                COMMON P(1000),AUX(1000),INDO(10),NCNT(300),JOVF,JUNF,
                   *BASE(2,10),SIG(10),IBLOC(2,10),KK,MM,XL90,XL10
0003                IK=KK
0004                IM=MM
0005                ID=0
0006                IF(IK-NK) 502,501,666
0007           666  PRINT 3000
0008           3000 FORMAT('  IK GREATER THAN NK    ')
0009           501  AMAX=P(IK)
0010                AMIN=AMAX
0011                ID=IM-NK
0012                GO TO 381
0013           502  IF(IM-NK) 360,360,361
0014           361  ID=IM-NK
0015                IM=NK
0016           360  AMAX=P(IK)
0017                AMIN=AMAX
0018                DO 350 J=IK,IM
0019                IF(AMAX-P(J)) 301,302,302
0020           301  AMAX=P(J)
0021           302  IF(AMIN-P(J)) 350,303,303
0022           303  AMIN=P(J).
0023           350  CONTINUE
0024                IF(ID) 380,380,381
0025           381  AMAXP=AUX(1)
0026                AMINP=AMAXP
0027                DO 650 J=1,ID
0028                IF(AMAXP-AUX(J)) 601,602,602
0029           601  AMAXP=AUX(J)
0030           602  IF(AMINP-AUX(J)) 650,603,603
0031           603  AMINP=AUX(J)
0032           650  CONTINUE
0033                IF(AMAX-AMAXP)700,701,701
0034           700  AMAX=AMAXP
0035           701  IF(AMIN-AMINP)380,380,703
0036           703  AMIN=AMINP
0037           380  A=AMAX-AMIN
0038                XL90=AMAX-TOL1*A
0039                XL10=AMIN+ TOL2*A
0040                RETURN
0041                END
```

```
FORTRAN IV G IEVEL 1, MOD 4            AMPX              DATE = 70122        02/35/57

0001                SUBROUTINE AMPX(IRUN)
0002                COMMON P(1000),AUX(1000),INDO(10),NCNT(300),JOVF,JUNF,
                   *BASE(2,10),SIG(10),IBLOC(2,10),KK,MM,XL90,XL10
0003                COMMON/CBA/IBCNT(2),N
0004                COMMON/AP/AMP(10000),NDATA
0005                IF(IRUN.EQ.1) MMM=1
0006                KKK=1
0007                LLL=1
0008                IF(MMM.EQ.1) LLL=2
0009                IF(MMM.EQ.0) KKK=2
0010                IJ=N
0011                DO 1 I=1,N
0012          400   IF(I-1) 402,401,402
0013          401   NTEMP=IBCNT(KKK)
0014                BA=BASE(KKK,NTEMP)
0015                GO TO 502
0016          402   IF(I-IJ) 1,403,1
0017          403   BA=BASE(LLL,1)
0018          502   NDATA=NDATA+1
0019                AMP(NDATA)=BA-SIG(I)
0020          1     CONTINUE
0021                IF(MMM.EQ.0) MMM=1
0022                IF(MMM.EQ.1) MMM=0
0023                RETURN
0024                END
```

```
FORTRAN IV G LEVEL 1, MOD 4            CHI                DATE = 70122          02/35/57

0001                  SUBROUTINE CHI(CSQ,Y1,ILO,IHI,C,NUSE,AVE,XLA,SD,XN,NTYP,SX)
0002                  DIMENSION Y(300,3) , Y1(300)
0003                  DO 1 I=1,300
0004                1 Y(I,1)=0.00
0005                  NUSE=0
0006                  KM=(ILO+IHI)/2
0007                  J=1
0008                  Y(J,2)=AVE-10.0*SD
                C       GROOP CLASS INTERVALS ON LOW END
0009                  DO 2 I= ILO,KM
0010                  Y(J,1)=Y1(I) + Y(J,1)
0011                  IF(Y(J,1)-5.0) 2,2,3
0012                3 Y(J,3)=C*I
0013                  NUSE = NUSE + 1
0014                  J = J + 1
0015                  Y(J,2) = C*I
0016                2 CONTINUE
                C       GROOP CLASS INTERVALS ON HIGH SIDE
0017                  I = IHI
0018                  Y(J,3) = AVE + 10.0*SD
0019                6 IF(I-KM) 10,10,4
0020                4 Y(J,1) = Y(J,1) + Y1(I)
0021                  IF(Y(J,1)-5.0) 11,11,5
0022                5 Y(J,2) = C*(I-1)
0023                  NUSE = NUSE + 1
0024                  J = J + 1
0025                  Y(J,3) = C*(I-1)
0026               11 I = I-1
0027                  GO TO 6
                C       COMPUTE THEORITICAL PROBABILITY
0028               10 CSQ = 0.00
0029                  DO 30 I=1,NUSE
0030                  XLL = Y(I,2)
0031                  XUL=Y(I,3)
0032               24 CALL SIMP( FTH,XLL,XUL,21,NTYP,AVE,SX,XLA)
                C       COMPUTE CHI SQUARE
0033                  IF(FTH) 31,31,30
0034               31 WRITE(6,100) I
0035              100 FORMAT('0    ZERO VALUE OF THEORITICAL PROBABILITY IN',I5,' TH
                     1 INTERVAL'/ 6X,'EXECUTION OF CHI SQUARE TEST DISCONTINUED')
0036                  RETURN
0037               30 CSQ=CSQ+((Y(I,1)-XN*FTH)**2)/(XN*FTH)
0038                  RETURN
0039                  END
```

Argument Variables

CSQ - Result of chi-square test.

Y1 - Array containing histogram.

ILO - Lowest class interval in histogram.

IHI - Highest class interval in histogram.

C - Width of class mark.

NUSE - Number of class intervals used by the chi-square routine.

AVE - Mean value of amplitudes.

XLA - Mean value of log-amplitudes.

SD - Standard deviation of amplitudes.

XN - Number of data points.

NTYP - Determines if chi-square test will be run for normal or log-normal test or both.

SX - Log standard deviation.

SUBROUTINE FFT (DT, FMAX)

This routine is called by the main program to coordinate the performance of the spectral analysis. Subroutines FOURT and PLOT are called to perform the Fourier transform and to plot the results. FFT will have PLOT plot directly from the calculated spectral data array or it will have it plot the average of a designated number of points in the array. This feature was incorporated to smooth out random variations.

Argument Variables

DT - Time between data samples.

FMAX - Maximum frequency to be used.

Labeled Common Variables

AMP - Array containing the time domain signal. This array is passed from AMPX.

FORTRAN IV G LEVEL 1, MOD 4 FFT DATE = 70122 02/35/57

```
0001            SUBROUTINE FFT(N,DT,FMAX)
0002            DIMENSION WORK(2500)
0003            COMMON/AP/AMP(10000),NDATA
0004            COMMON/GO/N1,N3,N4,FM,IDO
0005            COMMON/NPTS8/N8
0006            DIMENSION NN(2)
0007            PRINT 555,NDATA
0008            IF(NDATA-8192) 25,56,56
0009       25   NDIFF=8192-NDATA
0010            CALL FILL(NDIFF)
0011       56   PRINT 81,N8
0012       81   FORMAT(10X,'NUMBER OF ZEROS ADDED  =  ',I20//)
0013            NDATA=8192
0014       555  FORMAT(10X,' NUMBER OF DATA POINTS EXTRACTED  =',I20,///)
0015            N=NDATA
0016       99   FORMAT(/,'1FREQ(HZ)       MAGNITUDE')
0017            NN(1)=N
0018            DF=1.0/(N*DT)
0019            N2=(FMAX/DF)*2
0020            IF(N2.GT.N) N2=N
0021            CALL FOURT(AMP,NN,1,-1,0,WORK,2500)
0022            DO 5 J=2,N,2
0023            X=AMP(J-1)
0024            Y=AMP(J)
0025        5   AMP(J-1)=SQRT(X*X+Y*Y)/N
0026            WRITE(6,99)
0027            IF(IDO.EQ.1) GO TO 50
0028            CALL PLOT(AMP,DF,DF,N1,N2,N3)
0029       50   F=DF
0030            IF (IDO.EQ.3) GO TO 51
0031            PRINT 100
0032       100  FORMAT(/,' FREQ(HZ)         MAGNITUDE')
0033            SUM=0.0
0034            J=1
0035            NC=0
0036            DO 10 I=N1,N2,N3
0037            NC=NC+1
0038            SUM=AMP(I) +SUM
0039            IF(NC.LT.N4) GO TO 10
0040            NC=0
0041            AMP(J)= SUM/N4
0042            SUM=0.0
0043            IF(F.GT.FM) GO TO 11
0044            J=J+1
0045       10   F=F+ DF
0046       11   DFP=N4*DF
0047            SF=(DF + DFP)/2.0
0048            CALL PLOT(AMP,SF,DFP,1,J,1)
0049       51   CONTINUE
0050            RETURN
0051            END
```

NDATA - Number of data points in AMP array.

N1 - Designates the first point to be plotted from the spectral data array by PLOT.

N3 - Directs PLOT to skip N3 points between each plotted point in spectral data array.

N4 - Number of points to be averaged when using the averaging feature of this routine.

IDO - If IDO = 1 the "average" feature is to be used. If IDO = 3 the "average" feature is not to be used.

N8 - Number of points (zeros) added by FILL.

SUBROUTINE PRINT (NNN)

This subroutine accepts the error cumulation array from EXT after a run is completed. It prints out the error table and other error data.

Labeled Common Variables

IE - Array containing the sum of 7 types of errors for each of the 300 records.

IRCEND - The number of the last record to be processed.

SUBROUTINE SIMP (SUM, FLL, FUL, N, NTYP, A, B, C)

This is a Simpsons rule integration routine called by CHI.

Argument Variables

SUM - Result of integration.

FLL - Lower limit.

FUL - Upper limit.

N - Number of points - 21.

NTYP - Determines if routine will compute for a normal test, log-normal test or both.

A - Mean value of amplitudes

B - Log standard deviation.

C - Mean value of log-amplitude.

```
FORTRAN IV G LEVEL 1, MOD 4            PRINT            DATE = 70122          02/35/57

0001                SUBROUTINE PRINT(NNN)
0002                COMMON/PR/IE(7,300)
0003                COMMON/RAT/IRCEND
0004                DIMENSION IESUM(7)
0005                PRINT 3
0006           3    FORMAT(1H1,50X,'DATA PROCESSING IRREGULARTIES',/,10X,'ERROR CODES
                   *FOLLOW',////,
                   *10X,'NO BASE POINTS FOUND IN BASE SEARCH **********  1'/,
                   *10X,'NUMBER OF BASE POINTS EXCEEDS 10  ************  2'/,
                   *10X,'NUMBER OF SIGNAL POINTS EXCEEDS 10 ***********  3'/,
                   *10X,'NUMBER OF BASE POINTS INSUFFICIENT ***********  4'/,
                   *10X,'NUMBER OF SIGNAL POINTS INSUFFICIENT *********  5'/,
                   *10X,'NUMBER OF PASSES EXCEEDS LIMIT L1 ************  6'/,
                   *10X,'NUMBER OF ERRORS IN RECORD EXCEEDS 5 *********  7')
0007                DO 555 I=1,7
0008            555 IESUM(I)=0
0009                PRINT 1
0010           1    FORMAT(10X,'ERROR',11X,'1',13X,'2',13X,'3',13X,'4',13X,'5',13X,
                   *'6',13X,'7')
0011                PRINT 100
0012           100  FORMAT(10X,'RECORD',///)
0013                DO 55 I=1,IRCEND
0014                DO 55 K=1,7
0015            55  IESUM(K)=IESUM(K)+IE(K,I)
0016                DO 2 I=1,IRCEND
0017                DO 12 K=1,7
0018                IF(IE(K,I)) 15,12,15
0019           12   CONTINUE
0020                GO TO 2
0021           15   WRITE(6,5) I,(IE(K,I),K=1,7)
0022           5    FORMAT(10X,I3,10X,I4,10X,I4,10X,I4,10X,I4,10X,I4,10X,I4,10X,I4)
0023              2 CONTINUE
0024                PRINT 20
0025           20   FORMAT(10X,//,10X,'ERROR CODE',10X,'NUMBER OF ERRORS')
0026                DO 50 K=1,7
0027           50   PRINT21,K,IESUM(K)
0028            21  FORMAT(10X,I6,14X,I9)
0029                RETURN
0030                END
```

```
FORTRAN IV G LEVEL 1, MOD 4            SIMP              DATE = 70122          02/35/57

0001                SUBROUTINE SIMP(SUM,FLL,FUL,N,NTYP,A,B,C)
              C      INTEGRAND FUNCTION   REMOVE WHENCHANGING FUNCTION
0002                PBF(X,A,S) = (1.0/(S*SQRT(6.28318)))*EXP(-0.5*(((X-A)/S)**2))
0003                FNP=N-1
0004                DELX=(FUL-FLL)/FNP
0005                SUM=0.0
0006                SUM1=0.0
0007                SUM2=0.0
0008                DO 1 I=1,N
0009                FK=I-1
0010                X=FK*DELX+FLL
              C     CALL FOR INTERGRAND SUBROUTINE HERE
              C     CALL FOR INTERGRAND SUBROUTINE HERE
0011                IF(NTYP) 101,101,110
0012              101 VAL=PBF(X,A,B)
0013                GO TO 102
0014              110 IF(X) 20,20,100
0015               20 VAL=0.00
0016                GO TO 102
0017              100 XX=0.5*ALOG(X/A)
0018                VAL=PBF(XX,C,B)
0019                VAL=0.5*VAL/X
0020              102 CONTINUE
              C
0021                IF(I.EQ.1.OR.I.EQ.N) GO TO 2
0022                J=MOD(I,2)
0023                IF(J) 3,4,3
0024              3 SUM1=SUM1+VAL
0025                GO TO 1
0026              4 SUM2=SUM2+VAL
0027                GO TO 1
0028              2 SUM=SUM+VAL
0029              1 CONTINUE
0030                SUM=SUM+2.0*SUM1 + 4.0*SUM2
0031                SUM=SUM*DELX/3.0
0032                RETURN
0033                END
```

SUBROUTINE FILL (I)

This routine is called by subroutine EXT in cases where data points are discarded due to irregularities. FILL places zeros into the omitted positions.

Argument Variables

I - Number of data points discarded.

Labeled Common Variables

AMP - Array containing extracted data.

NDATA - Number of data points in AMP.

N8 - Number of zeros added by FILL.

```
FORTRAN IV G LEVEL 1, MOD 4            FILL              DATE = 70122          02/35/57

0001                SUBROUTINE FILL(I)
0002                COMMON/AP/AMP(10000),NDATA
0003                COMMON/NPTS8/N8
0004                J=(I+3)/6
0005                N8=N8+J
0006                DO 1 K=1,J
0007                NDATA=NDATA + 1
0008          1     AMP(NDATA)=0.
0009                RETURN
0010                END
```

DATA PROCESSING IRREGULARTIES

ERROR CODES FOLLOW

NO BASE POINTS FOUND IN BASE SEARCH ********** 1
NUMBER OF BASE POINTS EXCEEDS 10 ********** 2
NUMBER OF SIGNAL POINTS EXCEEDS 10 ********** 3
NUMBER OF BASE POINTS INSUFFICIENT ********** 4
NUMBER OF SIGNAL POINTS INSUFFICIENT ********** 5
NUMBER OF PASSES EXCEEDS LIMIT L1 ********** 6
NUMBER OF ERRORS IN RECORD EXCEEDS 5 ********** 7

ERROR RECORD	1	2	3	4	5	6	7
2	0	0	0	1	0	0	0
232	0	1	0	0	0	0	0
240	0	0	0	1	0	0	0
241	0	0	0	1	0	0	0
252	0	0	0	1	0	0	0
253	0	0	0	1	0	0	0
264	0	0	0	1	0	0	0
265	0	0	0	1	0	0	0
276	0	0	0	1	0	0	0
277	0	0	0	1	0	0	0
288	0	0	0	1	0	0	0
289	0	0	0	1	0	0	0
300	0	0	0	1	0	0	0

ERROR CODE	NUMBER OF ERRORS
1	0
2	1
3	0
4	12
5	0
6	0
7	0

ERROR TABLE

TAPE NUMBER 3397 TRACK 4 FILE 2

AMPLITUDE	LOG AMPLITUDE	COUNT	CUMULATIVE PROBABILITY
0.235000E 03	-0.347886E 00	0.100000E 01	0.120077E-03
0.245000E 03	-0.327050E 00	0.200000E 01	0.360230E-03
0.255000E 03	-0.307047E 00	0.200000E 01	0.600384E-03
0.265000E 03	-0.287814E 00	0.0	0.600384E-03
0.275000E 03	-0.269293E 00	0.0	0.600384E-03
0.285000E 03	-0.251434E 00	0.200000E 01	0.840538E-03
0.295000E 03	-0.234191E 00	0.100000E 01	0.960615E-03
0.305000E 03	-0.217523E 00	0.300000E 01	0.132085E-02
0.315000E 03	-0.201393E 00	0.600000E 01	0.204131E-02
0.325000E 03	-0.185766E 00	0.800000E 01	0.300192E-02
0.335000E 03	-0.170614E 00	0.400000E 01	0.348223E-02
0.345000E 03	-0.155907E 00	0.170000E 02	0.552353E-02
0.355000E 03	-0.141620E 00	0.190000E 02	0.780499E-02
0.365000E 03	-0.127730E 00	0.210000E 02	0.103266E-01
0.375000E 03	-0.114216E 00	0.390000E 02	0.150096E-01
0.385000E 03	-0.101057E 00	0.660000E 02	0.229347E-01
0.395000E 03	-0.882359E-01	0.720000E 02	0.315802E-01
0.405000E 03	-0.757353E-01	0.127000E 03	0.468300E-01
0.415000E 03	-0.635396E-01	0.178000E 03	0.682036E-01
0.425000E 03	-0.516343E-01	0.286000E 03	0.102546E 00
0.435000E 03	-0.400058E-01	0.381000E 03	0.148295E 00
0.445000E 03	-0.286417E-01	0.513000E 03	0.209894E 00
0.455000E 03	-0.175301E-01	0.739000E 03	0.298631E 00
0.465000E 03	-0.666013E-02	0.929000E 03	0.410182E 00
0.475000E 03	0.397811E-02	0.110800E 04	0.543228E 00
0.485000E 03	0.143953E-01	0.122700E 04	0.690562E 00
0.495000E 03	0.245999E-01	0.117400E 04	0.831532E 00
0.505000E 03	0.346000E-01	0.855000E 03	0.934198E 00
0.515000E 03	0.444044E-01	0.434000E 03	0.986311E 00
0.525000E 03	0.540202E-01	0.105000E 03	0.998919E 00
0.535000E 03	0.634542E-01	0.900000E 01	0.100000E 01

NUMBER OF OVERFLOWS 0
NUMBER OF UNDERFLOWS 0

NUMBER OF CLASS INTERVALS = 31

AVERAGE	STANDARD DEVIATION	SKEWNESS	KURTOSIS
0.471235E 03	0.323860E 02	-0.646181E 00	0.163909E 01
-0.127374E-02	0.364458E-01	-0.903620E 00	0.353928E 01

NUMBER OF DATA POINTS 8328

CHI SQUARE= 0.542616E 06
NUMBER OF CLASS INTERVALS USED = 23

CHI SQUARE= 0.534447E 07
NUMBER OF CLASS INTERVALS USED = 23

TYPICAL COMPUTER OUTPUT FOR
STATISTICAL ANALYSIS

TAPE NUMBER=3397 IDCAL=3 BASE=1 NUMBER OF CHANNELS=05 NUMBER OF SCANS=0200

TYPE BASE CALCULATION **********	*****	IBTYP	***** 2
TYPE STATISTICS CALLED FOR **********	*****	IFLAG	***** 4
NUMBER OF CLASS INTERVALS **********	*****	NCI	***** 100
NUMBER OF SCANS PER RECORD **********	*****	NOSCAN	***** 200
NUMBER OF CHANNELS ON TAPE **********	*****	NOCHAN	***** 5
TOLERANCE ON BASE LIMITS **********	*****	TOL1	***** 0.050
TOLERANCE ON SIGNAL LIMITS **********	*****	TOL2	***** 0.100
NUMBER OF SIGNAL AND BASE POINTS REQUIRED PER CYCLE ********	*****	TOL3	***** 3.000
NUMBER OF PASSES REQUIRED TO ABORT CYCLE **********	*****	L1	***** 10
NUMBER OF BASE POINTS REQUIRED FOR SIGNAL POINT SEARCH *****	*****	L2	***** 5
PUNCHED OUTPUT FLAG **********	*****	NPNCH	***** 1
PRINT ERROR TABLE FLAG **********	*****	IPRINT	***** 0
TYPE ANALYSIS ROUTINE WANTED **********	*****	ISSB	***** 2
INFORMATION FOR FFT ROUTINE **********	*****	FMAX	***** 40.000
	*****	DT	***** 0.006
	*****	FM	***** 30.000
	*****	N1	***** 3
	*****	N3	***** 2
	*****	N4	***** 5
	*****	IDO	***** 5

TYPICAL PARAMETER VALUES

APPENDIX B

This program generates a set of N random numbers having a log-normal distribution and a pre-selected mean and standard deviation. The program is in the form of a FORTRAN IV subroutine.

Theory: By definition a log-normal random deviate is one whose logarithms are normal random deviates. Thus if (X_i) is a set of log-normal random numbers then there must exist a set of normal random numbers (y_i) related to the X_i by

$$y_i = \ln X_i \qquad \text{B1}$$

Equation B1 may be generalized by the addition of appropriate scaling factors; i.e., we may let

$$y_i = a \ln X_i + b \qquad \text{B2}$$

Now by choosing the mean and variance of the (y_i) and the values of the scale factors a and b it is possible to generate a set of (X_i) having any desired mean and variance from a set of normal deviates (y_i). Solving B2 for X_i we have

$$X_i = \exp\left(\frac{y_i - b}{a}\right) \qquad \text{B3}$$

Since we wish to specify only two parameters, viz., the mean and standard deviation of the (X_i) it seems reasonable to assume that we will need only two parameters in equation B3. We therefore let a = 1 and take the mean of the (y_i) to be zero. B3 then becomes

$$X_i = \exp(-b) \exp(y_i) \qquad \text{B4}$$

taking the average of both sides of equation B4 we have

$$\overline{X} = \exp(-b)\ \overline{\exp(y_i)} \qquad \text{B5}$$

and also taking the second moment of (X_i) about zero

$$\overline{X^2} = \exp(-b)\ \overline{\exp(2y_i)} \qquad \text{B6}$$

the averages of the exponential functions in equation B5 and B6 can be evaluated easily

$$\overline{\exp(ny_i)} = (2\pi t^2)^{-1/2} \int_{-x}^{x} \exp(ny) \cdot \exp(y^2/2\sigma)dy \qquad \text{B7}$$

Combining equation B5, B6 and B7 we obtain expressions which may be solved for the scale factor b and the required standard deviation of the (y_i)

$$\sigma^2 = \ln(\mu/\overline{X}^2) \qquad \text{B8}$$

and

$$\exp(-b) = X\exp(-\sigma^2/2) \qquad \text{B9}$$

where μ is the second moment of the (X_i) about zero.

Program: The log-normal generator makes use of the normal random number generator included in the IBM Scientific Subroutine Package for the 360 computer. This routine (GAUSS) generates normal random numbers with any required mean and standard deviation. Coding for the program is shown in the accompanying listing. The argument list is as follows:

AVE - The required mean.

VAR - The required standard deviation.

Y - A vector of log-normal random numbers returned by the subroutine. Y is dimensioned by the calling program.

N - The number of random numbers to be generated.

IX - A "seed" required by GAUSS. IX must be a 5 digit odd integer.

Statements 3 to 6 compute the required standard deviation for the Gaussian-random numbers and the proper scaling factor. Statements 7 to 9 call GAUSS compute a log-normal random number from equation B5.

Fortran List for Log-Normal Generator

```
 1   SUBROUTINE LOGN(AVE, VAR, Y, N, IX)
 2   DIMENSION Y(1)
 3   VAR = VAR**2 + AVE **2
 4   SIG = ALOG(VAR/AVE**2)
 5   Z BAR = EXP(SIG/2.0)
 6   SIG = SQRT(SIG)
 7   DO 1   I = 1, N
 8   CALL GAUSS(IX, SIG, 0.0, X)
 9   1  V(I) = (AVE/Z BAR)*EXP(X)
10   RETURN
11   END
```

REFERENCES

1. Fried, D. L., Optical Propagation Measurements at Lake Emerson, Final Report, Langley Research Center, N.A.S.A., Hampton, Virginia, Contract No. NAS-1-7705.

2. Kerr, J. R., Multiwavelength Laser Propagation Study, Quarterly Progress Report No. 2, Oregon Graduate Center for Study and Research, Portland, Oregon, Sponsored by Advanced Research Projects Agency, ARPA Order No. 306.

3. Fitzmaurice, Bufton, and Minott, Wavelength Dependence of Laser Beam Scintillation, Goddard Space Flight Center, Greenbelt, Md.

4. Kolmogorov, A. N., The Local Structure of Turbulence in Incompressible Viscous Fluid for Very Large Reynolds Number, Doklady Akad. Nauk SSSR, 30, 301 (1941) German translation in Sommelband zur Statistischen Theorie der Turbuleny, Akademie-Verlog, Berlin (1958), p. 71.

5. Kolmogorov, A. N., Dissipation of Energy in Locally Isotropic Turbulence, Doklady Akad Nauk SSSR, 32, 16 (1941) German translation in Sommelband zur Statistischen Theorie der Turbeleny, Akademie-Verlag, Berlin (1958), p. 77.

6. Tatarski, V. I., Wave Propagation on a Turbulent Medium, Institute of Atmospheric Physics, Academy of Sciences of the U.S.S.R. Translated from the Russian by R. A. Silverman, Dover Publications, Inc., New York, 1967.

7. Beckman, Peter, Elements of Applied Probability Theory, Harcourt, Brace and World, Inc., 1967.

8. Mocker, H. W., "A 10.6 M Optical Heterodyne Communication System," Applied Optics, March, 1969, Vol. 8, No. 3, p. 677.

9. Cooley, J. W. and J. W. Tukey, "On Algorithm for the Machine Computation of Complex Fourier Series," Math of Comput. 19, 297 (1965).

10. Fried, D. L., "Propagation of a Spherical Wave in a Turbulent Medium," J. Opt. Soc. AM. 57, p. 175 (1967).

11. Fried, D. L., "Aperture Averaging of Scintillation," J. Opt. Soc. AM. 57, p. 175 (1967).

12. Fried, D. L., "Propagation of an Infinite Plane Wave in a Randomly Inhomogeneous Media," J. Opt. Soc. Am. 56, p. 1667 (1966).

13. Young, A. T., "Aperture Filtering and Averaging of Statistics," J. Opt. Soc. AM. 60, p. 248 (1970)

Appendix 4

REQUIREMENTS STUDY FOR THE AVLOC EXPERIMENT

This Report describes the various analyses which have been made in connection with the MSFC High Altitude Aircraft Test. These analyses include an investigation of the effects of the aircraft navigational errors on experimental accuracy, a survey of the engineering measurements to be conducted on this experiment and a survey of the meterological support requirements for the project. In addition a brief description of the High Altitude Aircraft Test program is given as background for the reader who may not be familiar with this project. Volume Two contains a complete report of both the experimental and theoretical investigations.

TABLE OF CONTENTS

DESCRIPTION OF THE MSFC HIGH ALTITUDE AIRCRAFT TEST FOR VISIBLE LASER COMMUNICATIONS

Introduction

The analysis reported in the following sections have been performed in support of the High Altitude Aircraft Test of Visible Laser Communications being conducted by MSFC personnel during 1971-1972. In order to orient the reader as to the relation of this work to the overall MSFC Aircraft Test program a brief description of that experiment will be given. A more comprehensive discussion of the experiment can be found in the High Altitude Aircraft Test project plan [2].

Program Objectives

The High Altitude Aircraft Test for Visible Laser Optical Communications (hereafter referred to as HAAT) is intended to perform three functions, viz., to collect scientific data on the propagation of visible wavelength radiation through the atmosphere, to provide engineering data needed for the evaluation of the techniques of optical communications and for the design of future systems, and to demonstrate the feasibility of optical techniques for communications between aircraft and ground or satellite and ground. These techniques include the ability of the satellite (or aircraft) to acquire the ground station and vice versa, the ability to accurately track the moving satellite and the ability to transmit high data rates with low error and high reliability.

Experimental System

The experimental system consists of an airborne optical communications terminal carried aboard a modified RB-57 aircraft and a ground station located on Redstone Arsenal, Alabama. Both the airborne and ground terminals are equipped with transmitting lasers so that two way communications may be established and both uplink and downlink propagation may be studied. In addition to communication equipment each terminal contains an optical tracking system which controls its pointing during the experiment. Thus each end of the system cooperatively tracks upon the other end throughout the course of the experiment. The ground station is equipped with a separate laser radar (designated the Ground Based Acquisition Aid or GBAA) for initial acquisition of the aircraft and for providing exact range and zenith angle information throughout the experiment. Both the airborne and ground terminals are fully instrumented to record all pertinent data relating both to system operation and to atmospheric effects on optical propagation.

The downlink channel will consist of a 6328 Å He-Ne laser beam pulse code modulated at 30 M.bits/sec. Downlink transmission will consist of either a real time television picture, a pseudo random code word for bit error rate measurements, or telemetry of data being collected aboard the aircraft. The uplink channel will consist of an amplitude modulated 4880 Å Argon laser beam which will be used for uplink scintillation measurement and to transmit commands to the airborne package.

The ground terminal receiving and transmitting optics consists of a 24-inch Cassegrainian telescope with the experimental package located at its Coudé focus. The incoming 6328 Å beam from the airborne He-Ne laser passes through a wavelength selective beam splitter to separate it from the 4880 Å uplink beam. It is then directed by means of a second beam splitter to two detectors. The first detector is a quadrant photomultiplier which provides fine pointing signals. These signals, along with the output of the angle encoders on the telescope mount, are fed into a SCC 4700 computer which performs the necessary coordinates transformations and generates the signals to drive the polar-equitorial telescope mount. In addition, both the angle encoder and the quadrant photomultiplier outputs are recorded to give angle of arrival fluctuation data.

The second part of the incoming beam is directed to two photomultiplier tubes. The output of one of these detectors is recorded to provide the wide bandwidth downlink communication, channel output, scintillation data, and bit error rate data.

The uplink beam is generated by an Argon laser which passes through a modulator and a beam steerer and out through the telescope. The beam steerer is driven by the computer so as to direct the uplink beam directly back along the incoming beam. The uplink beam is modulated with a 10.7 MHz sine wave and also with audio tones used to control the operation of the aircraft terminal.

In addition to the main tracking and communications system, the ground terminal contains a laser radar for acquisition and ranging (the GBAA). The acquisition radar is mounted on the main telescope

tube and bore-sighted with it. It consists of pulsed Argon laser, beam steering optics and receiving electronics. During acquisition phase, the beam is digitally scanned in a raster pattern, until a return from corner reflectors mounted on the aircraft is detected. At this time the GBAA enters a limited scan mode and the tracking and pointing function is passed to the detector in the primary receiver system. The GBAA continues to track the aircraft, however, and to provide range information. In the event that the primary tracker should lose the target, the acquisition radar will automatically re-enter the acquisition mode and reacquire the target. During this time the telescope drive will enter a coast mode so as to continue to point at the assumed position of the aircraft.

The airborne optical system will be mounted in a fixed position aboard the RB-57 aircraft and will view the ground in a steerable mirror which will be servocontrolled to point the outgoing beam in the proper direction. During acquisition the steerable mirror is pointed in the general direction of the ground station manually. When the ground based acquisition radar illuminates the aircraft, an acquisition sensor detects the upcoming beam and causes the system to enter a track mode. The incoming beam passes through a dichroic beam splitter which isolates it from the outgoing beam to an image dissector which provides tracking information and a photomultiplier which detects upcoming commands and measures scintillation. The transmitter section of the airborne terminal consists of a He-Ne laser which is superimposed on the incoming beam by means of the dichroic beam splitter. The outgoing beam is pulse code modulated at 30 megabits/sec with

either a pseudo random word for bit error rate measurements, with a video signal generated by a television camera aimed at the ground, or with telemetry.

Experiment Plan

The experiment plan calls for four missions at various times during the year. Each mission will consist of four fly overs of about three hours duration.

The aircraft will approach the Madkin Mountain ground station on a straight line path at an altitude of about 50,000 feet. Once acquired by the GBAA radar the aircraft will assume a circular flight path centered on the ground terminal thus maintaining a constant range from the ground station and constant zenith angle. Initially an altitude of 70,000 feet and a path diameter of 10 miles is planned. This corresponds to a start range of 74,800 feet and a zenith angle of 20.6 degrees, the minimum zenith angle obtainable with a circular path. By varying the altitude of the aircraft and the diameter of it's flight path the range and zenith angle can be varied at will.

The scientific measurements to be made during each fly-over are outlined in Table I. Detailed discussions of these experiments can be found in the referenced measurement program document [2].

Table I. Measurements Outline

Quantity Measured	Parameters	Analysis to Yield
1. Scintillation (downlink)	Receiving Aperture Range Zenith Angle	Log amplitude variance Probability density function Verify theoretical predictions concerning zenith angle, and range dependence. Aperture averaging effects: a. Reduction of signal variance b. Change of probability density function. Difference in up and down link.
2. Scintillation (uplink)	Receiving Aperture Range Transmitter Aperture	Log amplitude variance Probability density function Verify theoretical prediction concerning zenith angle and range dependence. Verify no uplink aperture averaging Effect of transmitting aperture size. Differences in uplink and downlink.
3. Angle of Arrival Fluctuations (downlink)	Range Zenith Angle Receiving Aperture	Variance Probability density function Aperture averaging Dependence on range and zenith angle. Differences between uplink and downlink.
4. Angle of Arrival Fluctuations (uplink)	Range Zenith Angle	Variance Probability density function Dependence on range and zenith angle. Differences between uplink and downlink.
5. Bit Error Rate	Range Zenith Angle Beam Divergence Transmitter Power	Verify theoretical prediction of BER dependence on system noise and irradiance fluctuation variance.

Table I. Measurements Outline (Cont'd)

Quantity Measured	Parameters	Analysis to Yield
6. Atmospheric Transmittance	None	Atmospheric transmittance at optical wavelengths.
7. Engineering Measurements		Determine ability to acquire and track. Evaluate system performance.

ANALYSIS OF THE ERRORS IN THE MSFC OPTICAL COMMUNICATIONS EXPERIMENT DUE TO FLIGHT PATH INACCURACIES

Introduction

Marshall Space Flight Center's High Altitude Aircraft Test of Visible Laser Communications (HAAT) is expected to provide scientific data concerning atmospheric turbulence and its effect on the propagation of laser beams over near vertical paths. If these data are to be meaningful, it is necessary that certain parameters such as aircraft range and zenith angle be held constant. Clearly no aircraft can fly a precise path, so some variation in these parameters must be accepted. It is the purpose of this report to examine the errors introduced into the experimental data as the result of deviation of the aircraft from its prescribed flight path and, based on this analysis, to suggest the maximum deviations which can be tolerated.

General Considerations

A description of the HAAT experiment is found in the HAAT project plan [2]. During the test the aircraft will fly a circular pattern over the ground station, ideally maintaining a constant range and zenith angle. The ground station will track the aircraft by means of a ground based acquisition aid (GBAA) also used for initial contact. The GBAA is an optical laser radar with ranging facilities and will provide continuous range and angle information. From the GBAA data the aircraft's position relative to the ground station will be accurately

known, a posteriori. It is therefore not a requirement that the aircraft fly precisely along a predetermined path but only that it remain upon a circle reasonably close to the desired pattern. It is the variations of the aircraft path from this somewhat arbitrary circle which are important. The GBAA data will also allow the elimination of any data segment for which the variation in the range or zenith angle are excessive.

If the aircraft were to fly a perfectly level, circular path then its range (r) and zenith angle (θ) would be constant. We anticipate that the aircraft's actual path will be some smooth curve which approximates the prescribed circular pattern. We will therefore assume that θ and r will be slowly varying functions of time.

The quantities to be measured (such as scintillation) are statistical quantities whose mean and variance depend upon r and θ as well as upon the statistics of the atmospheric turbulence. Since the atmosphere itself is a non-stationary system, the time variation of r and θ will simply serve to increase the variation in the statistical parameter of the measured quantity. It therefore seems reasonable to require that the variation in the statistical estimates of these parameters due to aircraft motion be small compared to the variations introduced by such unavoidable effects as atmospheric non-stationarity.

Table I in Appendix B of the HAAT program plan [3], which has been reproduced as Table I of this report, describes seven measurements which will be made. Eliminating from consideration the Engineering measurements and neglecting any difference in uplink and downlink

measurements, these may be reduced to four basic types of measurement viz.

1. Scintillation
2. Angle of Arrival Fluctuations
3. Bit Error Rate Measurements
4. Transmittance.

Each of these measurements will be considered.

Scintillation

The variance of the log-amplitude σ_ℓ for a spherical wave is given by [4]

$$\sigma_\ell = \int_0^Z C_N^2(h) \left[\frac{(z-s)s}{z}\right]^{5/6} ds \qquad (1)$$

where $C_N^2(h)$ is the index of refraction structure constant at an altitude h, z is the slant range and ds is an element of length along the propagation path. The actual situation which we wish to consider is that of a collimated, truncated gaussian beam. Since, however, we are only concerned with the order of magnitude of the variation of σ_ℓ on range and zenith angle, and since the form of the function $C_N^2(h)$ is not well known, we will assume that the relation of equation (1) describes the gaussian beam accurately enough for our purposes.

We will assume a form for $C_N^2(h)$ viz.

$$C_N^2(h) = C_0^2 \, h^{-1/3} \, e^{-h/h_0} \qquad (2)$$

where h_0 is a scale height usually taken to be 3200 m. Recent work [5] indicates that this value may be too large, however since for larger h_0, σ_ℓ is more sensitive to changes in altitude and zenith angle we will assume this value as a worst case.

For a zenith angle θ, h is related to s by

$$h = s \cos \theta \tag{3}$$

then

$$\sigma_\ell^2 = C_0^2 \cos^{-1/3} \theta \int_0^z s^{-1/3} e^{-\left(\frac{s \cos \theta}{h_0}\right)} \left[\frac{(z-s)s}{z} \right]^{5/6} ds \tag{4}$$

Now we let $u = s/z$, then

$$\sigma_\ell^2 = C_0^2 \cos^{-1/3} \theta \, z^{3/2} \int_0^1 u^{1/2}(1-u)^{5/6} e^{-u z \cos \theta / h_o} du \tag{5}$$

But $z \cos \theta$ is just the aircraft altitude h_m, therefore

$$\sigma_\ell^2 = C_0^2 \cos^{-11/6} h_m^{3/2} \int_0^1 u^{1/2}(1-u)^{5/6} e^{-\frac{h_m}{h_0} u} du \tag{6}$$

Now consider an aircraft flying in a circular path of radius R at an altitude h_m. As can be seen in Figure 1, if the radius of the circle changes by an amount ΔR then h_m remains constant and θ changes by an amount $\Delta\theta$ given by

$$\Delta\theta = \frac{\Delta X}{s} = \frac{\Delta R \cos \theta}{s} = \frac{h_m \Delta R}{s^2} \tag{7}$$

then the fractional change in the log amplitude variance is

$$\frac{\Delta\sigma_\ell^2}{\sigma_\ell^2} = \frac{1}{\sigma^2} \frac{\partial\sigma_\ell^2}{\partial\theta} \Delta\theta$$

$$= \left[+\frac{11}{6} C_0^2 \cos^{-17/6}\theta \sin\theta\, h_m^{3/2} I(h_m)\right] \cdot \Delta\theta$$

$$\Big/ \left[C_0^2 \cos^{-11/6}\theta\, h_m^{3/2} I(h_m)\right] \qquad (8)$$

Where $I(h_m)$ denotes the definite integral in Equation 6, Equation 8 reduces to

$$E_{\Delta R} = \frac{\Delta\sigma_\ell^2}{\sigma_\ell^2} = \frac{11}{6} \tan\theta\Delta\theta \qquad (9)$$

or

$$E_{\Delta R} = \frac{11}{6} \frac{R\Delta R}{s^2} \qquad (10)$$

Equation 10 allows us to estimate the variation in σ_ℓ^2 for a change in horizontal position of the aircraft. A similar equation may be derived for a change in altitude ΔH. As can be seen from Figure 2, a change in aircraft altitude changes both h_m and θ. The change in θ is given by

$$\Delta\theta = \frac{\Delta X}{s} = -\frac{\Delta H_m \sin\theta}{s} = -\frac{R\,\Delta H_m}{s^2} \qquad (11)$$

then

$$\frac{\Delta\sigma_\ell^2}{\sigma_\ell^2} = \frac{1}{\sigma_\ell^2} \left[\frac{\partial\sigma_\ell^2}{\partial\theta}\Delta\theta + \frac{\partial\sigma_\ell^2}{\partial h_m}\Delta h_m\right] \qquad (12)$$

C-3

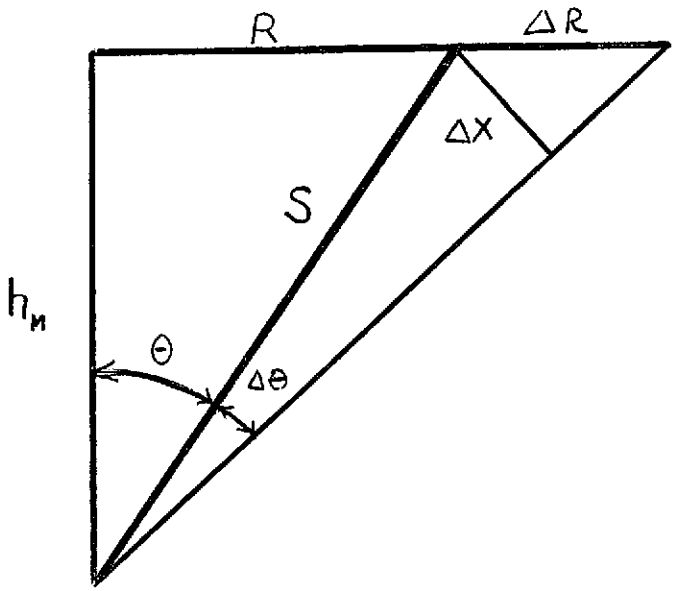

Figure 1

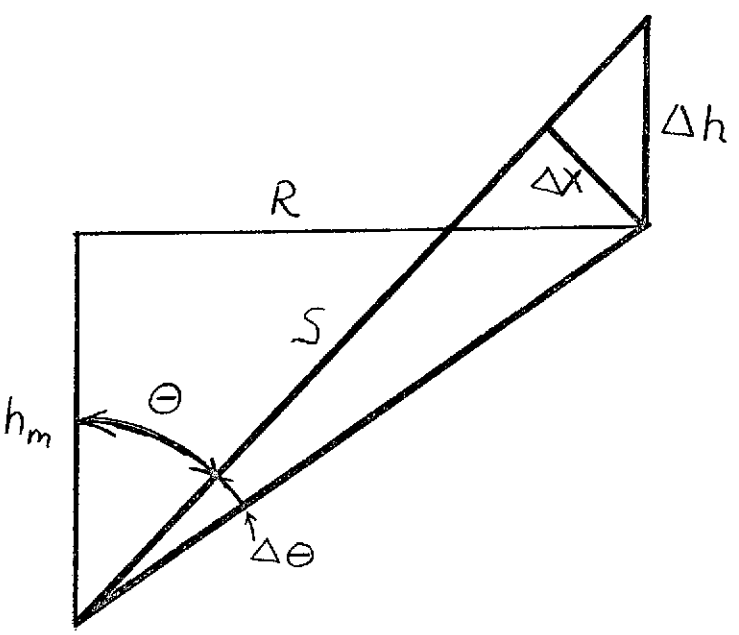

Figure 2

$$\frac{\Delta\sigma_\ell^2}{\sigma_\ell^2} = \frac{11}{6}\tan\theta\,\Delta\theta + \frac{3}{2}h_m^{-1}\Delta h_m + I^{-1}(h_m)\frac{\partial I(h_m)}{\partial h_m}\Delta h_m \qquad (13)$$

$$E_H = \frac{\Delta\sigma_\ell}{\sigma_\ell} = -\frac{11}{6}\frac{R^2}{S^2}\frac{\Delta H_m}{H_m} + \frac{3}{2}\frac{\Delta H_m}{H_m} + \frac{1}{I_m}\frac{\partial I_m(h_m)}{\partial h_m}\Delta H_m \qquad (14)$$

The last term in Equation 14 has been evaluated numerically on the IBM 360/50 computer using a double precision Simpson's rule integration. The values of this term are

- 2.45% per 1000 ft. at 42,000 feet
- 2.15% per 1000 ft. at 52,500 feet
- 1.90% per 1000 ft. at 63,000 feet.

Equation 10 and 14 specify the approximate errors in σ_ℓ^2 due to variation in ΔR and ΔH. These have been evaluated for the altitudes indicated above and for horizontal distances of 5 and 10 miles. The results are shown in Table II. The values for ΔE_H are seen to be quite small and may have either sign. This behavior may be understood by considering that for a positive ΔH, corresponding to an upward motion of the aircraft, the log amplitude variance is increased due to an increase in the propagation path length.

Table II

Altitude (1000's ft)	Range (Miles)	Slant Range (1000's ft.)	ΔE_R %/1000 ft.	ΔE_H %/1000 ft.	$\lvert\Delta E\rvert+\lvert\Delta H\rvert$ %/1000 ft.
42.0	5	49.2	2.0%	-.11%	2.1%
52.5	5	58.8	1.4%	+.005%	1.4%
63.0	5	68.3	1.04%	+.05%	1.1%
42.0	10	67.2	2.15%	.85%	3.0%
52.5	10	74.5	1.75%	1.11%	2.9%
63.0	10	82.1	1.44%	1.17%	2.6%

This effect is relatively slight; however, since C_N^2 at the altitudes we are considering is very small. Furthermore, it is compensated for by the decrease in zenith angle which tends to "swing" the propagation path up out of the more turbulent lower atmosphere. The variation in the horizontal distance has a larger effect since a positive ΔR (the aircraft moves outward from the ground station) both lengthens the propagation path and lowers it into a more turbulent region.

Angle of Arrival Fluctuations

The variance of the apparent angle of arrival can be shown to depend on the five-thirds power of the correlation length r_o[6.7], i.e.,

$$\langle \Delta\theta^2 \rangle \propto 1/r_o^{5/3} \tag{15}$$

For a spherical wave propagating from the ground to an aircraft at a slant range z. r_o may be expressed as

$$1/r_o^{5/2} \propto \int_0^Z C_N^2(h) \left(\frac{s}{z}\right)^{5/3} ds \tag{16}$$

or

$$1/r_o^{5/3} \propto \int_0^{z \cos\theta/h_o} (h_o u)^{-1/3} e^{-u} \left(\frac{u\, h_o}{z \cos\theta}\right)^{5/3} \left(\frac{h_o du}{\cos\theta}\right) \tag{17}$$

where we have let $u = s \cos\theta/h_o$. We note that $z \cos\theta$ is the aircraft altitude h_m, therefore

$$\langle \Delta\theta^2 \rangle \propto \frac{h_o^{7/3}}{h_m^{5/3} \cos\theta} \int_0^{h_m/h_o} e^{-u} u^{4/3} du \tag{18}$$

The integral in Equation 18 is the incomplete gamma function $r(h/h_o, 7/3)$ which, at the altitudes that we are considering, is a slowly varying function of h_m. We will therefore take it to be a constant and write

$$\langle \Delta\theta^2 \rangle \propto h_m^{-5/3} \cos^{-1} \theta \tag{19}$$

For changes in horizontal range

$$E_{\Delta R} = \frac{\Delta \langle \Delta\theta^2 \rangle}{\langle \Delta\theta^2 \rangle} = \text{Tan } \theta \, \Delta\theta \tag{20}$$

or

$$E_{\Delta R} = \frac{R\Delta R}{s^2} \tag{21}$$

By comparing this expression with Equation 10, we see that the angle of arrival measurement errors are smaller than the scintillation measurement errors by a factor of 6/11 for changes in R. Hence the requirement on the accuracy of R is not determined by the angle of arrival measurements.

For changes in the aircraft altitude we may replace cos θ by h_m/s hence

$$\langle \Delta\theta^2 \rangle \propto h_m^{-7/3} \, s = h_m^{-7/8} \sqrt{R^2 + h_m^2} \tag{22}$$

then

$$E_{\Delta H} = (-\frac{7}{3} H_m^{-1} + H_m s^{-2}) \Delta H_m \tag{23}$$

For a five-mile radius E_H varies from 3.8% at 42,000 feet to 2.5% at 63,000 feet.

For downlink angle of arrival, the integral in Equation 16 is replaced by

$$\int_0^Z C_N^2(h) \left(\frac{z-s}{z}\right)^{5/3} ds$$

No calculation for downlink angle of arrival fluctuation has been made.

Bit Error Rate Measurements

The probability of error for a binary coded channel in the presence of log normal scintillation has been given by Fried [8] as

$$P_E = [2\pi (8\beta^4\sigma_\ell^2 X_T + \beta^2 X_T)]^{-1/2}$$

$$x [\exp \{- \frac{1}{2} (4\beta^4\sigma_\ell^2 X_T + \beta^2 X_T)\}] \qquad (24)$$

where β is the signal to noise ratio in the receiver and σ_ℓ^2 is the log amplitude variance of the scintillation. The parameter X_T is related to σ_ℓ and β by

$$\sigma_\ell^2 = -(\ell n\ X_T)/(4 + 8\beta^2 X_T) \qquad (25)$$

Equation 24 was derived under the assumption that the receiver noise is white gaussian noise. This assumption may not be justified for an optical receiver where the principle noise source is the Shott noise in the photodetector. A more precise treatment of detection in an optical communications system has been given by Hoversten [9]. For the purpose of estimating the dependence of P_E on the small changes in range the gaussian noise model should be adequate, however, so that Equation 24 may be used.

Inspection of Equation 24 reveals that the probability of error, P_E, depends only on the signal to noise ratio β and the log amplitude variance of the scintillation σ_ℓ^2. Provided that we may assume that the receiver noise remains constant then β is proportional to the received power which in turn varies as the square of the slant range. Hence,

$$\frac{\Delta\beta}{\beta} = 2\,\frac{\Delta S}{S} \tag{26}$$

For a 1000 foot change in slant range, a 5 mile radius path and altitudes of 42,000 and 63,000 feet this error amounts to 4.76% and 2.44%, respectively.

The changes in σ_ℓ^2 have been discussed in a preceeding section. It therefore remains only to demonstrate how these changes will effect P_E.

Equation 24 may be simplified by noting that for a small change in β or σ_ℓ^2 the first factor will be slowly varying compared to the exponential. We may therefore treat it as constant. Eliminating σ_ℓ we obtain

$$P_E = K \exp\left[-\frac{1}{2}\left(\frac{4\beta^4 \ln X_T \cdot X_T}{4 + 8\beta^2 X_T} + \beta^2 X_T\right)\right] \tag{27}$$

or

$$P_E = K \exp\left[-f(X_T,\beta)\right] \tag{28}$$

then

$$\frac{1}{P_E}\,\frac{\partial P_E}{\partial X_T} = -\frac{\partial f}{\partial X_T} \tag{29}$$

and

$$\frac{1}{P_E} \frac{\partial P_E}{\partial \beta} = - \frac{\partial f}{\partial \beta} \tag{30}$$

From Equation 25 it is seen that X_T may take on values from a very small positive number (deep scintillation) to +1 (no scintillation) while β can take on any positive value. For the case of fairly large signal to noise ratio and small scintillation $f(\beta, X_T)$ will reduce to

$$f(\beta, X_T) = \frac{1}{2} \beta^2 \left(X_T + \frac{1}{2} \ln X_T\right) \tag{31}$$

then

$$\frac{\partial f}{\partial X_T} = \frac{1}{2} \beta^2 \left(1 + \frac{1}{2X_T}\right) \approx \frac{3}{4} \beta^2 \tag{32}$$

$$\frac{\partial f}{\partial \beta} = \left(X_T + \frac{1}{2} \ln X_T\right) \approx \beta X_T \tag{33}$$

Then

$$\frac{\Delta P_E}{P_E} = - \frac{\partial P_E}{\partial X_T} \cdot \frac{\partial X_T}{\partial \sigma_\ell^2} \Delta \sigma_\ell^2 - \frac{\partial P_E}{\partial \beta} \Delta \beta \tag{34}$$

$$\frac{\Delta P_E}{P_E} = - \left(\frac{3}{4} \beta^2\right) \left(\frac{1}{8\beta^2 X_T}\right) \Delta \sigma_\ell^2 - \beta X_T \Delta \beta \tag{35}$$

$$\frac{\Delta P_E}{P_E} = - \frac{3}{32} \frac{1}{X_T} \Delta \sigma_\ell - \beta X_T \Delta \beta \tag{36}$$

Now for the assumed conditions, i.e., β large and X_T approximately equal to unity the first term is small so that

$$\frac{\Delta P_E}{P_E} = - \beta X_T \Delta \beta \tag{37}$$

From this analysis it is clear that even these with the simplifying assumptions the bit error rate may be a strong function of the signal to noise ratio, particularly for the case of large β. It may therefore be necessary to limit the experimental conditions to those producing large bit error rates.

A more exact analysis could be carried out by avoiding the simplifying assumptions which we have made and differentiating equation directly. However, due to the uncertainty as to the accuracy of the gaussian noise model it was not felt that such an analysis would be worthwhile.

Atmospheric Attenuation

The atmospheric transmission τ_A is given by [10]

$$\tau_A = \frac{\pi(\alpha S)^2 \bar{I}}{P_T} \tag{38}$$

where S is the slant range to the aircraft; α the laser beam divergence angle, P_T the mean transmitted power and $\bar{I}$ the mean received power. In the preceeding section it was shown that for an altitude of 63,000 feet, I would change by about 2.44% per 1000 feet change in slant range. For attenuation measurements this variation is averaged so that small changes in the slant range have little effect on the observed value of τ_A provided that the average value of the slant range is accurately known. This information should be available from the GBAA. We therefore conclude that for changes in aircraft position of the order of a thousand feet will introduce errors of only a fraction of a percent into the measured value of τ_A. This is far less than the errors which may be expected in the measurement of $\bar{I}$ and P_T due to inaccuracies

in the calibration of the detectors.

The atmospheric extinction constant K is related to τ_A by

$$K = -\frac{1}{M} \ln \tau_A \tag{39}$$

Where M is the air mass, M is proportional to

$$\int_0^S e^{-h/h_o} \, ds \tag{40}$$

Where S is the slant range and h is height above the ground. For the altitudes we are considering this integral is constant to within about 1/2%.

Conclusions

From the preceeding analysis, it is clear that the quantities to be measured on the HAAT experiment are relatively insensitive to small changes in either the altitude of the aircraft or its horizontal distance from the ground station. Of the two the latter is the more critical. In general, changes in aircraft position of 1000 feet will produce variations of only 1 or 2% in the measured statistical parameters. A typical data segment will probably be 1 or 2 minutes long. Experimental results indicate that the measured values of log amplitude variance taken a few minutes apart may differ by a considerable amount. It is therefore not unreasonable to expect the log amplitude variance to change by a few percent during the course of a measurement. If this is the case, then an additional variation of a few percent due to flight path inaccuracies will not be objectionable.

A possible exception is the bit error rate measurements. At very small bit error rates, the error rate becomes a very sensitive function of signal to noise ratio and therefore a sensitive function of received power. This, combined with the fact that a long time is required to measure a very small bit error rate, may make it difficult to compare the measured BER with theory.

Recommendations

It is recommended that the initial operational plan specify navigation tolerances during data acquisition of $\pm$500 feet in range from the ground station and $\pm$500 feet in altitude. These tolerances are to be held for one complete orbit around the ground station.

If it appears likely, either from discussion with Air Force personnel or from experience on early flights in the program, that these tolerances impose excessive restraints upon the operation of the aircraft, then they may be relaxed by as much as a factor of 2 or 3 without jeopardizing the validity of the experiment.

METEROLOGICAL DATA REQUIREMENTS

Introduction

The High Altitude Aircraft Test for Visible Laser Optical Communications requires that meterological data be collected prior to and during each test flight so that the optical measurements may be correlated with such gross atmospheric parameters as temperature, barometric pressure, relative humidity, and wind profile. In addition meteorological data will be useful in revealing unusual atmospheric conditions, such as a temperature inversion, which might lead to anomalous experimental results. A second, and equally important, requirement for meteorological data is to assist is scheduling the test at the most advantageous times from the point of view of favorable weather conditions. Also the test conductor must be provided with current and accurate forecast so that in the event of deteriorating weather conditions he will have the best possible information on which to base a decision to cancel or postpone the test flight.

Several sources of meteorological data are available. These include instrumentation which will be located at the Madkin Mountain ground terminal, the MSFC Atmospheric research station facilities located approximately three miles southwest of the ground terminal, the FAA Aircraft Advisory westher facilities located at the Huntsville - Decatur Airport five miles to the west, and several other weather stations on Redstone Arsenal operated for other purposes. In addition use will

be made of the normal NOAA wide area weather information services. The MSFC Atmospheric Research Station will be the principal source of meteorological measurements and will assume primary responsibility for the collection and evaluation of weather information from all sources and for providing weather forecasts to the test conductor.

We have, at the direction of the contracting officers representative (COR), undertaken to review the meteorological support requirements for the High Altitude Aircraft Program. A preliminary statement of the meteorological data to be collected in connection with these test is given in the HAAT program plan [11]. We have carefully reviewed the meteorological measurements specified in that document to determine their value in analyzing the optical propagation data which will be obtained and to insure that no additional meterological data will be required. Several conferences have been held between the project director and MSFC Atmospheric Research Station personnel. On the basis of these conferences and our review, specific recommendations for meteorological data requirements have been formulated. We have also considered the question of what, if any, specific criteria can be established for the minimum weather conditions under which a flight test will be conducted.

Application to Measurements Program

Meteorological data will be used in the analysis of both the optical propagation experiments and the engineering experiments performed during the high sltitude aircraft test. Areas in which meteorological data will be employed include the following.

a) General Weather Conditions. For the optical propagation data to be meaningful it is necessary that the general weather conditions under which it was collected be carefully and quantitatively documented. The same is true, perhaps even to a greater degree, for the analysis of the communication and tracking systems performance. For this reason careful meteorological observations must be made throughout each flight. Special importance must be attached to the identification of any unusual conditions, such as temperature inversions or high, thin cloud cover, which might not be readily apparent to a casual observer.

b) Wind Profile. The frequency spectrum of the optical scintillation depends upon the component of wind velocity transverse to the optical path. Wind profile measurements will therefore be directly applicable to the analysis of the scintillation data. Fried [12] has developed expressions for the scintillation spectrum as a function of wind speed assuming that the wind speed is constant along the optical path. To our knowledge no analysis has been performed for the case of wind speed which varies along the optical path. Therefore additional theoretical work may be required in this area in order to properly interpret the results of the aircraft test.

c) Estimation of Structure Constant Profile. In order to adequately compare the experimental results to theory it would be desirable that the atmospheric structure constant, C_N^2 be measured as a function of altitude during each test. Methods of determining C_N^2 from the temperature structure constant have been proposed by Ochs [13,14]. It does not appear, however, that the instrumentation to make these measurements capable of being flown on a weather balloon will be

available in time for use on this project. It will therefore be necessary to assume a standard profile for C_N^2 and to attempt to infer from conventional meteorological data the validity of this assumption. Information as such factors as temperature lapse rates will be useful in detecting conditions under which the C_N^2 profile may deviate from normal.

Test Scheduling

One of the most important applications of meteorological information will be it's use in scheduling the test flights at times when the weather conditions are likely to be the most favorable and in deciding when conditions warrent the postponement or cancellation of a test. The problem of scheduling will consist of three phases, viz. (1) Advanced scheduling of flight periods, (2) selection of specific flight times and (3) the decision to delay or abort a test in the event of deteriorating weather conditions.

We recommend that the following procedure and criteria be adopted for scheduling of flight test from a weather standpoint and for cancelling of a mission once it has begun.

A. Advanced Scheduling

The test will be carried out in sequencies of four flights. The operational periods for each sequence will be determined as far in advance as possible. In order to schedule the operational periods at times when most favorable weather conditions are likely to prevail it will be necessary to compile statistical data concerning the typical weather patterns at various times of the year in the Huntsville

area. This data will include such factors as the average number of clear days per month, the typical monthly rainfall, etc. Based on statistics available for the past several years preferred operational periods will be established.

B. Selection of Specific Flight Times

One week before the beginning of each operational period tentative flight schedules will be established. The specific dates and times chosen will be based primarily upon a prediction of a low percent cloud cover and the absence of fog, haze or other conditions which might adversely effect the operation of the experimental system. The schedules must be considered tentative at this point since the reliability of one-week forecast is not very great.

Flight schedules will be reviewed at 5 days, 3 days, 48 hours and 24 hours before the beginning of each test. Rescheduling will be possible at each of these points if revised forecasts indicate an increased probability of fog, haze or excessive cloud cover.

C. Cancellation of Test

For the 24 hour period prior to the flight revised forecasts will be made every 6 hours and then hourly for the 6 hour period immediately preceeding the flight.

D. Criteria for Postponement of Test

It is recommended that the following criteria be used in scheduling and delaying a test flight.

1. Predicted cloud cover greater than 10 percent.

2. Any prediction of fog, haze, or cirrus clouds which might reduce atmospheric transmission below 70%.

Data Requirements

On the basis of our survey of the meteorological data required to support the High Altitude Aircraft Test and as the result of several conferences held with the MSFC meteorologist we recommend that the following meteorological measurements be made.

A. Madkin Mountain Ground Station

A meteorological shelter will be installed near the Ground Terminal on Madkin Mountain. Instrumentation will consist of a hydrothermograph to provide a continuous recording of relative humidity and temperature and a recording anamometer to measure wind speed and direction. Measurements at this site are required from 24 hours prior to the beginning of each test flight until 24 hours after the conclusion of the test.

B. At MSFC Atmospheric Station

1. Hourly observations from 6 hours prior to the beginning of each flight test until 1 hour prior to the beginning of the test, and then every 1/2 hour until the conclusion of the test. Observations will consist of:

a) Temperature

b) Barometric pressure

c) Relative Humidity

d) Wind Speed and Direction

e) Clouds, percent cover, type and approximate altitude

f) Surface visibility

2. Radiosonde Releases to provide temperature, relative humidity, wind speed and wind direction as a function of altitude from the surface

to 110,000 feet at 1000 foot intervals. Relative humidity measurement will not be made above 40,000 feet due to its low value above this level. It is expected that all of the sondes may not reach the specified altitude. This is not critical, however, since data above the operating altitude of the test aircraft is of only minor interest.

Two radiosonde releases are required for each flight test. The first will be made enough in advance of the arrival of the aircraft over station so that a complete profile will be available at the beginning of the test. The second release will be made near the mid-point of the test. In the event that the aircraft remains on station for the maximum time (4 hours) a third release near the end of the test would be very desirable.

C. Wide Area Weather Information

To aid in evaluating the local weather data and in predicting conditions at the time of each test wide area weather information is required. Meteorological FAX charts will therefore be supplied for surface, 500 mb., 700 mb. and 850 mb. every six hours of 48 hours preceeding and 24 hours following each flight.

ENGINEERING MEASUREMENTS PROGRAM

Introduction

The High Altitude Aircraft Test program plan contains, as Appendix B, a detailed measurements program for the scientific experiments which will be conducted. Engineering measurements are briefly outlined in Section III.C.5 (page 22) of the subject document. It was desired by the cognizant MSFC personnel that the engineering aspects of the HAAT program be documented in detail comparable to the scientific measurement program. We have, therefore, prepared at the request of the contracting officers representative this engineering measurements plan which describes the engineering and system analysis aspects of the Aircraft Test program.

Engineering Measurements

The measurements described in Sections III.C.1 through III.C.4 of the Measurements Program for the High Altitude Aircraft Test of Visible Laser Optical Communications are intended to yield fundamental information concerning the turbulence and transmission of the earth's atmosphere and their effects on wave propagation at optical frequencies. They will also provide critical data needed to design future optical communications systems for ground to satellite applications. In addition a number of engineering measurements will be made for the purpose of evaluating the performance of the tracking and communications systems and confirming the feasibility of the design concepts employed. These measurements will include:

a. Measurement of the return signal strength (joules/pulse) in the ground based acquisition aid (GBAA).

b. Determination of the maximum range for acquisition with the GBAA.

c. Measurement of the frequency of loss-of-track and time to reacquire.

d. Observation and video-recording of a real time television transmission.

e. Monitoring of certain "house keeping data" which will provide information on the operation and reliability of the various subsystems.

This data will be analyzed and evaluated in conjunction with other flight measurements, such as scintillation, and data from peripheral experiments as described below.

Engineering Analysis

1. Objectives

From an engineering viewpoint the high altitude aircraft test are intended to perform a number of functions. These include:

a. To demonstrate the feasibility of the technical approaches taken to the problems of acquiring and cooperatively tracking.

b. To demonstrate the feasibility of high data rate optical communication over vertical paths through the atmosphere.

c. To demonstrate the reliability of optical tracking and communication systems under actual operational conditions not too dissimilar to those which would be encountered in an earth to space link.

d. To provide engineering data which will be valuable in the design of future optical communications systems.

e. To identify the sources of error in the tracking and communications systems and to estimate their relative importance in terms of overall system operation.

In order to achieve these objectives a detailed evaluation of the operation of each subsystem should be performed. In the following section we have considered each subsystem and identified certain areas which we feel should be investigated and recommended measurements which should provide useful engineering data. In the following discussion it is assumed that the system is operating normally and within design specifications. Needless to say an important aspect of any engineering evaluation is the identification of those areas in which the system does not perform as expected or does not meet its design specifications. Since it may not always be possible to anticipate what these areas will be or what measurements should be made we have excluded measurements on malfunctioning systems from this discussion. Such measurements should more properly be considered trouble-shooting. We also exclude from consideration routine measurements which would fall into the category of acceptance-testing.

2. Ground Based Acquisition Aid (GBAA)

In the acquisition mode of operation the ground based acquisition aid (GBAA) depends upon the return of a single laser pulse in order to detect the incoming aircraft. This makes the system very sensitive to the effects of atmospheric scintillation since acquisition could be missed if the critical pulse occurred at an instant of deep fade. The designers of the GBAA (ITT Corp.) have attempted to minimize this possibility by dispersing the retro-reflectors on the

aircraft over distances large compared to the correlation distances for atmospheric scintillation. In this way it becomes unlikely that all retro-reflectors will be in a region of fade at the same instant. This technique is in effect a form of aperture averaging for the returned signal. Considerable effort has been devoted to the analysis of the intensity of the returned pulses and the effect of dispersing the retro-reflector arrays [15].

It is important to the design of future acquisition and tracking systems that the effects of scintillation be experimentally determined and the effectiveness of dispersing the retro-reflectors be evaluated. This may be accomplished during the high altitude aircraft test by measuring the returned signal strength and comparing the observed data with the theoretical predictions. Quantities to be measured should include:

a. The mean intensity of the returned laser pulse.

b. The probability density function of the returned pulse amplitude.

In order to compare these measurements with the theoretical predictions both quantities should be measured simultaneously with scintillations experiments performed with the up and downlink communications systems.

A second engineering measurement on the GBAA will consist of determining the frequency of loss-of-track and the ability of the system to reacquire. It is expected that due to scintillation or system noise the GBAA will occasionally loose track of the aircraft. When this occurs the GBAA will automatically switch from the track-mode to a reqcquire mode and the presence of this condition will be indicated

by a light on the GBAA control console. In order to measure the frequence of loss-of-track it will only be necessary to connect a counter to record the number of times the reacquire mode indicator is turned on. It might also be of interest to arrange a timer which would be started when the reacquire mode is entered and stopped when the track mode is entered. In this way the mean time required to reacquire the aircraft could be determined.

The expected frequency of loss-of-track will depend upon the detection probability for a pulse and thus may be computed in a manner similar to that used to determine the probability of acquisition. Comparison with the observed frequency with which track is lost will therefore provide an additional verification of the atmospheric model used in designing the GBAA.

3. Main Tracking System

Errors in the main optical tracking system are expected to arise from three sources; atmospheric scintillation, mechanical errors in the telescope mount and associated drive motors, and errors in the control electronics. Analysis of the tracking system should not only determine the overall tracking accuracy of the system but also should attempt to identify the contribution of each of these factors to the total system error.

Available data will consist of the telescope mount position encoders read-out, the signal to the fine pointing beam storers and the output signal from the tracking detector. The sum of these three signals will be the instantaneous bearing of the target aircraft. From this it will be necessary to remove the actual aircraft motion and the apparent

pointing fluctuations due to atmospheric scintillation. Changes in the measured bearing due to actual aircraft motion can be assumed to be slow and smoothly changing so that the variance of the fluctuations about an instantaneous mean can be attributed entirely to system error or atmospheric effects. Simultaneous observation of scintillation will provide a measure of the integrated atmospheric turbulence along the optical path from which the angle of arrival fluctuations may be estimated.* After correcting the variance of the observed tracking fluctuations for actual target motion and atmospheric effects the remaining variation may be attributed to electrical or mechanical tracking errors. While this method is at best rough it is felt that it should yield a fair estimate of the tracking system performance.

4. Communications System

The principal engineering analysis which will be performed on the communications system will be measurements of bit error rates for the downlink P.C.M. system. These measurements have been described in detail in the scientific measurement program document so will not be discussed further here.

In addition to quantative bit error rate measurements a real time television picture will be transmitted to allow an evaluation of picture quality. By alternating between bit error rate measurement and

---

*This estimate will not be exact since scintillation and apparent angle of arrival fluctuation depend upon the index of refraction structure constant multiplied by an appropriate lever function and integrated along the optical path. Since this lever function is not the same in both cases it will be necessary to make as assumption concerning the structure constant profile which may effect the result.

video transmission it will be possible to determine the bit error rate for each sample picture. Thus the subjective evaluation of picture quality amy be correlated with a measured bit error rate. Considerable research has been conducted to correlate bit error rates and picture qualities for R.F. television systems. However, because of the differences in the statistical nature of conventional communication channels and atmospheric channels it will be of interest to repeat these studies for an optical communications system.

The uplink communications channel will be used only to transmit operational commands to the airborne experiment package. Unless it should prove to be unreliable, which is not expected to be the case, it's operation will not be well suited to any type of quantitative analysis or evaluation.

Conclusions

In attempting to document an engineering measurements program one encounters certain difficulties not presented by a scientific measurement program. As a scientific experiment the high altitude aircraft project involves certain well defined aspects of optical propagation which one wishes to investigate. It is therefore possible to detail in advance exactly what data is required and what measurement should be made. From an engineering point of view the most interesting and important aspects of the experiment may well be those in which the experiment does not perform exactly as expected. If a system operates precisely as it was designed then there is no engineering problem of any importance left. This consideration makes it impossible to detail in

advance all the engineering experiments which will probably be conducted in connection with the project. Secondly, unlike a scientific experiment where much qualitative data is collected, engineering experiments involve much more qualitative or subjective observation on the part of the personnel involved. That is to say an engineering experiment is often more of a learning experience for the engineer than a formal process of data taking and therefore much less subject to advance planning and documentation.

In the preceeding sections several areas have been identified in which it is felt an analysis of the operation of the High Altitude Aircraft Experiment hardware will lead to engineering data of value in the design of future optical communication systems. A number of measurements have been suggested to obtain this data. It is expected that as the MSFC operating personnel gain experience with the operation of the system many other engineering measurements will present themselves.

REFERENCES

1. Webb, William E., Final Report on NASA Contract NAS8-30507, BER Report No. 111-70, University, Alabama, November, 1969.

2. High Altitude Aircraft Experiment Test for Visible Laser Optical Communications. NASA Internal Document, August, 1970.

3. Ibid. Appendix B, p. 14.

4. Fried, D. L., Optical Science Consultants Report. TR-001, August, 1970.

5. Lawrence, R. S. and J. W. Strohbehn, "A Survey of Clear Air Propagation Effects Relevant to Optical Communications", Proc. IEEE. 58, 1523, (1970).

6. Fried, D. L., "Statistics of a Geometric Representation of Wave Front Distortion", J. Opt. Soc. Am. 55, p. 1472, (1965).

7. Webb, W. E., "Study of Atmospheric Effects on Optical Communications and Optical Systems", Final Report on NASA Contract NAS8-30507, BER Report No. 111-70, University of Alabama, November, 1969.

8. Fried, D. L., and Schmeltzer, R. A., "The Effects of Atmospheric Scintillation on an Optical Data Channel - Laser Radar and Binary Communications", Appl. Opt. 6, p. 1729, (1967).

9. Hoversten, E. V., R. O. Harger, and S. J. Halme, "Communications Theory for the Turbulent Atmosphere", Proc. IEEE, 58, 1626 (1970).

10. Reference 2. Appendix B, p. 43.

11. Reference 2. Appendix B, p. 23.

12. Fried, D. L., "Atmospheric Modulation Noise in an Optical Heterodyne Receiver", IEEE J. Quantum Electronics, QE-3, 213 (1967).

13. Lawrence, R. S., Ochs, G. R., and Clifford, S. F., "Measurements of Atmospheric Turbulence Relative to Optical Propagation," J. Opt. Soc. Am. 60, 1970, p. 826.

14. Ochs, G. R., "A Resistance Thermomenter for Measuring Air Temperature Fluctuations," ESSA Report, No. IER-47-ITSA-46, October, 1967.

15. Fried, D. L., "Analysis of the Atmospheric Loss Factor for the Ground Based Acquisition Aid Portion of the High Altitude Experiment", Optical Sciences Consultants Report, TR-001, Yorba Linda, Calif., August, 1970 (prepared for ITT Corp., San Francisco, Calif.).

APPENDIX 5

PATH ANALYSIS FOR AVLOC PROJECT

The following report on the atmospheric propagation experiments performed during the AVLOC flight was prepared at the request of Dr. Joe Randall and is intended as a portion of the MSFC final report on project AVLOC.

Data used in this report has been taken from "Measurement Report on Altitude Aircraft Test" Vol. I (AVLOC Flight 9), Vol. II (AVLOC Flight 12) and Vol. III (AVLOC Flight 15), final report on NASA Contract NAS8-29194, by Northrop Services Inc., Huntsville, Alabama. The description of the data reduction procedures used by Northrop Services Inc. also follows closely that found in the referenced report.

Certain paragraphs in the following report have been omitted when the pertinent data were not available. It is intended that the omitted paragraphs will be supplied by MSFC personnel who are preparing other sections of the final AVLOC report.

Reference numbers are also omitted since they will be specified during final editing in a manner consistent with the complete AVLOC report. Likewise the equation numbers will have to be modified to agree with the numbering of the equations in the other parts of the report.

PROPAGATION EXPERIMENTS

Introduction

The principal objectives of the AVLOC test were the engineering evaluation of an operational optical communications system and the scientific investigation of optical propagation over vertical paths throught the atmosphere. In order to fulfill the second objective extensive measurements of scintillation, bit error rates, angle of arrival fluctuations and atmospheric attenuation were planed. Each of these quantities was to be investigated as a function of receiving and transmitting aperture, range and zenith angle, and all measurements except bit error rates were to be made on both up link and down link beams. Since the AVLOC tests were to extend over the period of a year it was also expected that seasonal variations in propagation characteristics and the effects of meterological conditions could be studied.

The following table, reproduced from the original measurements plan, lists the proposed propagation experiments.

Table . MEASUREMENTS OUTLINE

Quantity Measured	Parameters	Analysis to Yield
1. Scintillation (downlink)	Receiving Aperture Range Zenith Angle	Log amplitude variance. Probability density function. Verify theoretical predictions concerning zenith angle, and range dependence. Aperture averaging effects: a. Reduction of signal variance. b. Change of probability density function. Difference in uplink and downlink.
2. Scintillation (uplink)	Receiving Aperture Range Zenith Angle Transmitter Aperture	Log amplitude variance. Probability density function. Verify theoretical prediction concerning zenith angle and range dependence. Verify no uplink aperture averaging. Effect of transmitting aperture size. Differences in uplink and downlink.
3. Angle of Arrival Fluctuations (downlink)	Range Zenith Angle Receiving Aperture	Variance. Probability density function. Aperture averaging. Dependence on range and zenith angle. Differences between uplink and downlink.
4. Angle of arrival Fluctuations (uplink)	Range Zenith Angle	Variance. Probability density function. Dependence on range and zenith angle. Differences between uplink and downlink.
5. Bit Error Rate	Range Zenith Angle Beam Divergence Transmitter Power	Verify theoretical prediction of BER dependence on system noise and irradiance fluctuation variance.

6.	Atmospheric Transmittance	None	Atmospheric transmittance at optical wavelengths.
7.	Engineering Measurements		Determine ability to acquire and track. Evaluate system performance.

Early in the project's design phase it was realized that certain of these measurements presented greater experimental difficulties than had been anticipated. For example, accurate measurements of atmospheric transmission requires a precisely calibrated detector on the aircraft to monitor transmitted power and an exact knowledge of the beam profile. It soon became apparent that it would be very costly to implement a meaningful transmission measurement. Since funds were limited this experiment was eliminated from the measurements plan. Likewise it was decided that meaningful measurement of the angle of arrival fluctuations would impose excessive requirements on the accuracy of the tracking system and these experiments were also eliminated. Thus at the beginning of the operational phase of the project the planned measurement consisted of uplink scintillation, downlink scintillation, bit error rates and a qualitative investigation of the effect of atmospheric attenuation.

Equipment problems during the early flights severely limited the amount of time available for data collection and prevented the completion of even the reduced measurements program. Useful data was collected only on flights 9, 12, and 15 and during these flights the system was fully operational only part of the time. We were therefore unable to conduct extensive investigation into the effect of transmitter and receiver aperture size nor could bit error rate measurements be made. It was also discovered when the data was reduced that saturation in an amplifier had destroyed most of downlink scintillation data.

In summary, reliable data has been obtained only for the uplink scintillation experiments although some qualitative information concerning atmospheric transmission is also available.

Data Collected

The following is a summary of the experimental data collected aboard the aircraft and at the ground station.

Aircraft Data. The data collected aboard the aircraft is shown in Table 2. All data was recorded on magnetic tape.

Table 2. Aircraft Data

Tape Channel	Quantity
1	Image Disector Error, Y component
2	Image Disector Error, Z component
3	Beam Steerer Angle, Y component
4	Beam Steerer Angle, Z component
5	Vibration, Pitch
6	Vibration, Yaw
7	Vibration, Longitudinal
8	Log Amplitude Scintillation
9	Linear Amplitude Scintillation
10	PAM DATA

The image disector errors (ch. 1 and 2) are error voltages generated in the tracking system that are proportional to the angle of arrival of the incoming beam. The beam steerer angles (ch. 3 and 4) are the voltages

applied to the beam steerers. Vibration data (ch. 5 - 7) was obtained from three vibration sensors mounted along mutually orthogonal axes on the airborne communications package. Linear amplitude scintillation (ch. 9) is the instantaneous received power at the aircraft while log amplitude scintillation (ch. 8) is the same signal after passing through a logrithmic amplifier. Channel 10 (PAM data) consists of a number of measurements that were made periodically and multiplexed onto a single channel for recording. The PAM data is listed in Table 3. A complete description of the way in which this data was obtained can be found in the system description elsewhere in this report.

TABLE 3. PAM DATA

VCO Channel	Data	Quantity Recorded
3	Beacon Presence	ON/OFF
4	TV filter	OUT/IN
5	Receiver Aperture	OUT/IN
6	Beam Divergence	Arc Seconds
7	Laser Shutter	OUT/IN
8	Tracker Attenuation	Position
9	Receiver Attenuation	OUT/IN
10	Fine Track	ON/OFF
11	60 Hz Power	Voltage
12	400 Hz Power	Voltage
13	28V DC unregulated	Voltage
14	28V DC regulated	Voltage
15	5V DC	Voltage
16	15V DC	Voltage
17	AOCP Temperature	Deg. C.
18	Cannister Temperature	Deg. C.

Ground Station Data

This section intentionally left blank

DATA REDUCTION

Aircraft Data

Selection of Data Slices. Data was recorded on analog magnetic tape throughout the entire time that the RB-57 aircraft was over station. Oscillograms were first made from the analog tapes and inspected to determine those periods during which uninterrupted power was being received at the aircraft and the airborne tracking system was operating normally. Based on this inspection time slices were selected for further processing.

Analog/Digital Conversion. Selected data was digitized and recorded on digital magnetic tape for computer processing. A sampling rate of 2000 samples per second was used to provide an upper frequency cut off of 1 KHz. The quantization level of 1024 (10 bits/sample) was used to accomodate the required 60 db dynamic range.

Probability Density and Moments. The probability density function (PDF) and cumulative distribution function is computed for each channel of the selected data slices. Based on the PDF, the first four central

moments, i.e., mean, variance, third moment and fourth moment are computed. Next, the skewness and kurtosis are computed from these moments. For normal (gaussian) distribution, the kurtosis will be equal to 3 and skewness equal to zero.

Test for Normality of Probability Distribution. The fact of kurtosis being equal to 3 and skewness being zero is not enough to establish the normality of any distribution. At best, it is only a quick check. The standard statistical test for goodness-of-fit for normality is the chi-square test. This is a one-way test giving the upper confidence limit for any prescribed level of significance. One problem in using the chi-square test is the choice of the class number and class limits for the PDF, since it is known that different choices may yield different results. A procedure for minimizing the subjectiveness has been proposed by Mann and Wald (refs. , and). This procedure computes the number of classes based on the number of data points used and the desired level of significance. Further, the corresponding class limits are chosen in such a way that the theoretical distribution under test in each class interval is equal. The Mann-Wald procedure is used in the present data processing.

Power Spectral Density. The fast Fourier Transform (FFT) is used for computing the power spectral density (PSD) of the data channel of interest. The particular version for the PSD employed in this study is based on time averaging over short, modified periodograms obtained by the FFT (ref.). Further, use is made of the complex-conjugate relationship of the FFT for

real time series, so that two real data series can be transformed simultaneously in order to cut the required computation time approximately in half (ref.).

Correlation Coefficient. To determine quantitatively the degree of dependence between any two data series, the correlation coefficient is computed. It is defined as the normalized time-lagged product between the given two random time series of interest. Its value should be within $\pm$ 1.

Summary of Data Recorded. Useful data was obtained only on flights 9, 12 and 15. The data segments that were digitized and processed are listed in the following tables.

Table 4. AVLOC Flight 9 Aircraft Data

Data Piece No.	A/D Time (seconds)
2	15
3	10
4	50
5	20
6	10
7	30
8	40
9	10
10	10
11	20
12	50
13	30
14	30
15	20
16	50
Total Time	395 seconds

Table 5. AVLOC Flight 12 Aircraft Data

Data Piece No.	A/D Time (Seconds)
1	200
2	70
3	100
4	190
5	80
6	80
7	100
8	200
9	70
10	190
11	80
12	100
13	
14	
Total	1,460 Seconds

Table 6. AVLOC Flight 15 Aircraft Data

Data Piece No.	A/D Time (Seconds)
1	26
2	30
3	60
4	30
5	30
Total Time	176 Seconds

GROUND STATION DATA

This section intentionally left blank

DATA ANALYSIS

Uplink Scintillation

The uplink scintillation was measured by a tracking photodetector in the AOCP which measured the instantaneous received power. The photodetector output was recorded in three modes; linear, logarithmic and base band. The base band channel consisted of direct recording of the detector output. In order to avoid the effects of background radiation the uplink beacon was modulated at 10.7 KHz, and the amplitude of this frequency component recorded (linear channel). The 10.7 KHz signal was also passed through a log-amplifier before recording (logarithmic channel). Inspection of the data has shown that the amplitude scintillation was so large that the linear range of both the linear and base band channels was exceeded. The logarithemic channel was well within the dynamic range of the system. For this reason we have based all analysis on the logarithmic channel data.

The available data consist of 15 segments from flight 9, 14 segments from flight 12, and 3 segments from flight 15 as indicated in tables 4 and 5. At least one 10 second segment was selected from each data piece for analysis.

A summary of the reduced data is included in appendix .

Log Normalicy

According to the most generally accepted theory of atmospheric turbulance amplitude scintillation is expected to follow a log normal probability distribution, i.e., the logarithm of the amplitude fluctuations should be a gaussian random variable. To test this hypotheses three statistical techniques were used, the method of moments, the chi-square test and plots

of the cumulative probability of the log and linear scintillation on "probability paper". In the last method the horizontal coordinate scale is such that if the data is indeed normal the resulting plot will be a straight line. Plots for the log and linear recordings of a typical data segment are shown in the following figures. Other data segments yielded essentially similar results.

Inspection of the probability distribution curves and the statistical moments indicates that in all cases the observed scintillation more nearly approximated a log-normal distribution than a gaussian. The goodness-of-fit to the log-normal distribution was moderately good. There was a general trend for the fit to become worse as the amplitude variance increased. We have carefully considered all possible sources of experimental error that might bias the observed probability distributions; a discussion of the possible sources of error is given in a following section. Although we have been unable to identify any single error that could be expected to cause the observed discrepancy with log-normalicy it is still possible that the effect might be due to the accumulation of errors from several sources.

In summary, the observed data shows a strong tendency toward log-normalicy. On the basis of the observed data we are unable to determine with certainty whether the observed departure from the expected distribution is due to experimental error or represents a real deviation of the propagation process from the theoretically predicted result.

CUMULATIVE PROBABILITY
DENSITY PLOT (LOG)

Flight 12

Channel 8

Data Piece 6

Figure 1

CUMMULATIVE PROBABILITY
DENSITY PLOT (LINEAR)

Flight 12

Channel 9

Data Piece 6

Figure 2

Amplitude Variance

As previously stated the base band and linear scintillation data showed saturation effects because the dynamic range of the signal exceeded the linear range of the recording channel. For this reason we have taken the variance from the log scintillation channel only.

It is convenient to convert the variance of the logarithmic signal to intensity variance. This may be accomplished as follows. We assume that the log channel output is a voltage V which is related to the received intensity I by

$$V = \alpha \ln I + \gamma \qquad 1$$

Likewise the output of the linear channel S is given by

$$S = \beta I \qquad 2$$

Where α, β and γ are constants that depend upon the amplifier gains in the two channels. Solving equation 1 for I we have

$$I = \exp\left[\frac{V - \gamma}{\alpha}\right] \qquad 3$$

hence

$$S = \beta \exp\left[\frac{V - \gamma}{\alpha}\right] \qquad 4$$

or

$$S = \exp\left[\frac{V - \gamma}{\alpha} + \ln\beta\right] \qquad 5$$

we may replace the quantity $-\gamma/\alpha + \ln\beta$ by a new constant δ

$$S = e^{\delta} \cdot e^{V/\alpha} \tag{6}$$

Now let S_o be the mean value of S.

$$S_o = e^{\delta} \langle e^{\gamma/\alpha} \rangle \tag{7}$$

The variance of S is

$$C_s = \langle (S-S_o)^2 \rangle \tag{8}$$

$$C_S = \langle (e^{\delta} e^{v/\alpha} - e^{\delta} \langle e^{v/\alpha} \rangle)^2 \rangle \tag{9}$$

$$C_s = e^{2\delta} \langle e^{v/\alpha} \rangle^2 \left\langle \left(\frac{e^{v/\alpha}}{\langle e^{v/\alpha} \rangle} - 1 \right)^2 \right\rangle \tag{10}$$

Now we assume that I is log normal, hence V is a gaussian random variable.

For any gaussian random variable X

$$\langle e^{ax} \rangle = \exp\left[a\langle x \rangle + \frac{a^2}{2} \langle (x-\langle x \rangle)^2 \rangle\right] \tag{11}$$

$$\langle e^{ax} \rangle = \exp\left[a\langle x \rangle + \frac{a^2}{2} Cx\right] \tag{12}$$

a = a constant. Hence

$$\langle e^{v/2} \rangle = \exp\left[\frac{\langle V \rangle}{\alpha} + \frac{CV}{2\alpha^2}\right] \tag{13}$$

$$C_s = e^{2\delta} \langle e^{v/\alpha} \rangle^2 \left\langle \frac{e^{2v/\alpha}}{\langle e^{v/2} \rangle^{\alpha}} - 2\frac{e^{v/\alpha}}{\langle e^{v/\alpha} \rangle} + 1 \right\rangle \tag{14}$$

$$C_s = S_o^2 \left\langle \frac{e^{2v/\alpha}}{\langle e^{v/\alpha} \rangle^2} - 2\frac{\langle e^{v/\alpha} \rangle}{\langle e^{v/\alpha} \rangle} + 1 \right\rangle \tag{15}$$

$$C_s = S_o^2 \left[\frac{\langle e^{2v/\alpha} \rangle}{\langle e^{v/\alpha} \rangle^2} - 1 \right] \tag{16}$$

then using the above relationship

$$C_s = S_o^2 \left[\frac{\exp \frac{2\langle V \rangle}{\alpha} + \frac{2Cv}{2}}{\exp 2 \frac{\langle V \rangle}{\alpha} + \frac{Cv}{2\alpha^2}} - 1 \right] \qquad 17$$

$$C_s = S_o^2 \left[\exp\left[\frac{Cv}{\alpha^2}\right] - 1 \right] \qquad 18$$

or introducing the standard deviations σ_s and σ_r is place of the variances

$$\sigma_s = \sqrt{C_s} \text{ and } \sigma_v = \sqrt{C_v} \qquad 19$$

we finally obtain.

$$\sigma_s / S_o = \left[e^{(v/\alpha)^2} - 1 \right]^{1/2} \qquad 20$$

But since

$$\sigma_s = \beta \sigma_I \qquad 21$$

and

$$S_o = \beta I_o \qquad 22$$

$$\sigma_I / I_o = \left[e^{(\sigma v/\alpha)^2} - 1 \right]^{1/2} \qquad 23$$

which is the required expression for the normalized standard deviation of the intensity fluctuations.

The one remaining constant in equation 20 and 23 can be evaluated from the calibration curve of the scintillation detector. Based on post flight calibration data, α has been found to be 0.532 volts.

The following table gives the log variance C_v and the normalized intensity variance σ_I/I_o for each data segment. The mean and standard deviation of (σ_I/I_o) for each flight is given in Table 8.

The quantities shown in Table 8 are the mean and standard deviation of the received power and hence are proportional to the mean and standard deviation of irradiance. The S. D. of power is in fact equal to the S. D. of irradiance because of the normalization. Most theoretical results, however, are expressed in terms of the log amplitude variance C_1. This quantity is easily obtained from the data as follows. C_1 is defined as

$$C_1 = \langle (1-\bar{1})^2 \rangle \qquad 24$$

where 1 is the log amplitude

$$1 = \ln(A/\bar{A}) = 1/2\ln(I/\bar{I}) \qquad 25$$

Making use of equation 1 and the definition of C_V

$$C_v = \langle (V - \bar{V})^2 \rangle \qquad 26$$

we have

$$C_v = \left\langle \left(\alpha \ln \frac{I}{\delta} - \left\langle \alpha \ln \frac{I}{\delta} \right\rangle\right)^2 \right\rangle \qquad 27$$

which upon expanding the square and collecting terms becomes

Table 7
Mean and Variance for Log Scintillation (Uplink)

Flight	Data Piece No.*	Mean V_o	Standard Deviation σv	Normalizes Intensity Standard Deviation σ_I/I_o
9	2	3.114	.332	.690
9	3	3.139	.325	.673
9	4A	3.185	.320	.660
9	4B	3.206	.329	.683
9	5	3.097	.282	.566
9	6	3.147	.344	.720
9	7	3.129	.298	.607
9	8A	3.028	.198	.385
9	8B	3.038	.198	.385
9	9	3.307	.312	.641
9	10	3.077	.307	.629
9	11	3.153	.330	.685
9	12A	3.140	.326	.675
9	12B	3.094	.276	.556
9	13A	3.090	.143	.274
9	13B	3.085	.151	.290
9	14	3.271	.302	.617
9	15	3.114	.289	.586
9	16	3.068	.308	.631
12	1	2.776	.315	.648
12	2	2.689	.434	.972
12	3		.433	.944
12	4	2.650	.380	.816
12	5	2.743	.401	.874
12	6	2.446	.293	.595
12	7	3.549	.428	.493
12	8	2.955	.422	.936
12	9	2.966	.334	.695
12	10	2.774	.335	.698
12	11	0.191	1.588	8.605**
12	12	Missing		
12	13	0.189	1.773	25.813**
12	14	3.0468	.426	.948
15	1	3.116	.424	.942
15	2	2.976	.479	1.118
15	3	3.021	.499	1.188
15	4	Missing		
15	5	Missing		

*A and B indicates two 10 sec. segments taken from the same data piece.

**These data not used.

Table 8
Averages for Individual Flights

Flight 9	Average	Standard Deviation
Mean	3.130	0.070
Normalized S.D.	0.576	0.134
Flight 12		
Mean	2.859	0.283
Normalized S.D.	0.767	0.156
Flight 15		
Mean	3.038	0.058
Normalized S.D.	1.083	0.103

$$C_v = \alpha^2 \left\langle (\ln I - \langle \ln I \rangle)^2 \right\rangle \qquad 28$$

likewise

$$C_1 = 1/4 \left\langle (\ln I - \langle \ln I \rangle)^2 \right\rangle \qquad 29$$

hence

$$C_1 = \frac{1}{4\alpha^2} C_v \qquad 30$$

Using this expression we may calculate the log amplitude variance and corrosponding S. D. from the variance of the signal voltage V. The results for each flight are given in the following table.

Table 9
Log Amplitude Variance

Flight 9
$\sigma_1 = .2873$ S.D. $(\sigma_1) = .59$
$C_1 = .074$

Flight 12
$\sigma_1 = .3819$ S.D. $(\sigma_1) = .051$
$C_1 = .133$

Flight 15
$\sigma_1 = .4673$ S.D. $(\sigma_1) = .032$
$C_1 = .190$

Average all Flights
$C_1 = .132$

The observed scintillation variances are of the order of magnitude that one would expect from atmospheric propagation theory and an in general agreement with other experimental data. Minott, Bufton and Fitz Maurice [ ] report an average C_L of 0.18 for data collected during GSFC Balloon Atmospheric Propagation Experiment (BAPE I). This is in good agreement with the AVLOC value of 0.13.

Propagation theory predicts that for an infinitely small source the log amplitude variance is given by [ ]

$$C_L(0) = .56k^{7/6}\int_0^Z dsD_n^2(S)[Z-S)(\frac{S}{Z})]^{5/6} \qquad 31$$

where Z is the source to receiver distance measured along the propagation path, k is the propagation number and $C_N^2(s)$ is the index of refraction structure constant which expresses the strength of turbulence at each point along the propagation path. A model of the turbulent atmosphere proposed by Hufnagel and Stanley [ ] predicts that $C_N^2(h)$ will be given by

$$C_N^2(h) = C_{N_o}^2 h^{-1/3} e^{-h/h_o} \qquad 32$$

where h_o is a scale factor usually taken to be 1000 meters, h is attitude, and $C_{N_o}^2$ is a constant that expresses the gross turbulence strength. Both $C_{N_o}^2$ and h_o depend strongly upon local meteorological conditions. It is generally agreed that while equation 32 predicts the gross variation of C_N^2 with altitude, the actual turbulence structure is layered and shows strong

local fluctuations not predicted by this model. These turbulence layers are associated with wind sheers in the upper atmosphere and often occur near the tropopause. For these reasons a proper analysis of log amplitude variance would require a knowledge of the turbulence profile obtained independently of the optical measurement. Such data could be obtained from radiosonde borne microthermal probes but was not available during the AVLOC test.

Equation 31 must be corrected for the finite source diameter of the laser beam and for aperture averaging effects at the receiver. Fried [ ] has shown that this correction depends on the normalized source size

$$\Omega = \frac{k\alpha_o^2}{h_o} \sec \theta \qquad 33$$

where α_o is the real part of the complex gaussian beam parameter and θ is the zenith angle. Once Ω has been computed the required correction can be obtained from curves in the quoted reference.

Fried [ ] has investigated the effects of aperture averaging and found that the signal variance is given by

$$\sigma_S^2 = 2\pi \int_0^D \rho d\rho \; K_o(\rho_1 D) \; C_I(\rho) \qquad 34$$

Where D is the receiver aperture diameter, C_I the intensity covariance at the receiver and K_o the diffraction limited optical transfer function of the receiver. From equation 33 one may compute an averaging function θ which is the ratio of the observed signal variance to the signal variance

in the absence of aperture averaging. For an infinite plane wave propagating from space to earth one finds that θ depends on the turbulence strength $C_I(0)$ and a normalized aperture

$$D/\sqrt{4h_o \sec\theta/k} \qquad 35$$

For our test condition Fried results indicate that θ will be greater than 0.9. This theory is not strictly applicable to the AVLOC test for these reasons, viz, we have a gaussian beam wave not a plane wave, the propagation direction is from earth to space, and it neglects the effect of the central obscuration in the cassigrainian receiving telescope. Never the less Fried's results should provide an estimate of the magnitude of the aperture effects. Clearly this effect is small, probably less than the probable error in the data, and can be neglected.

Because of the lack of precise knowledge of the turbulence profile that existed during the AVLOC test and the absence of a theory of aperture averaging that is applicable without extensive modification we have not undertaken a precise comparison of the observed log amplitude variance with those predicted by theory. However, using Hufnagel's model with the usual choice of h_o and $C_{N_o}^2$, equation 31 predicts values of $C_1(0)$ on the order of 0.1 which is in relatively good agreement with the observed log-amplitude variances.

Power Spectral Density

Power spectral density (PSD) is defined as the Fourier transform of

the irradiance covariance function and is equivalent to the average received power per unit bandwidth at each frequency. Power spectral densities have been computed for each data segment. A typical PSD is shown in the next figure. The PSDs from other data segments were essentially similar.

All PSD's showed a more or less linear decrease with increasing frequency from a few HZ to 1000 HZ, the later value being the maximum frequency component obtainable with the selected sampling rate. In all cases the power density decreased about one order of magnitude at 100 HZ and two orders of magnitude at 1000 HZ.

Measurement Accuracy

Although the observed scintillation data tended strongly toward a log normal distribution the lack of strict log normalicy has caused some concern that the data may be biased by extraneous noise. We have considered all apparent sources of extraneous noise that might contribute to the observed scintillation and have concluded that none could reasonably be expected to account for this effect. Each of the possible sources of experimental error is discussed in the following paragraphs.

a. Detector Noise

The power signal to noise ratio S/N in the detector can be estimated from the photomultiplier tube parameters. S/N is given by

$$S/N = \frac{(i_s)^2}{(i_{N_1})^2 + (i_{N_2})^2}$$

POWER SPECTRAL DENSITY CURVE

Data	**6**
CH	**8**
FLT	**12**

Where $(i_s)^2$ is the mean square detector current due to the signal, $(i_{N_1})^2$ that due to shot noise in the photomultiplier tube and $(i_{N_2})^2$ that due to Johnson noise in the load resistor. As usual $(i_{N_2})^2$ may be neglected since both the signal and shot noise terms are multiplied by the square of the tube gain and the Johnson noise term is not. Now

$$i_S = \frac{GPe\eta}{hV_s} (2m) \cos\omega mt$$

where

G = PM Tube Gain

η = Quantum Efficiency

e = electronic charge

P = received signal power

h = Plank's constant

V_s = signal frequency

m = modulation indes

ω_m = modulation frequency.

and

$$(i_{N_1})^2 = 2G^2 (i_c + i_d) \Delta V$$

i_c = current due to incident radiation

i_d = dark current

ΔV = post detection bandwidth

$i_c = Pe\eta/hv_s$

hence

$$S/N = \frac{2i_c^2 m^2}{e(i + i_c)\, v}$$

where a factor of 2 has been introduced from the time average of $(i_s)^2$ we assume the following parameters:

$$\eta = 15\%$$

$$I_d = 1.2 \times 10^{-9} \text{ amps}$$

$$P = 6 \times 10^{-9} \text{ watts}$$

$$v_s = 6.16 \times 10^{14} \text{ Hz}$$

$$\Delta v = 5 \times 10^{3} \text{ Hz}$$

$$m = .3$$

The values of n and I_d are typical of the RCA 8644 photomultiplier tube used for scintillation detection in the AOCP, P is the average power measured on all flights and m represents a worse case (minimum) modulation index. With these values the estimated power signal to noise ratio is 10^5 corresponding to a voltage signal to noise ratio of approximately 300.

The shot noise induced by back ground radiation has been neglected in the preceeding calculations since all test were conducted at night.

The normalized standard deviation of intensity (σ_I/I_o) was typically on the order of .5. Hence it follows that the observed fluctuation in the output signal due to scintillation would be approximately 150 times greater than those due to detector noise.

b. Amplifier noise, recorder characteristics, electrical pickup.

All data channel amplifiers and recorders were designed to accommodate the expected data without introducing either excessive noise or biasing the data by reduced bandwidth or dynamic range. Throughout the flight test the data channel amplifier and data acquisition systems appeared to operate normally; we do not believe, therefore, that they represent a significant source of experimental error.

The scintillation data, along with all other data channels, did show a weak but persistant 56 Hz component which was been identified as electrical pickup from the aircrafts (nominally) 60 Hz power system. In our estimation, however, this 60 Hz pickup was not strong enough to bias the experimental data.

c. Pointing

One possible source of error is false scintillation caused by pointing error. Since the beam has a gaussian rather than uniform intensity profile any pointing error will cause a decrease in the irradiance at the receiver. If the pointing error is time dependent it will cause irradiance fluctuations that will be indistinguishable from scintillation. The gaussian beam profile may be expressed as

$$I = I_o \, e^{-\theta/\theta_o}$$

where θ_o is the angular beam width. Then the intensity fluctuation ΔI caused by a pointing error $\Delta\theta$ is

$$\Delta I = I_o - I = I_o - I_o e^{-\Delta\theta/\theta_o}$$

or

$$\Delta I/I_o = 1 - e^{-\Delta\theta/\theta_o}$$

A reasonable criteria is that $(\Delta I/I_o)^2$ be much less than the intensity variance due to scintillation. The observed intensity variances are on the order of 1/4 hence we might require.

$$1 - e^{-\Delta\theta/\theta_o} \quad .01$$

$$e^{-\Delta\theta/\theta_o} = \quad .99$$

or

$$\Delta\theta/\theta \approx .01$$

That is, the pointing error should be less than 1% of the beam width to insure that the error in observed variance is no more than a few percent (about 2 1/2%). On the AVLOC test the observed pointing errors were about 1 arc seconds and the beam width θ_o was about 180 arc seconds. We conclude therefore that pointing error could not cause an error of more than about 2% in the observed intensity variance.

The above analysis assumes a smooth, gaussian intensity profile. If, the beam contained "hot spots" the false scintillation induced by even a small pointing error could be much worse. The possibility of this having occurred cannot be eliminated with complete certainty; however, observation of the transmitted beam has indicated that the intensity pro-

file is smooth and free from detectable "hot spots".

As a final check on the effect of point accuracy we have cross correlated the instantaneous power received at the aircraft with beam steerer voltages in the ground station transmitter. If pointing was in fact introducing appreciable false scintillation we would expect to see a strong positive corrolation. No significant correlation was found.

d. Aircraft Induced Turbulence

Scintillation due to the turbulence around the aircraft is not significant because of the thinness of the turbulence layer and its proximity to the receiver. Referring to equation we see that the aircraft turbulence would contribute an amount.

$$\Delta C_e(0) = .56\, k^{7/6} \int_{Z-\Delta Z}^{Z} C_N^2(AC)\, [(Z-S(\tfrac{S}{Z})]^{5/7}\, dS$$

to the observed log amplitude variance. Clearly with ΔZ small (a few meters) and the weighting function $[(Z-S)(\frac{S}{Z})]^{5/6}$ approximately zero ($Z \approx S$) this term will be negligable.

e. Vibration

To ensure that the observed scintillation did not include vibration induced noise the vibration of the AOCP was monitored along three orthogonial axis by piezo electro sensors. Power spectra densities of the vibration were computed and the vibration data was cross correlated with scintillation.

The lateral vibration (yaw) showed a strong, rather sharp resonance at 10 Hz and a weaker broad resonance near 100 Hz. Above 200 Hz the vibration fell quickly to zero. The longitudinal vibration data had a single strong peak at 200 Hz. Both axis also have a number of other sharp spikes. Especially noticable are those at 55 Hz, 110 Hz, etc. which probably are related to the aircrafts 60 Hz (nominal) power frequency.

None of the features in the vibration PSD could be identified in the scintillation PSD; neither was their any significant correlation between these data. We therefore conclude that aircraft vibration has no effect on the recorded data.